SYNTHESIS OF DISPIRO-PORPHODIMETHENES AND THEIR TRANSFORMATIONS TO OTHERWISE INACCESSIBLE PORPHYRIN PRODUCTS

By

HUBERT S. GILL, IV

A DISSERTATION PRESENTED TO THE GRADUATE SCHOOL
OF THE UNIVERSITY OF FLORIDA IN PARTIAL FULFILLMENT
OF THE REQUIREMENTS FOR THE DEGREE OF
DOCTOR OF PHILOSOPHY

UNIVERSITY OF FLORIDA

2004

This work is dedicated to my parents, Sue and Hubert Gill, for their endless love, support, and sacrifice throughout my life, and in memory of Chris Whitehead and Lydia Matveeva, two colleagues who contributed to this work, but departed this earth before its completion.

ACKNOWLEDGMENTS

I would like to extend my thanks and appreciation to those who have contributed to my development as a scientist, beginning with my family members, who encouraged my curiosity and tolerated my experimentation from the time I was able to strike a match, mix household chemicals, and insert metal objects into wall outlets. I thank my mom, Sue, and sister, Savannah, for keeping me alive, and my dad, Hubert, for encouraging them to do so. I would also like to thank my dad for taking me on "field trips." Weather we were fishing on the Outer Banks, watching PBS, wandering through the woods identifying trees and animals, or trying to distill cedar oil and making nothing but creosote, he has always been there for me, encouraging me to do my best and never stop pursuing any endeavor that I began. This advice has been particularly relevant during the course of this dissertation. My grandparents, Frances and Hubert, who both passed away since I moved to Gainesville, I am also forever indebted to. My granddad taught me to be a meticulous tinkerer. My grandma and her sister, my Aunt Dick, were both rock hounds, and they provided early lessons in geology and the symmetrical beauty of crystals.

My high school chemistry teacher and friend for life, Phillip Dail, provided my formal introduction to chemistry, and taught me, my sister, and countless others not only about the natural laws of God's world but also more profound things concerning life and friendship. I have him to thank for guiding me towards chemistry as my primary scientific discipline. My undergraduate academic advisor at FSU, Ken Goldsby, who is

also a phenomenal educator, took me under his wing and provided me with my first synthetic research experience, taught me everything I know about electrochemistry, and introduced me to the wonderful perspective on the universe provided by group theory. Ken also encouraged my initial interest in inorganic biochemistry, which led me to the University of Florida.

A few days after I emailed my future advisor, Prof. Michael Scott, telling him that I was interested in his work, he called me at home, waking me in the early am from a deep sleep directly into a conversation that would change my life. I knew immediately that I could work with Mike, and even through the course of five years of close academic contact with occasional moments of doubt; I know that I made the right decision by joining his group. I owe much thanks to Mike, who is undoubtedly one of the few professors in the world who possesses the patience, good temperament, and other intangible qualities required to direct the research of one who takes direction as poorly as I . I thank him for indulging my tangential curiosity, while keeping me close enough to the line required to finish this work.

Mike and Dr. Michael Harmjanz, the person responsible for indoctrinating me into the brutally rewarding, low-yielding, and colorful world of porphyrin synthesis, deserve more credit for this dissertation than I do. Michael taught me most of the synthetic techniques that I did not made up as I went along, and the brainstorming sessions that we had in my first two years here have been sorely missed since his departure. One person who helped to fill this void is Isaac Finger, an undergraduate researcher who has been working with me for the past three years. His scientific curiosity and outside the box

perspective has provided inspiration and insight, and often quite unintentionally, he has advanced this work in many ways that cannot be directly accounted for.

An immeasurable amount of gratitude is owed to Dr. Ivana Božiderević, my lab mate and friend for the past five years. Without her I never would have made it through this. The other members of our research group, past and present, who I would like to thank include, in order of appearance, Matt, Martin, Andrew, Cooper, Nella, Ranjan, Javier, Dolores, Pieter, Candace, Eric, Hanna, Ozge, Eric, Erik, Priya, Flo, and Claudia. I appreciate all of your help and tolerance of my mess.

I would also like to extend my thanks to the professors that taught my graduate courses: Dr. Scott, Dr. Richardson, Dr. Abboud, Dr. Richards, and Dr. Horenstein, as well as those who have served on my committee: Dr.Abboud, Dr. Talham, Dr. Martin, and Dr. James.

TABLE OF CONTENTS

page

LIST OF TABLES

LIST OF FIGURES

Abstract of Dissertation Presented to the Graduate School
of the University of Florida in Partial Fulfillment of the
Requirements for the Degree of Doctor of Philosophy

SYNTHESIS OF DISPIRO-PORPHODIMETHENES AND THEIR TRANSFORMATIONS TO OTHERWISE INACCESSABLE PORPHYRIN PRODUCTS

By

Hubert S. Gill, IV

December 2004

Chair: Michael J. Scott
Major Department: Chemistry

The MacDonald [2 + 2]-type condensation of readily available 5-aryl-substituted dipyrromethanes with acenaphthenequinone leads to *trans*-dispiro-porphodimethenes. Coordination of various late transition metals by these porphodimethenes typically proceeds smoothly and in high yield. In addition to providing insight to this underrepresented class of tetrapyrrolic macrocycles, these porphodimethenes serve as precursors to otherwise inaccessible *trans*-bis-naphthyl porphyrins bearing various functional groups in intimate proximity to the porphyrin plane. The porphyrins with two alcohol or carboxylate moieties are susceptible to oxidative ring-closing reactions that are chemically and electrochemically switchable, with both the open porphyrin form and the closed porphodimethene form being stable over a large concurrent potential range. In addition to possibilities for the design of novel redox-switchable sensors or optical materials, this unusual reactivity has broader implications for biological processes, particularly oxidative heme catabolism. These dispiro-metalloporphodimethenes are also

excellent synthetic precursors for the preparation of unprecedented porphyrin architectures via unusual light-activated oxidative rearrangements. The products of these cascade reactions are intrinsically non-planar, conformationally distorted metalloporphyrins. The palladium complexes of these porphyrins have been shown to generate singlet oxygen with 100% quantum yields. Further oxidative dehydrogenation of these non-planar porphyrins generates exceedingly large, sheet-like porphyrins bearing two polycyclic aromatic ring systems fused to the porphyrin core. These porphyrins have an extensively delocalized π-system, and their UV-visible-near IR spectra feature the lowest energy electronic transitions observed for monomeric porphyrin species to date.

CHAPTER 1
TETRAPYRROLIC MACROCYCLES

Introduction

Pyrrolic macrocycles, such as porphyrins, corroles, chlorins, and bacteriochlorins (Figure 1-1) are used throughout nature in an abundance of proteins and enzymes for diverse functions including catalysis, light-harvesting, dioxygen transport, and as prosthetic groups for electron transfer in redox enzymes.[1] Driven by the desire to understand these systems and in order to mimic these processes for practical utility, chemists have perused the synthesis of naturally occurring tetrapyrrolic macrocycles, their intermediates, and their modified analogues over the past century.[2] These extensive synthetic investigations have offered insight into the biological function of natural tetrapyrroles, and they have provided catalysts for various synthetic transformations, photosensitizers for cancer chemotherapy, electrochemical sensors, and receptors for molecular recognition and anion binding.[3]

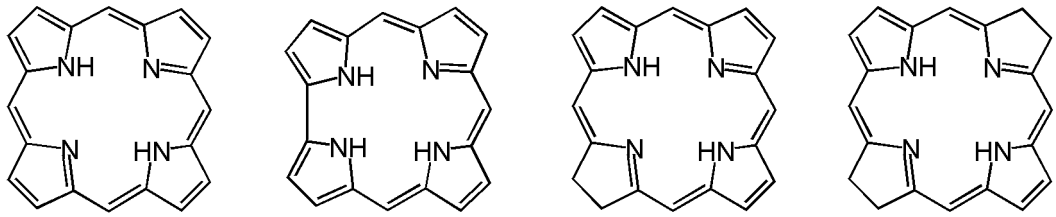

Figure 1-1. Illustration of some naturally occurring tetrapyrrolic macrocycles.

Reduced Forms of the Porphyrin Skeleton

As illustrated by the biological synthesis of uroporphyrins and protoporphyrins from porphobilinogen (Figure 1-3), natural porphyrin formation involves first the

condensation and cyclization of pyrroles, followed by the oxidation of the resulting porphyrinogen by six electrons and removal of six protons, four from the *meso*-positions and two from the pyrrole nitrogens (see Figure 1-3 for porphyrin nomenclature[4]).[5] Upon initial oxidation of porphyrinogen, the oxidation process is difficult to arrest, and partially oxidized intermediates such as porphomethenes, phlorins, and porphodimethenes have rarely been isolated (Figure 1-4). The presence of porphodimethene macrocycles has been indicated spectroscopically during the controlled oxidations of tetraaryloctaalkyl-porphyrinogens, which proceed slowly relative to the oxidation of most other porphyrinogens.[6,7]

The irreversibility of the oxidative process is due to the considerable thermodynamic stabilization gained upon the formation of the large aromatic porphyrin macrocycle. It is likely that the similar aromatic stabilization found for chlorins and bacteriochlorins is responsible for their ubiquitous utilization in nature. As opposed to paying the high energy penalty for breaking aromaticity by reducing the *meso*-positions, the option of reducing up to four of the β-positions pair-wise, forming the chlorin and bacteriochlorin systems, is typically favored because the β positions on the B and D pyrrole rings are not involved in the 18-annulene aromatic path (Figure 1-5).

In 1974, Buchler and Puppe reported the preparation of the first air-stable porphodimethenes.[8] Their procedure employed the reductive methylation of octaethylporphyrinato zinc(II), which has ethyl protected β-positions, sterically discouraging the alkylation of these carbons (Figure 1-6). The scope of this reaction was later expanded to produce metalloporphodimethenes bearing various metals and other alkyl substituents at the saturated *meso*-carbons.[9-13] The addition of alkyl groups to the 5-

and 15-positions of metalloporphyrins in a *syn*-diaxial conformation provides stabilization at these sp^3 centers, and even under oxidative potentials, the complexes were not found to dehydrogenate.[14]

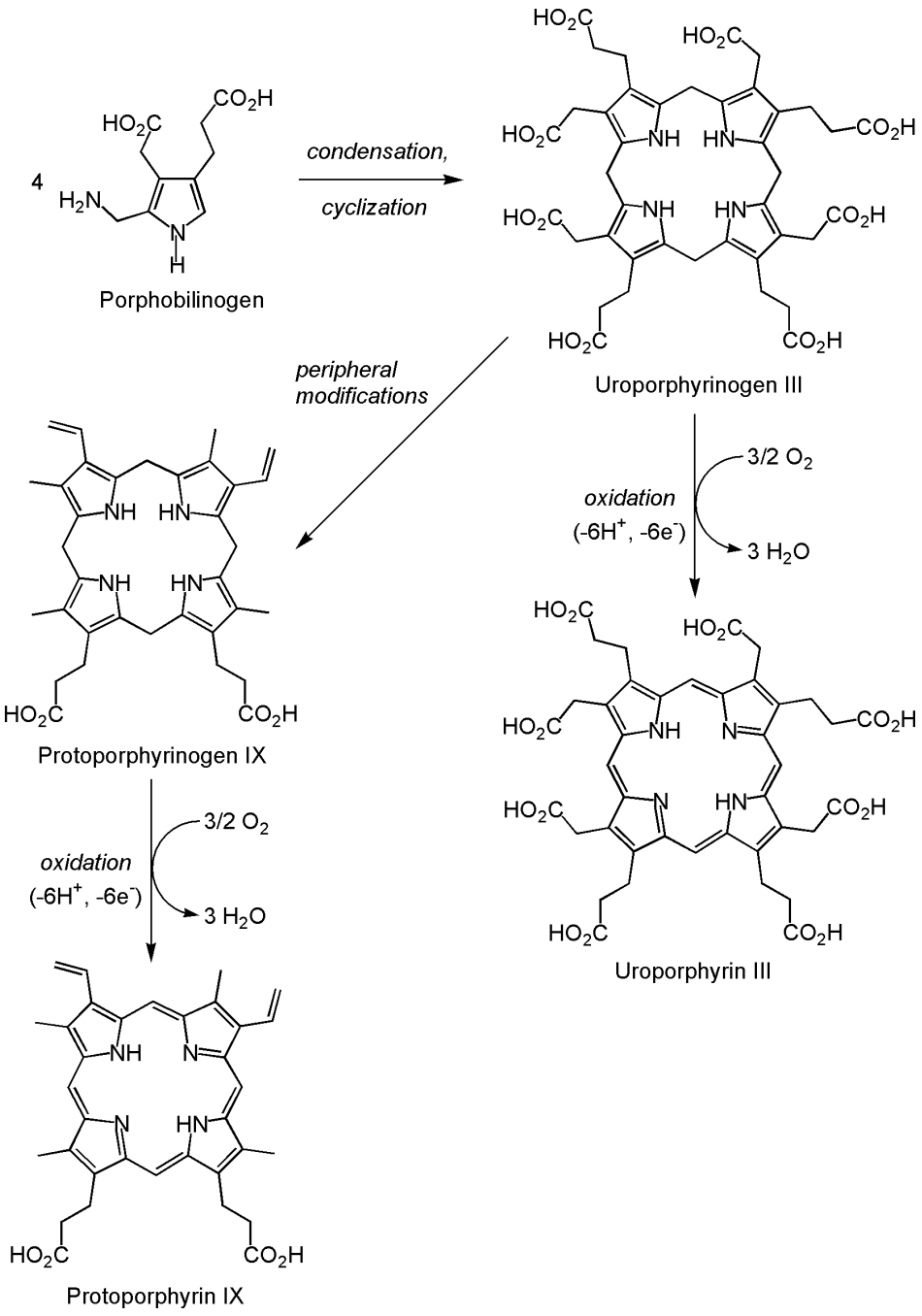

Figure 1-2. Diagram of the biological synthesis of porphyrins illustrating the step-wise condensation to form porphyrinogens and oxidation to form the fully aromatic porphyrins.

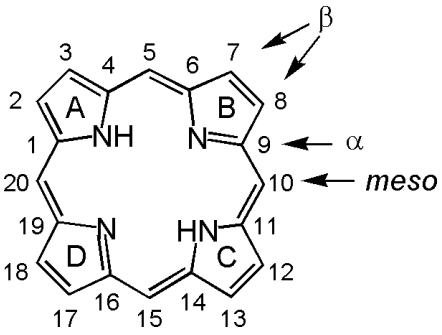

Figure 1-3. Diagram of porphyrin depicting the numbering scheme and nomenclature used for tetrapyrrolic macrocycles.

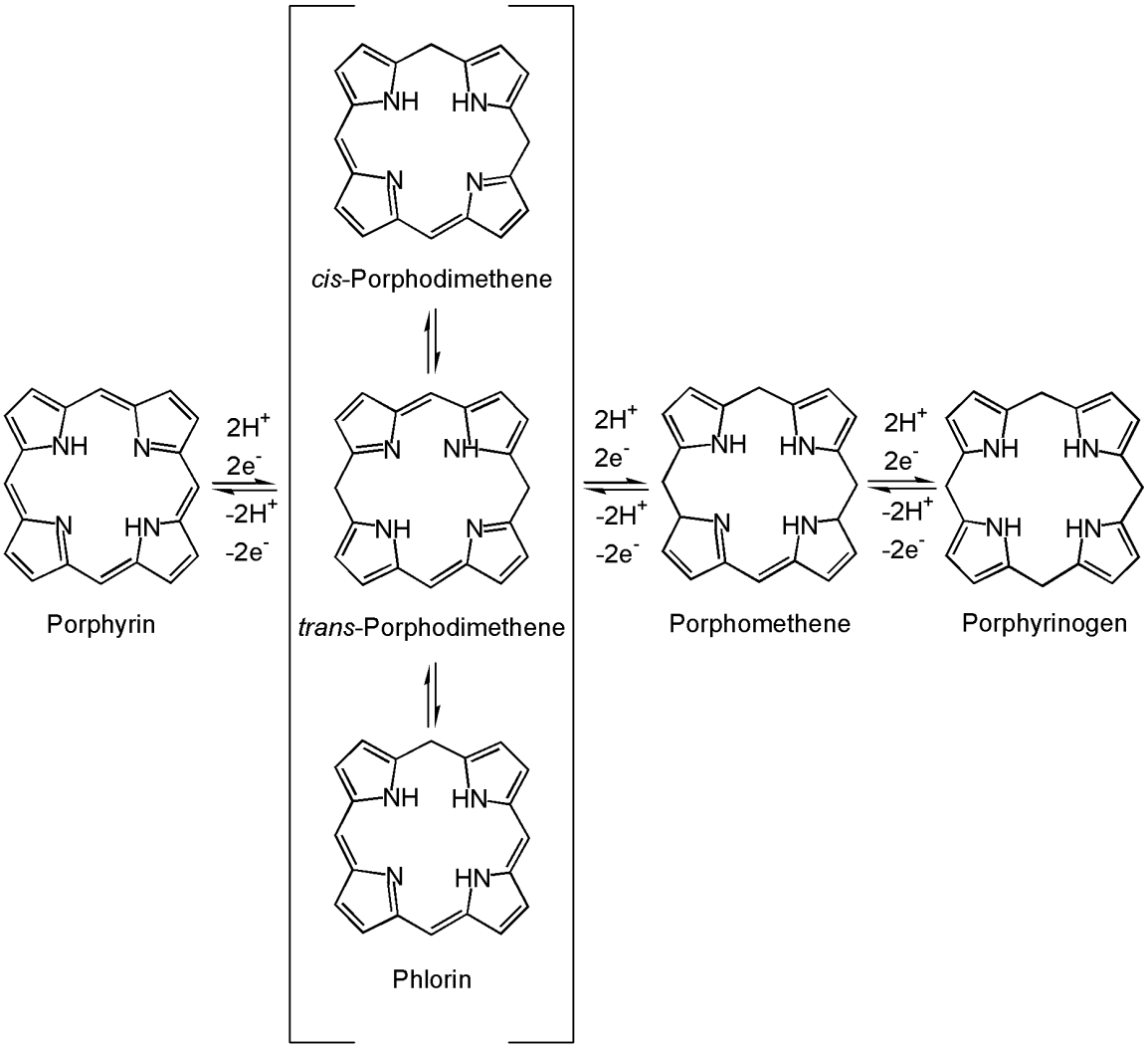

Figure 1-4. Illustration of the redox relationships between various intermediates in the oxidation pathway from porphyrinogen to porphyrin.

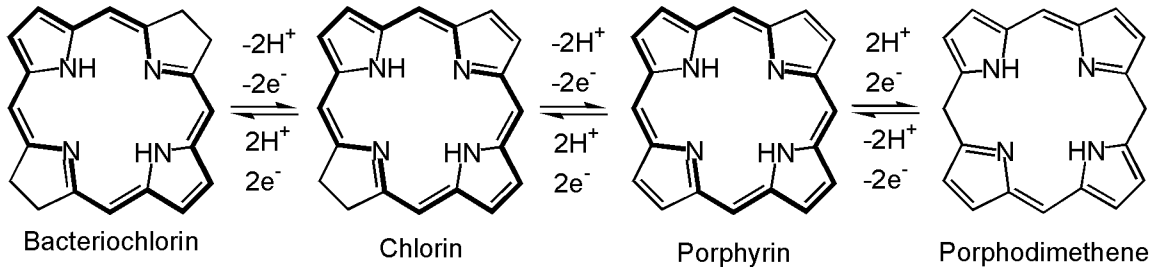

Figure 1-5. Depiction of the alternative routes for the reduction of porphyrin by hydrogenation of the β-positions leading to chlorin and bacteriochlorin, highlighting the 18-annulene pathway of aromaticity retained.

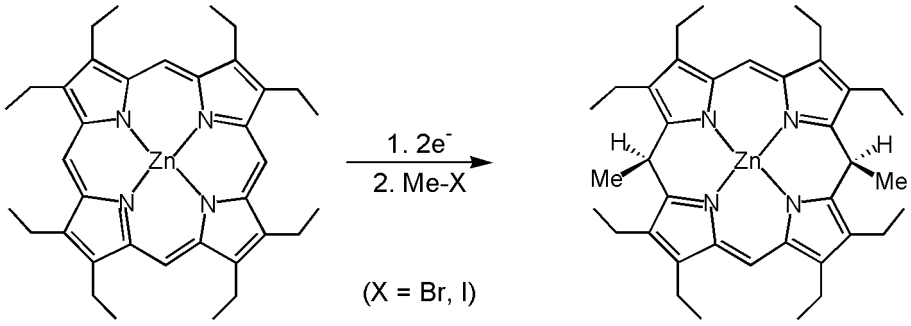

Figure 1-6. Depiction of the reductive alkylation of octaethylporphyrinato zinc(II), producing the first isolated air-stable porphodimethene.

In addition to the routine characterization of these *trans*-porphodimethenes, Buchler and coworkers undertook extensive investigations of their physical properties including X-ray structural determinations,[8-10,15-17] as well as electrochemical, magnetic, Mössbauer, and ESR measurements.[10,13,14,18] Although these studies generated an interest in porphodimethenes within the scientific community, viable alternative schemes for the synthesis of these macrocycles were slow to emerge. No other general methods for the preparation of isomerically pure porphodimethenes were reported prior to the inception of the work presented in Chapter 2, and multi-gram quantities of this class of macrocycles were not accessible prior to 1999.

Synthesis of *meso*-Tetraarylporphyrins

One modification to the porphyrin core that has been utilized extensively is the introduction of aryl substituents at the *meso*-carbons of the macrocycles.[19] Substitution for the hydrogens found at these positions in most naturally occurring porphyrins with various aromatic substituents in artificial porphyrins provides stabilization with respect to oxidative degredation and photobleaching of the chromophore[20] as well as providing points for further synthetic elaboration and fine-tuning of steric and solubility properties.[19] The synthesis of *meso*-tetraphenylporphyrin [H_2(TPP)] was first described in 1935 by Rothemund and subsequently detailed in 1941 by Rothemund and Menotti, who heated pyrrole and benzaldehyde at high concentrations in pyridine to 200°C in a sealed vessel for 48 h (Figure 1-7).[21,22] Upon slow cooling to room temperature, H_2(TPP) crystallized and was isolated in 7.5-9% yield.

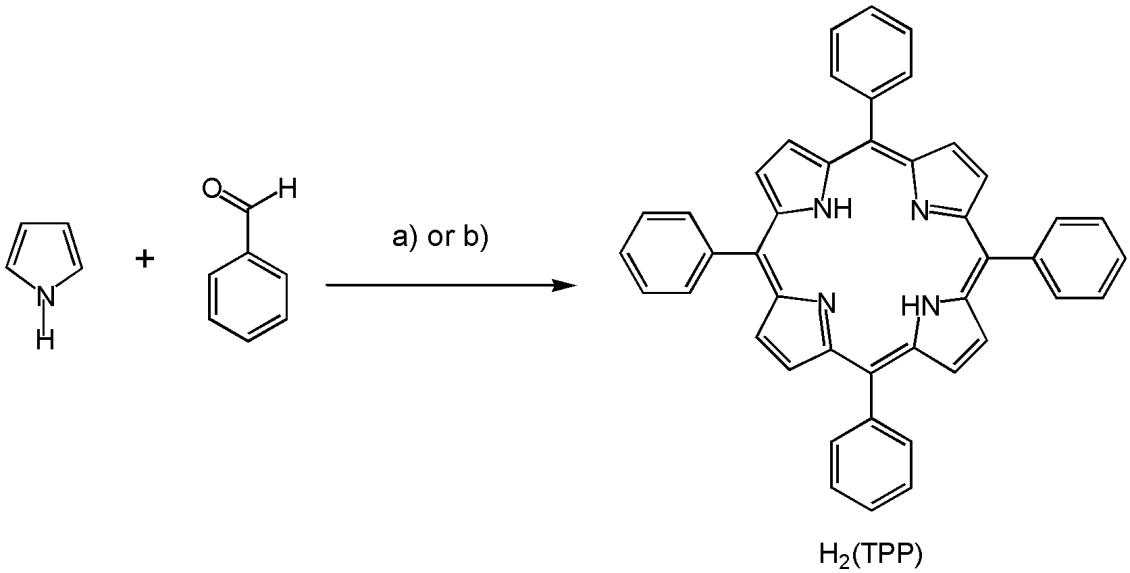

Figure 1-7. Diagram of two syntheses of tetraphenylporphyrin. a) Rothmund's method with pyridine as the solvent in a sealed vessel at 220°C. b) the Adler-Longo method employing refluxing organic acid with the reaction open to the air.

The procedures of Rothemund were expanded upon very little and no new methodology for the preparation of tetraarylporphyrins was published until 1964, when Adler, Shergali, and Longo reported their synthesis of H_2(TPP) via the condensation of benzaldehyde and pyrrole in refluxing acetic acid, with the reaction vessel open to the air (Figure 1-7).[23] This synthesis provided a substantial increase in yield over that obtained by the Rothemund method (~20%). Due to the lower solubility of the porphyrin products in comparison to acetic acid, propionic acid has become the solvent of choice for this preparation because the microcrystalline porphyrins may be isolated directly from the reaction mixture by filtration. The extension of this work using various aromatic aldehydes allowed for numerous aryl substituents to be symmetrically incorporated at the *meso*-positions of the porphyrin periphery. Although a significant improvement to Rothmund's synthesis, the use of organic acids as solvent and the high temperatures required restrict the functional group tolerance and cause side reactions, leading to lower yields.

The aforementioned limitations and lack of synthetic judiciousness led Lindsey and coworkers to reexamine the approach to *meso*-substituted porphyrin synthesis with a focus on rational, step-wise procedures under gentle conditions. The optimization of these conditions was deliberate and tedious, requiring seven years to develop (1979-1986) prior to publication. The synthesis, illustrated in Figure 1-8, is a two-step one-flask room-temperature reaction sequence which results in superior yields for most symmetric *meso*-tetraarylporphyrins in comparison to any other method.[24,25]

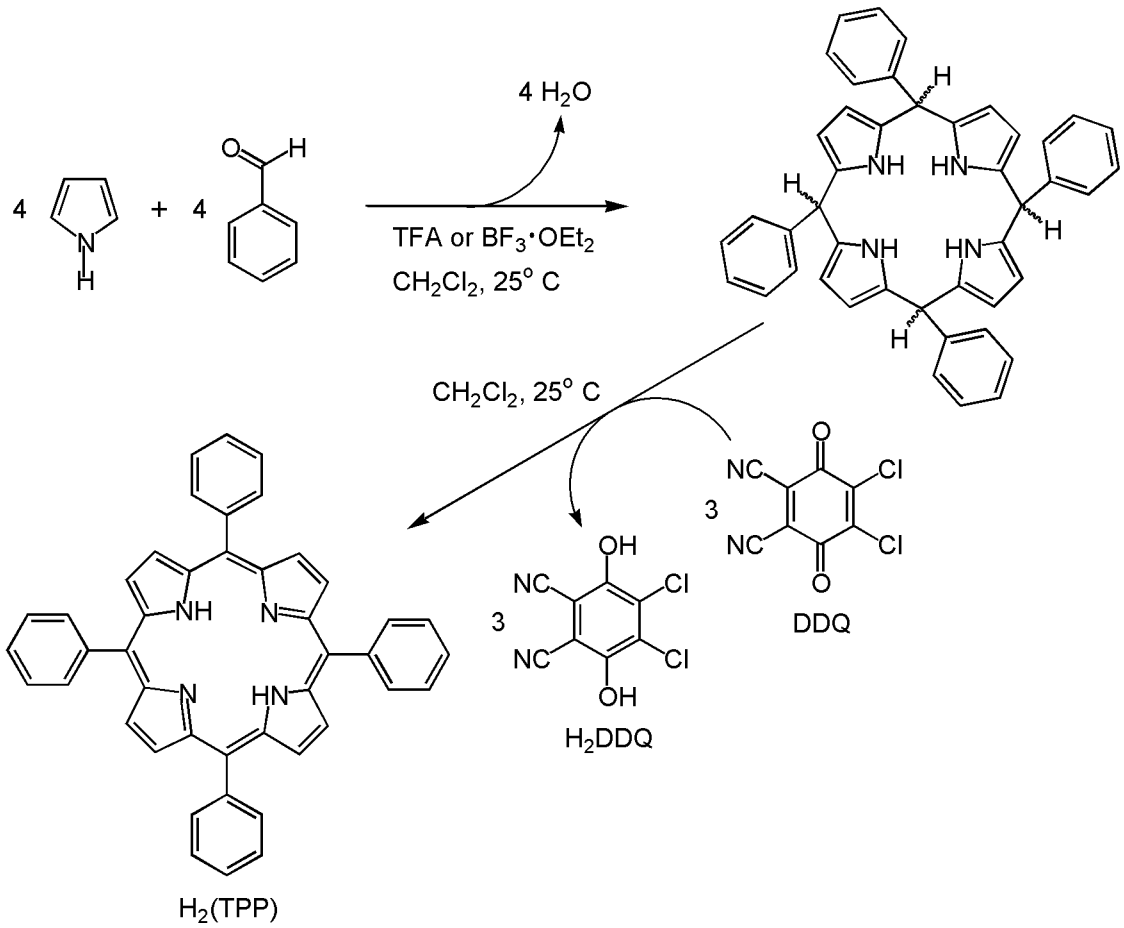

Figure 1-8. Diagram of the two-step, one-pot synthesis of tetraarylporphyrins by Lindsey's methodology.

Some advantageous aspects of this methodology include 1) gentle reaction conditions, allowing for great diversity of aldehydes and preventing side reactions with high activation energies, 2) catalytic activation of the aldehydes with low concentrations of acids (1mM for $BF_3{\cdot}OEt_2$; 20-50 mM for trifluoroacetic acid), limiting the formation of the well-known but poorly characterized pyrrole-red and other oligopyrrole byproducts, 3) high dilution of the reagents in dichloromethane (10 mM), encouraging the formation of cyclic rather than long-chain oligomeric products, 4) formation of the cyclic porphyrinogen skeleton under gentle, reversible conditions prior to the addition of oxidant, preventing premature oxidation which can lead to chain termination or prevent

cyclization, and 5) the use of very active quinone oxidants, rather than atmospheric oxygen, for the dehydrogenation of the porphyrinogen intermediate, allowing for rapid, porphyrin formation under mild conditions. While the reaction efficiency varies considerably depending upon the steric and electronic properties of the aldehyde precursor, typical yields range from 20–40% [35-40% for H_2(TPP)],[19,24,25] and even yields claimed to be in excess of 60% have been reported for some aldehydes.[26]

Synthesis of Asymmetric Tetraarylporphyrins

For purposes including the preparation of porphyrins for biological model systems and various materials applications, asymmetric porphyrins bearing two, three, or four different aryl substituents at regiospecific *meso*-positions are desirable synthetic targets. As depicted in Figure 1-9, mixed condensation approaches using two different aldehydes to form mixtures of porphyrins is a plausible approach to obtain A_xB_{4-x} porphyrins, but a statistical distribution of isomers is always formed. The binomial distribution may be used to project the outcome of such mixed condensations, assuming equal reactivity of the aldehydes employed in the statistical reaction.[27] A 1:1 ratio predicts 6.25% A_4, 25% A_3B, 25% *cis*-A_2B_2, 12.5% *trans*-A_2B_2, 25% AB_3, and 6.25% B_4. Aldehyde ratios may be adjusted to favor the desired product, and the yield of mono-substituted (A_3B) porphyrins may be increased by changing the ratio to 3:1 in favor of aldehyde A, producing 42.2% of the A_3B isomer. The most difficult asymmetric porphyrin to obtain from this approach is the *trans*-A_2B_2 isomer, which should not exceed 12.5%, regardless the ratio employed.

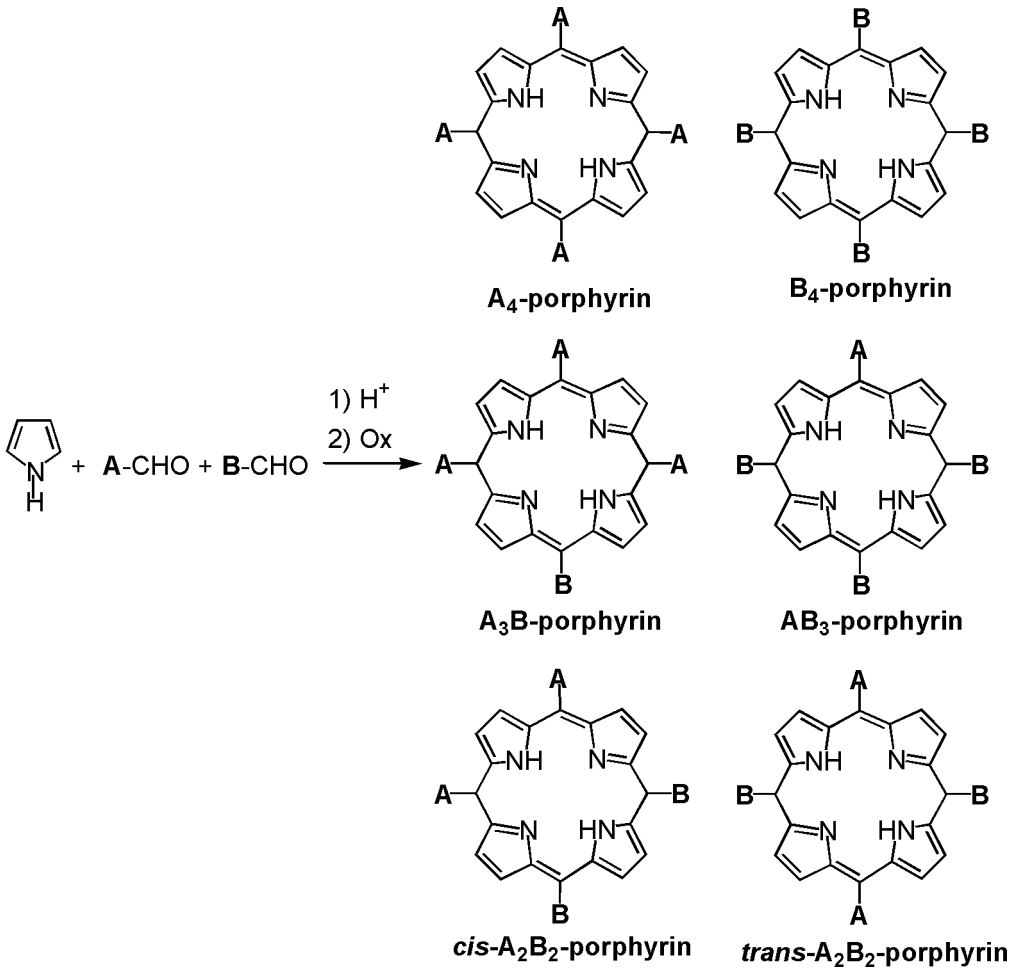

Figure 1-9. Illustration of the possible porphyrin isomers resulting from the mixed condensation of two aldehydes and pyrrole.

In some cases, the isomers can be resolved chromatographically, but this separation is laborious, often requiring multiple columns for successful purification. Owing to the inherently low yields for tetraarylporphyrin syntheses coupled with the statistical distribution of products obtained and the limitations involving isolation, quantities of the desired porphyrin isomer obtained are often meager, limiting the scope of this approach. In spite of these difficulties, the desire to utilize such asymmetric porphyrins for various applications eventually led to the preparation of numerous asymmetric porphyrins bearing two different *meso*-substituents by the Adler-Longo method.

Although the increased yields and broader functional group tolerance of the Lindsey method make mixed condensations more fruitful in comparison to the Adler-Longo synthesis, the isolation of specific isomers remains difficult in most cases. Additionally, the synthesis of porphyrins bearing three or four unique *meso*-substituents by this method is quite impractical regardless of the yield, as the statistical distribution of compounds increases exponentially with the number of aldehydes in the reaction mixture. For these reasons, Lindsey and coworkers devised new, directed approaches for the preparation of asymmetric porphyrins, replacing elaborate chromatography with elegant syntheses. These procedures may be divided into two distinct types, the syntheses of *trans*-A_2B_2-tetraarylporphyrins and the syntheses of porphyrins bearing up to four different *meso*-aryl substituents with controlled regioselectivity.

The rational preparation of *trans*-A_2B_2-tetraarylporphyrins was achieved by modified MacDonald [2+2] reactions, which employ the acid catalyzed condensation of 5-aryldipyrromethanes with aldehyde followed by oxidation with DDQ (Figure 1-10).[28] The dipyrromethanes required for this reaction are prepared by the condensation of pyrrole and aldehyde with $BF_3 \cdot OEt_2$ as the acid catalyst and pyrrole as the solvent.[28] In many cases, the optimization of acid concentration for the [2+2] reaction is crucial, as high acid concentrations promote scrambling of the aryl moieties, resulting in a distribution of isomers as found for mixed condensations.[29-31] Under optimized conditions, yields ranging from 28-48% are typical, far surpassing the mixed-condensation approach while avoiding chromatography entirely.[31]

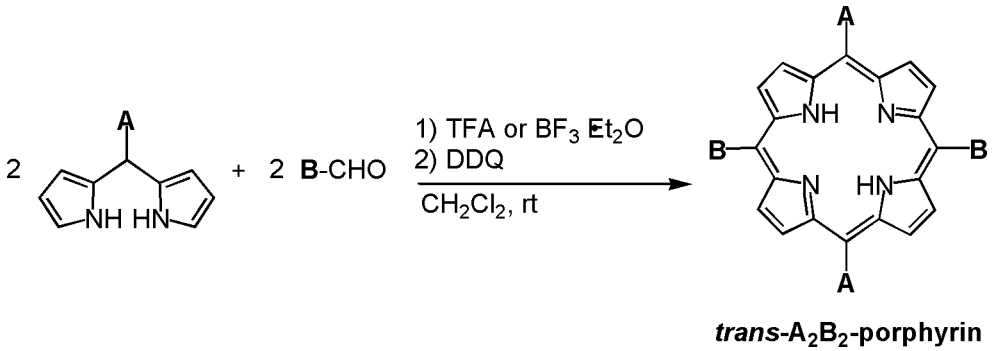

Figure 1-10. Diagram of the modified MacDonald [2+2] condensation under Lindsey conditions to provide *trans*-A_2B_2 porphyrins without chromatography.

The preparation of AB_2C or ABCD porphyrins in a rational manner represents perhaps the most elegant synthesis of tetraarylporphyrins to date, and their products have been employed for numerous applications, including the assembly of complex porphyrin architectures for molecular electronics and light harvesting.[32-36] As illustrated in Figure 1-11, the synthesis of porphyrins bearing up to four different *meso*-aryl substituents begins with the symmetric or step-wise acylation of dipyrromethanes.[37] The carbonyls are then reduced to carbinols with $NaBH_4$. Condensation with another dipyrromethane produces the asymmetric porphyrinogen, and subsequent oxidation with DDQ generates the porphyrin. Yields for these reaction sequences are in some cases meager, ranging from 6 to 30% overall, but they provide the only reasonable route to such complex porphyrins and utilize minimal column chromatography.

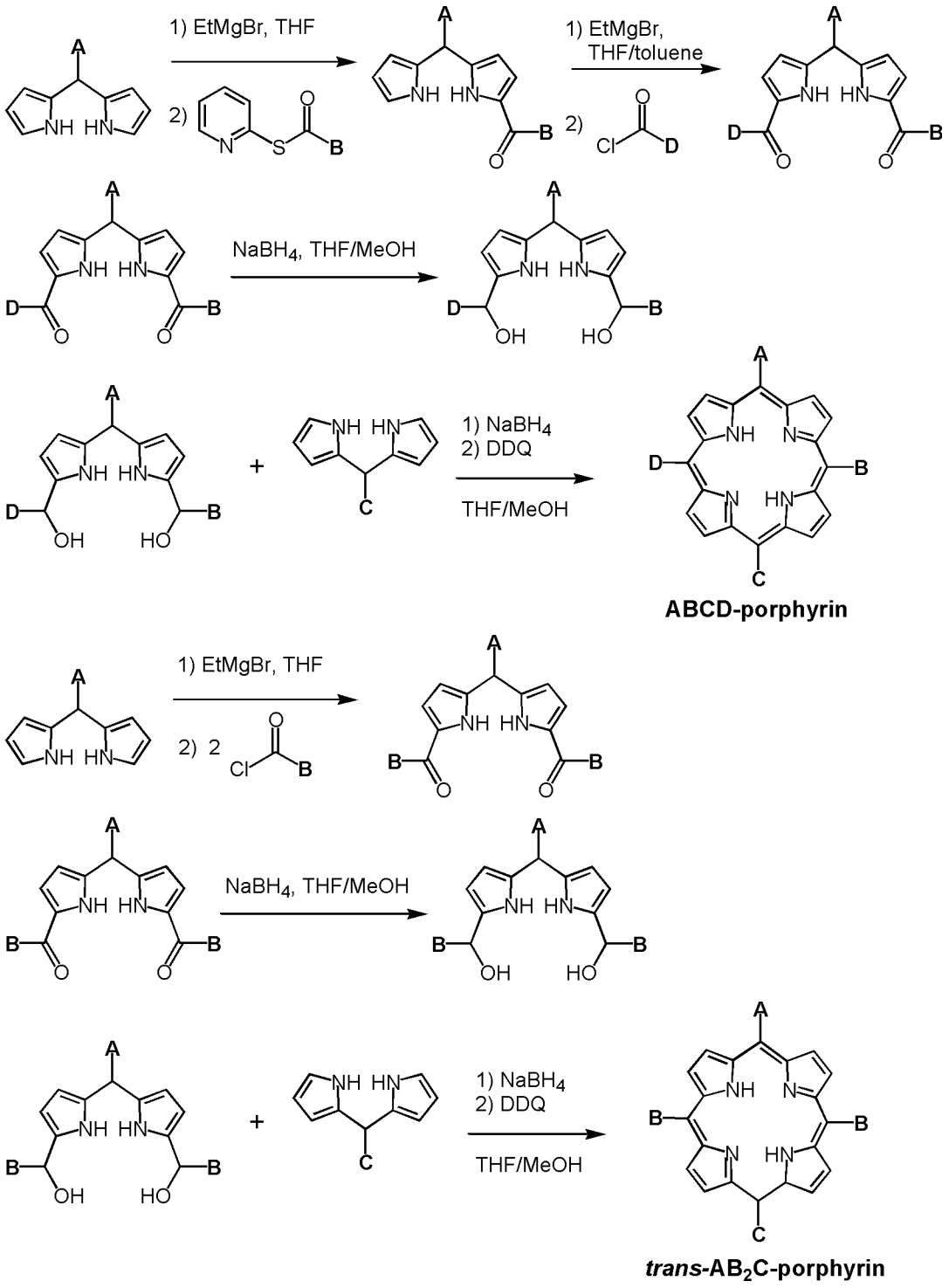

Figure 1-11. Diagram of the rational methodology for the preparation of highly asymmetric porphyrins.

Electronic Absorption Spectra of Tetrapyrrolic Macrocycles

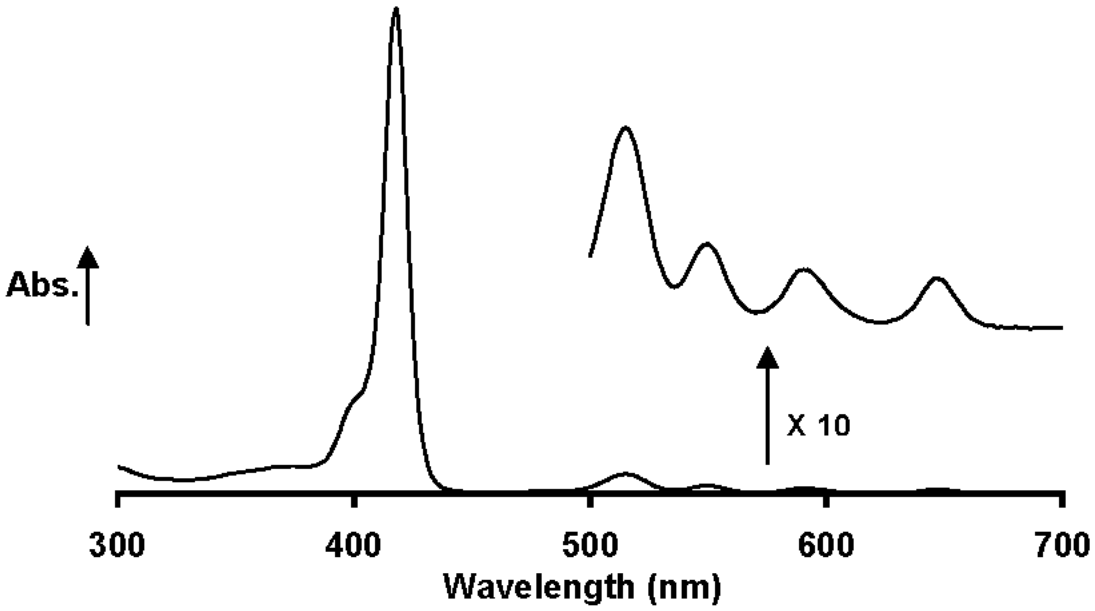

Figure 1-12. Illustration of the UV-visible spectrum of H_2(TPP) measured in CH_2Cl_2.

As their name origin from the Greek *porphura* (purple) implies, typical porphyrins exhibit a deep-purple hue, and all porphyrins are intensely colored. The electronic absorption spectra of conventional porphyrins, such as octaethylporphyrin or tetraphenylporphyrin, are characterized by a strong, single band in the high-energy region of the visible spectrum ranging from ~400 – 440 nm, referred to as the Soret or B band, and a series of bands appearing in the low-energy visible region from ~500 – 700 nm, which are identified as the Q bands (Figure 1-12). Both of these spectral features arise from π-π^* transitions, and are described by the Gouterman four-orbital model.[38] This paradigm invokes the two highest occupied molecular orbitals [a_{1u}(HOMO) and a_{2u}(HOMO-1)], which are of similar but distinct energies, and the two lowest, nearly degenerate, unoccupied molecular orbitals [e_{gy}(LUMO) and e_{gx}(LUMO)], which are considered to have equal energies (Figure 1-13).

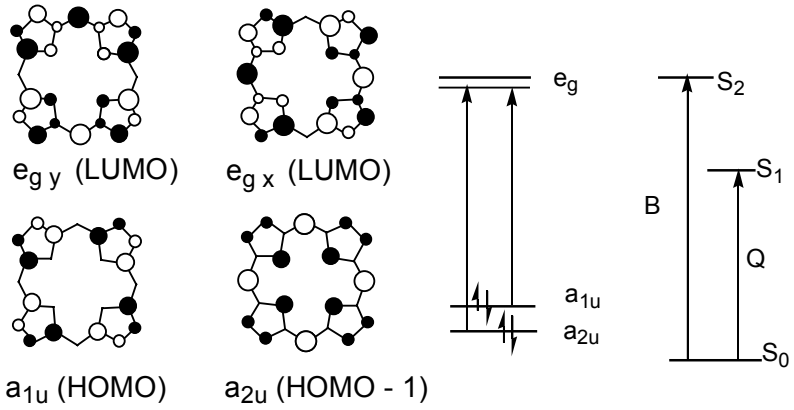

Figure 1-13. Illustration of the frontier orbitals, their relative energies, and the states arising from configurational interactions of H_2(TPP). Adapted from Anderson.[39]

Based upon this molecular orbital description, two bands of comparable energies in the visible region are predicted ($a_{1u} \rightarrow e_g$ and $a_{2u} \rightarrow e_g$), but as observed in the spectrum of H_2(TPP), the wavelengths of the two absorptions are quite dissimilar. This disparity has been attributed to a process known as configurational interaction; wherein the four orbitals combine to form three states (Figure 1-13). Constructive interference arising from this hybridization provides the intense, high-energy Soret band from the $S_0 \rightarrow S_1$ absorption, and destructive interference results in the Q bands from the $S_0 \rightarrow S_2$ absorption.[39] The multiple features observed in the latter have been attributed to a slight modification to this model, which allows for two, rather than one, absorptions from two quasi-forbidden transitions, and one vibrational satellite for each of these absorptions.[40]

Metallation of porphyrin chromophores alters the wavelengths and band patterns in their electronic absorption spectra. Most late transition metals induce a slight red-shift for the Soret band, but palladium typically provides a blue-shifted Soret band in comparison to their free-base analogues.[41] The pattern observed for the Q bands is

changed upon metallation, with the vibrational satellites for the two low-energy transitions being lost, resulting in two long wavelength bands (Figure 1-14).

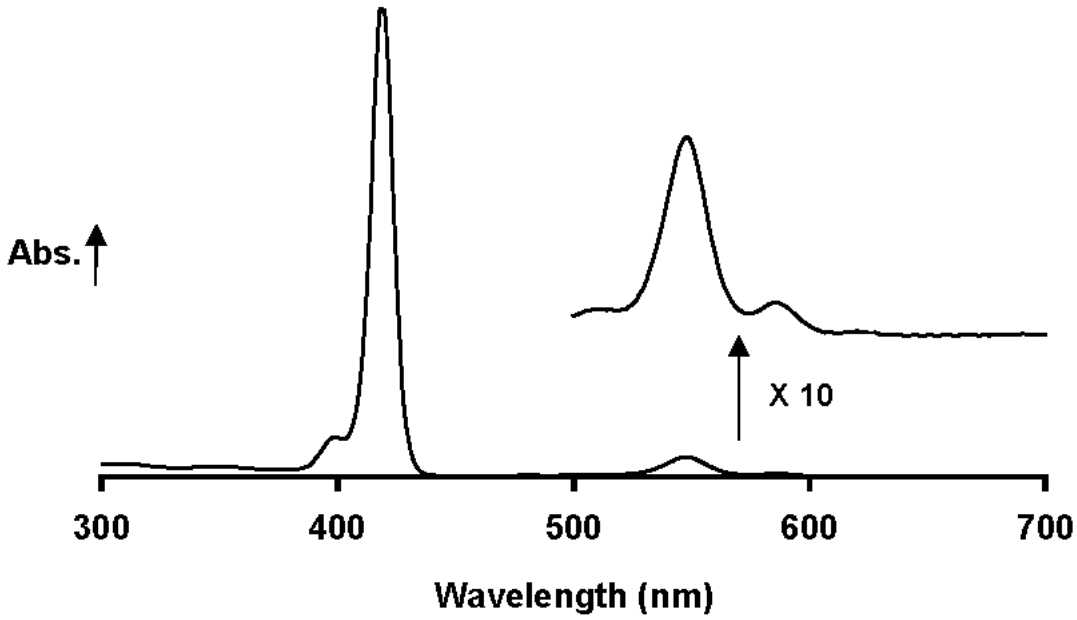

Figure 1-14. Illustration of the UV-visible spectrum of Zn(TPP) measured in CH_2Cl_2.

Given the delicate balance implied by these models, the spectral features of porphyrins, especially the Q-bands, are quite sensitive to perturbations of the electronic structure of the chromophore. These changes can arise from altering the symmetries and/ or energies of the porphyrin frontier orbitals. Reduction of the *meso*- or β-positions provides such asymmetry. The spectra of chlorins and bacteriochlorins differ substantially from analogous porphyrins, but due to the retention of the 18-annulene aromatic pathway, they retain the gross spectral features implied by the four-orbital model. Reduction of one or more *meso*-position of the porphyrin chromophore, resulting in the loss of aromaticity and configurational interactions, causes drastic changes in the electronic absorption spectra of the resulting macrocycles.

Asymmetrical substitution about the porphyrin periphery, as described in the previous section, might be expected to provide such electronic changes, especially given the widely divergent aryl moieties that may be incorporated by Lindsey's methodology. Although fine-tuning of the spectral properties of the porphyrin chromophore can be achieved by this method, large changes are not observed, even upon the incorporation of strongly electron donating or withdrawing groups. This lack of spectral modulation is due to the large aryl – porphyrin dihedral angles that result from steric interactions of the *ortho*-aryl and β-pyrrole hydrogens, resulting in little π-overlap between the aromatic systems. In order to provide examples of porphyrins with drastically modified electronic structures for theoretical investigation and practical utility, the preparation of macrocycles with annealed exocyclic ring systems and unusual symmetries is of great interest.

Porphyrin Electrochemistry

The rich electronic absorption spectra of porphyrins are matched by their equally remarkable electrochemical properties. Owing to the considerable electronic delocalization endowed by the large porphyrin π-system, cation and anion radical species are quite stabilized via resonance, allowing for reversible oxidations and reductions at relatively low potentials for most free-base porphyrins and porphyrins coordinating redox-inert metals. Furthermore, the dianionc and dicationic species are often accessible, and these redox processes are also typically reversible. The cyclic voltammogram of H_2(TPP), depicted in Figure 1-15, illustrates the four reversible redox processes. Incorporation of late transition metals into porphyrin macrocycles typically causes the

potentials required for these ligand oxidations to shift to less positive values and makes the potentials required for the reductions more negative.

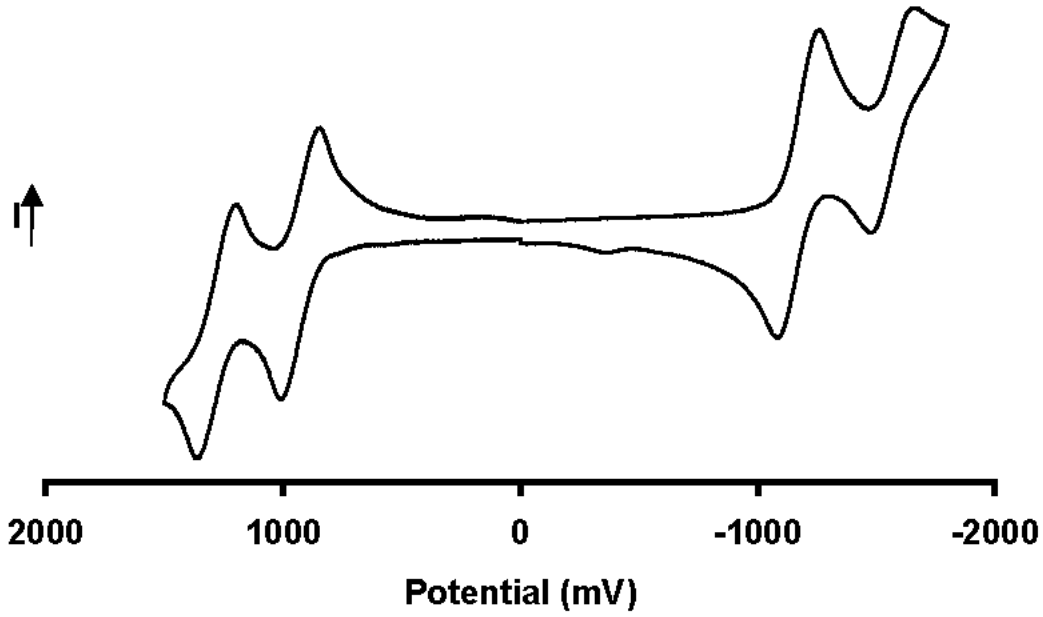

Figure 1-15. Illustration of the cyclic voltammogram for H_2(TPP) measured in CH_2Cl_2 with TBAH as the supporting electrolyte. Pt disc, Pt wire, and Ag/ AgCl were used as the working, counter, and reference electrodes, respectively. Potentials reported vs. the Ag/ AgCl reference electrode.

Oxidized and reduced porphyrin species are employed by biological systems for numerous purposes, including photosynthesis and numerous catalytic processes. For example, the reactive species in the catalytic cycles of peroxidase and cytochromes P450 are best described as oxoferryl porphyrin anion radical cations $\{[O^{-2}=Fe^{IV}(Por^{\cdot -})]^{\cdot +}\}$[42] Another illustration of the importance of redox-active tetrapyrroles in Nature is provided by primary processes in photosynthesis. In addition to other transient radical tetrapyrrolic species involved in energy transfer from antennae pigments to the reaction center, the 'special pair' of bacteriochlorophylls at this reaction center provides the species responsible for all light-dependant life on Earth. Upon excitation, this dimer

forms a charge-separated cation/ anion pair, which acts as both the oxidant *and* reductant for subsequent steps, ultimately resulting in the net electrolysis of water, which provides protons to drive ATP synthase and molecular oxygen.

To provide insight into these and other processes essential to life, the electrochemical behavior of naturally occurring tetrapyrroles has been thoroughly examined. To complement the investigations of biological systems, numerous model compounds have been prepared and electrochemically characterized. In addition to the artificial porphyrins directly relevant to biology, synthetic macrocycles with unusual redox properties are desirable synthetic targets to provide examples to further aid in the understanding of fundamental physical processes. Furthermore, porphyrins with exceptionally low oxidation and/ or reduction potentials may provide useful catalysts, novel electronic materials, or highly efficient artificial photosystems.

CHAPTER 2
SYNTHESES OF DISPIRO-PORPHODIMETHENES AND THEIR METALLATED DERIVATIVES

Introduction

As delineated in Chapter 1, Buchler and Puppe isolated the first air-stable porphodimethene, which was made electrochemically by the reductive methylation of octaethylporphyrinato zinc(II).[8] Over the years this methodology has been extended to metalloporphodimethenes with various alkyl substituents at the sp^3 *meso*-carbons,[9-18,43] but no other report of isomerically pure porphodimethenes in reasonable yields appeared in the literature prior to the beginning of our work in this area. Our group was interested in preparing air-stable, porphodimethenes for use as synthons for porphyrins that would be otherwise synthetically inaccessible.

Michael Harmjanz, a former postdoctoral fellow in our group, devised a route to the first dispiro-porphodimethenes. Inspired by the modified MacDonald [2+2] synthesis of *trans*-A_2B_2 porphyrins presented in Chapter 1 (Figure 1-9)[28] and the observation that acenaphthenequinone undergoes condensation with pyrroles in a manner analogous to aromatic aldehydes (Figure 2-1),[44] Harmjanz and Scott reacted acenaphthenequinone with 5-mesityldipyrromethane using $BF_3{\cdot}OEt_2$ as the acid catalyst (Figure 2-2). Upon oxidation with two equivalents of DDQ and filtration over alumina, the first dispiro-porphodimethenes were isolated as a mixture of *syn*- and *anti*-isomers.[45] These isomers were separated by column chromatography, producing the porphodimethenes as bright-orange solids upon removal of the solvents.

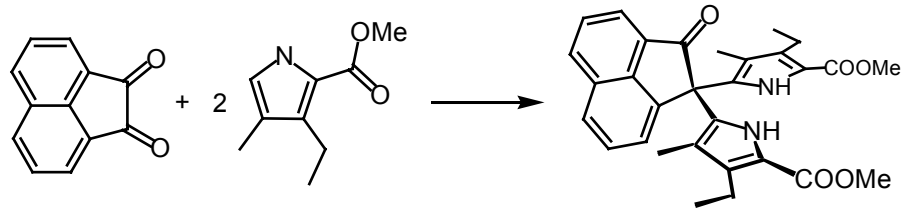

Figure 2-1. Illustration of the aldehyde-like reactivity of acenaphthenequinone in condensation reactions with pyrroles.

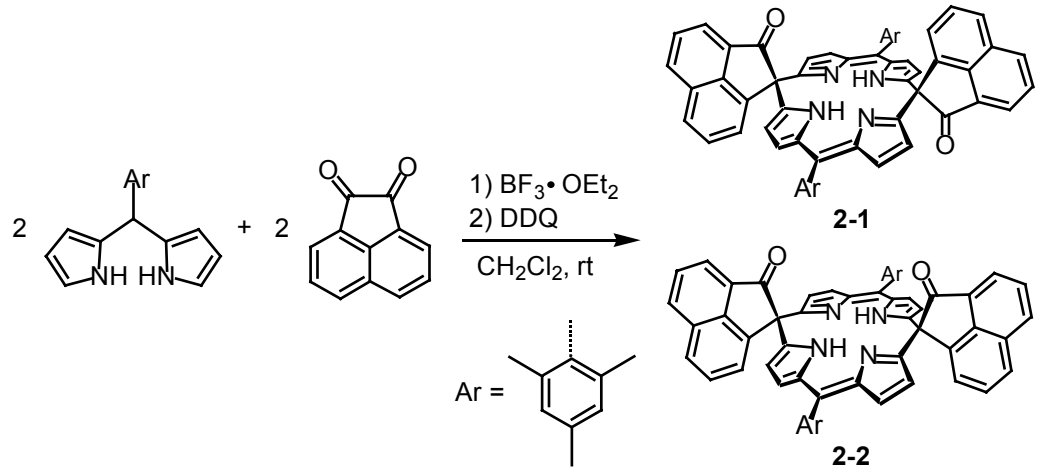

Figure 2-2. Depiction of the first synthetic scheme to provide dispiro-porphodimethenes.

Months prior to the initial communication of this reaction, Floriani and coworkers reported the preparation of stable porphodimethenes via the reductive dealkylation of a tin porphyrinogen, producing a hexaalkyl tin porphodimethene (Figure 2-3).[46] Almost concurrently with our first publication in this area, Sessler and coworkers reported the MacDonald [2+2] condensation of acetone with dipyrromethane to produce tetramethyl porphodimethene, as well as larger expanded congers that were all separable by column chromatography (Figure 2-4).[47] Both of these procedures produce large quantities of porphodimethenes, suitable for the study of the macrocycle class, but as mentioned for Buchler's porphodimethenes, other than metallation and demetallation reactions, these molecules are ill suited for further synthetic elaboration including step-wise oxidations to form functionalized porphyrins.

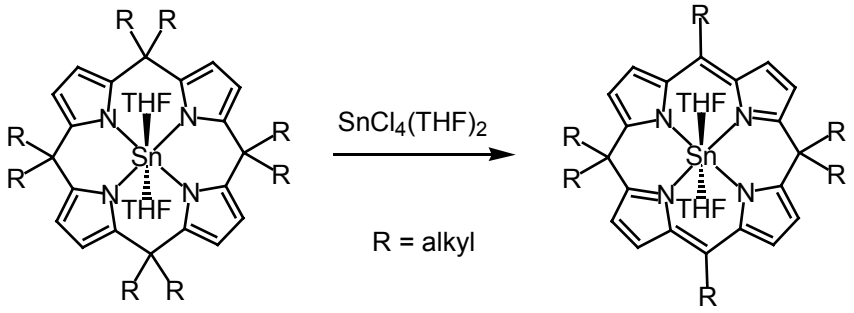

Figure 2-3. Diagram of the reductive dealkylation of a tin porphyrinogen.

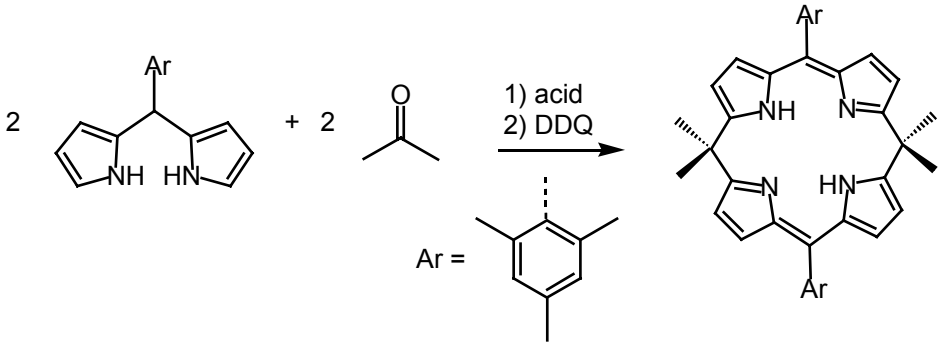

Figure 2-4. Depiction of the [2 + 2] condensation of dipyrromethane with acetone.

Porphyrins are frequently metallated for numerous reasons including the protection of the pyrrolic nitrogens during synthetic modifications, the activation of *meso*- and/ or β-positions to enhance reactivity at these positions, the alteration of physical properties including electrochemical and photophysical behavior,[41] and the application for uses such as catalysis, molecular recognition, or supramolecular construction.[3] By analogy, porphodimethenes and metalloporphodimethenes are expected to exhibit divergent reactivity and physical properties. Few examples of free-base porphodimethenes have been reported,[43,45,47-56] and no focused investigations comparing metalloporphodimethenes with the corresponding unmetallated macrocycles have been undertaken. In addition to providing insight into the effects of metallation on these tetrapyrroles, dispiro-metalloporphodimethenes may be compared to metalloporphyrins and are more suited to contrasting with other porphodimethenes in the literature, as most

of these macrocycles have been characterized as their metal complexes. With these issues in mind, we were interested in incorporating various transition metals into dispiro-porphodimethenes to study these differences in properties and reactivity relative to free-base dispiro-porphodimethenes, other metalloporphodimethenes, and metalloporphyrins.

Results and Discussion

Subsequent to the initial preparation of compounds **2-1** and **2-2**, our efforts were directed in three areas, investigation of the scope of porphodimethene synthesis by this general method, examination of the physical properties of dispiro-porphodimethenes, and study of the reactivity of these unique macrocycles. Investigation of the scope for the condensation of vicinal diketones with dipyrromethanes thus far includes variation of the acid catalyst, the aryl substituent on the dipyrromethene, and the ketone used. Physical methods employed to examine the properties of dispiro-porphodimethenes include UV-visible spectrophotometry, NMR spectroscopy, cyclic voltammetry (Chapter 5), X-ray crystallography,[56,57] and photophysical techniques.[58] The reactivity of the resulting porphodimethenes has been explored in terms of metallation, ring-opening (Chapter 3), and rearrangement reactions (Chapter 5).

Synthesis and Metallation Reactions of Dispiro-Porphodimethenes

Alternate acid catalyst

The type of acid catalyst employed in porphyrin synthesis under Lindsey's modified MacDonald [2+2] conditions is know to effect the yield of porphyrin products.[30,31] In addition to investigating the effect of the acid catalyst on the yield and isomer ratios of dispiro-porphodimethenes, we were interested in finding an alternate acid catalyst, as $BF_3 \cdot OEt_2$ requires air and water-free conditions. Due to the low concentrations required for [2+2] reactions of this type, the scale of the preparation is

somewhat limited by the necessity of solvent distillation and Schlenk conditions, and the use of an acid catalyst without such rigorous constraints would facilitate the production of larger quantities of porphodimethenes.

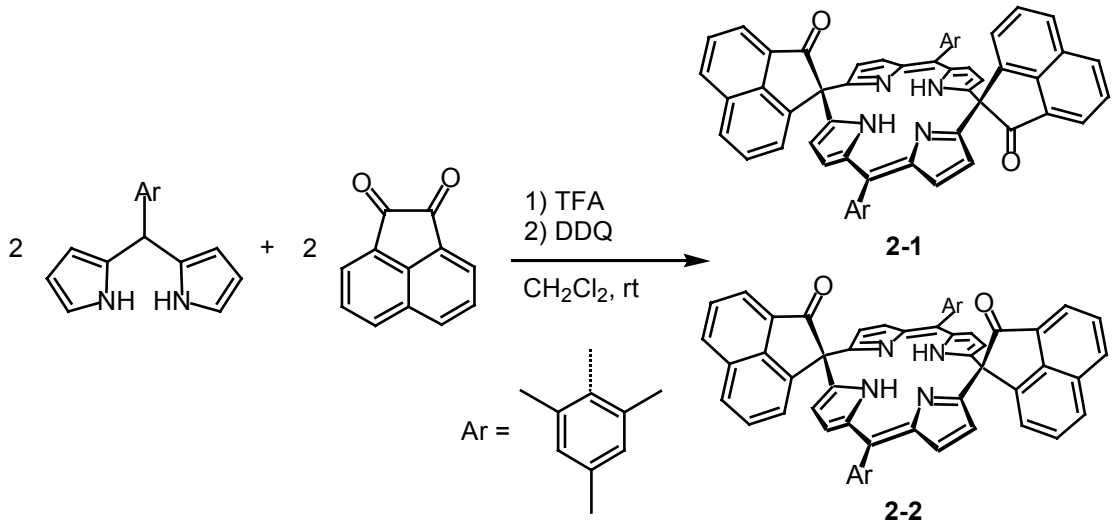

Figure 2-5. Depiction of dispiro-porphodimethene synthesis using an alternative acid catalyst.

Following the general approach developed by Harmjanz, a solution of 5-mesityldipyrromethane and acenaphthenequinone in non-distilled CH_2Cl_2 open to the air was treated with catalytic amounts of TFA, followed by oxidation with DDQ (Figure 2-5). Procedures used to isolate **2-1** and **2-2** were unchanged from those employed by Harmjanz for the $BF_3{\cdot}OEt_2$ reaction. A marginal decrease in combined yield was observed with TFA as the catalyst (24%) in comparison to the reaction with $BF_3{\cdot}OEt_2$ (26%). The isomeric ratio was also found to be somewhat sensitive to acid catalyst, with an isomer yield ratio of 16%: 8% (*anti* to *syn*) observed for TFA and 15%: 11% for $BF_3{\cdot}OEt_2$. While the differences are small, these results do illustrate the utility of TFA as an alternate acid catalyst, and the relative ease associated with this change make the slight decrease in overall yield acceptable. Furthermore, for the purpose of reactivity

studies a single porphodimethene isomer is preferable, and the TFA-catalyzed reaction offers the highest yield for any one isomer (16% for **2-1**) and can provide multi-gram quantities of this compound without requiring solvent distillation or air-free synthetic manipulations.

Variation of aryl functional groups

In order to further examine the scope of the reaction, the aryl substituent on the dipyrromethane precursor was varied. The reaction proved to be quite convenient and versatile. Porphodimethenes with numerous functional groups, imparting different steric and electronic properties, were prepared using this general pathway (Figure 2-6).[56]

In this study, the combined yields of the two porphodimethene isomers (*syn* and *anti*) vary from 7 (**2-15** and **2-16**) to 26% (**2-1** and **2-2**), and as witnessed for the formation of porphyrins by [2 + 2] condensations,[31] the yields are strongly dependent on the electronic and steric nature of the dipyrromethane starting materials (Table 2-1). Although no concerted attempt was made to maximize the yields for the porphodimethenes by varying conditions, the procedures optimized by Lindsey et al for the preparation of A_2B_2 porphyrins by [2 + 2] condensations using either $BF_3{\cdot}OEt_2$ or TFA were used for the reactions.[28]

For the first step in the purification process, the reaction mixtures were filtered through a column of neutral alumina. This allows for the quick isolation of the porphodimethenes as a mixture of *syn*- and *anti*-isomers. These isomers were then separated by column chromatography using silica gel with toluene or a CH_2Cl_2/ hexanes mixture as the eluting solvent.

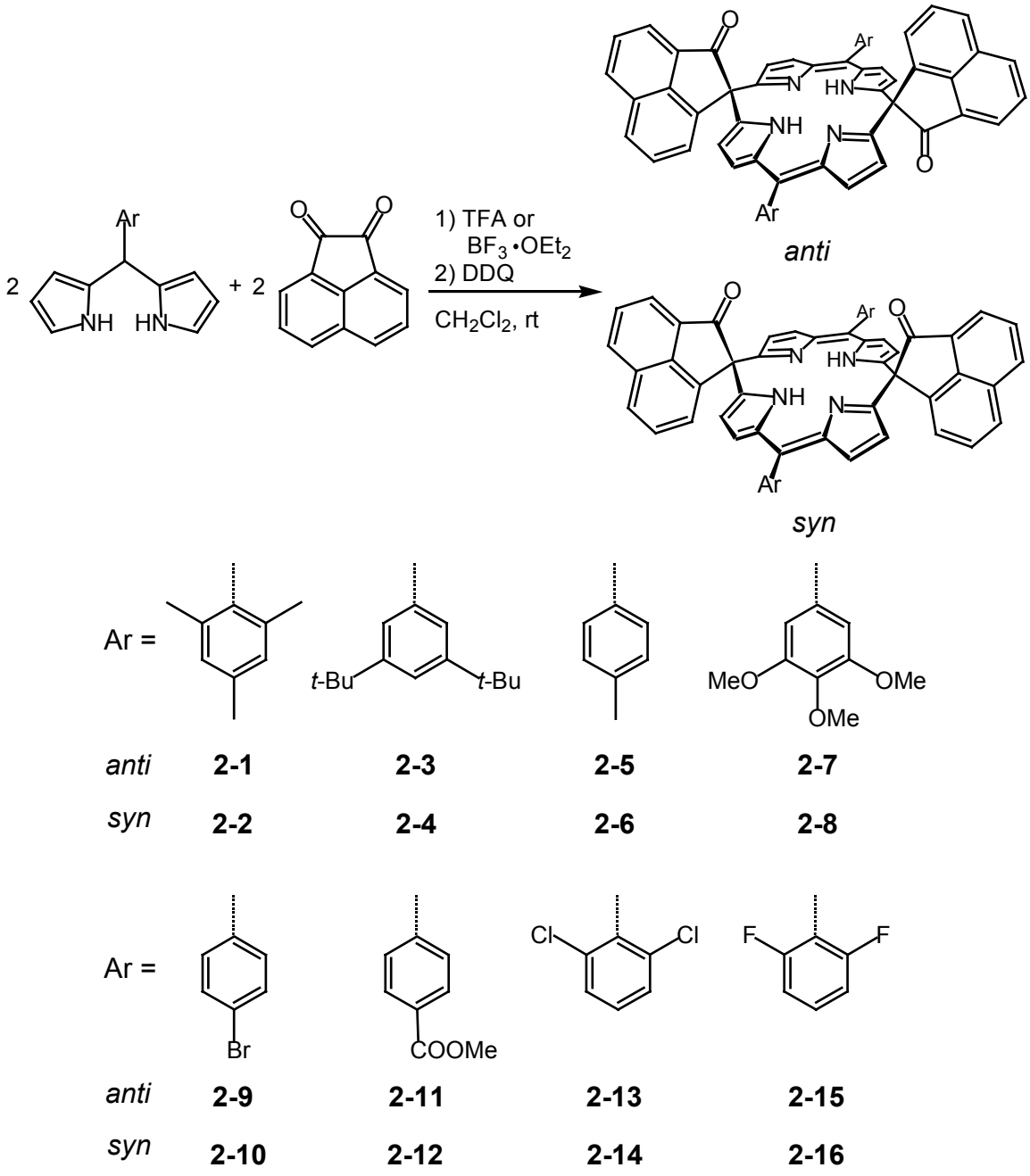

Figure 2-6. Illustration of the range of aryl groups incorporated into dispiro-porphodimethenes.

Variation of vicinal diketone

Another aspect of the scope of dispiro-porphodimethene synthesis that we were interested in examining was the use of vicinal diketones other than acenaphthenequinone

in the condensation reaction. Harmjanz and Ivana Božidarević investigated the reactivity of aceanthrenequinone, phenanthrenequinone, and pyrenequinone with 5-mesityldipyrromethane (Figure 2-7).[55] The reaction proved to be versatile with respect to diverse polycyclic aromatic vicinal diketones, producing porphodimethenes with various polycyclic aromatic ketones at the sp^3 *meso*-carbons. This study illustrates the considerable variability for isomer distribution depending on the choice of diketone employed, with the *anti*-isomer being the only product isolated from the phenanthrenequinone reaction.

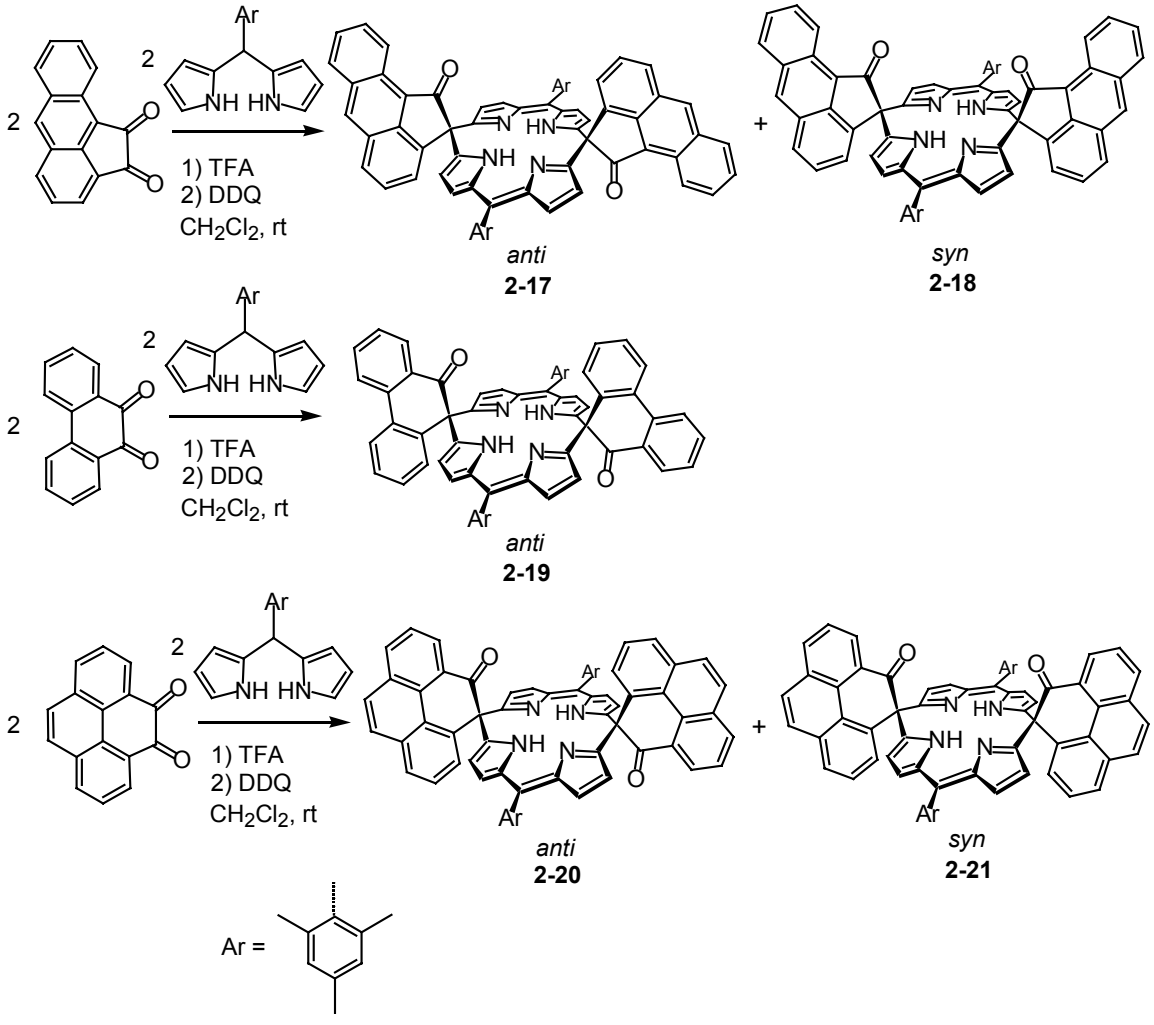

Figure 2-7. Depiction of the scope of the condensation reaction with respect to variation of vicinal diketone.

Preparation of dispiro-porphodimethenes with peripheral *t*-butyl groups

In the course of the reactivity studies presented in Chapter 5, it became evident that some of the porphyrin products derived from **2-1** needed enhanced solubility, and the 3,5-di-*tert*-butylphenyl derivative (**2-3**) did not improve the solubility of these products appreciably. In order to provide a porphodimethene precursor that would impart improved solubility to these porphyrins, the preparation of an acenaphthenequinone with additional steric bulk about the periphery was undertaken. The introduction of *tert*-butyl groups to the 4-and 7-positions of the acenaphthenequinone seemed like a plausible approach, and Dr. Javier Santamaria initially prepared **2-25** through a four-step reaction sequence (Figure 2-8).[52] Due to the extensive column chromatography employed for this preliminary preparation, the methodology was subsequently modified as described in the experimental section, simplifying the procedure and increasing the practicable scale for the reaction sequence.

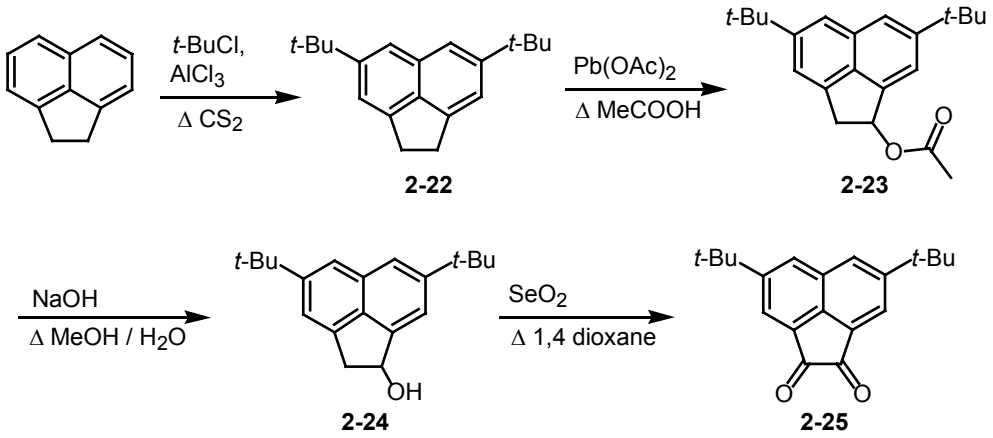

Figure 2-8. Diagram of the preparation of acenaphthenequinone bearing two *t*-butyl groups.

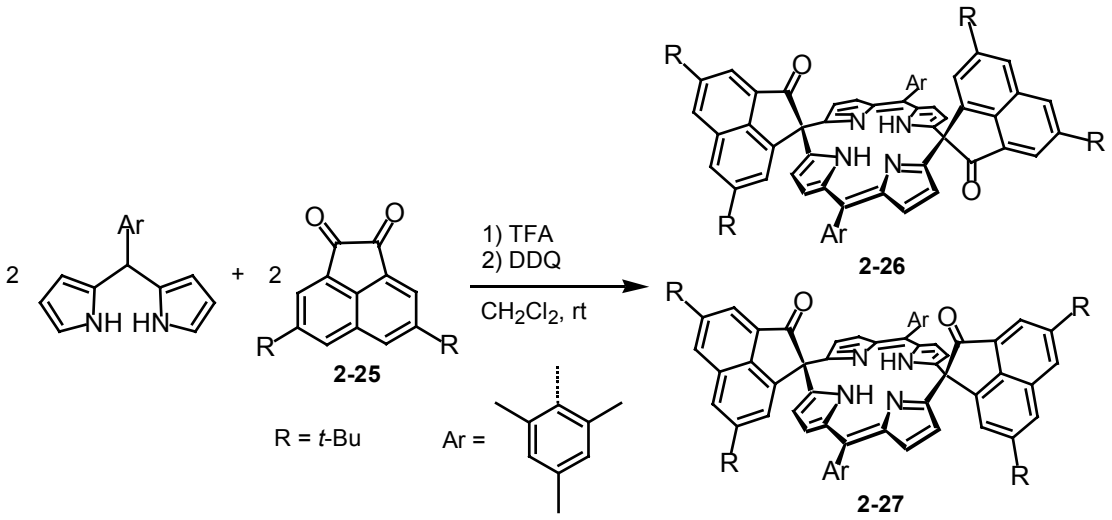

Figure 2-9. Preparation of dispiro-porphodimethenes for use as precursors for porphyrins with enhanced solubility.

Following the methodology presented for **2-1** and **2-2** with TFA as the acid catalyst, the preparation porphodimethenes bearing *tert*-butyl groups on each of the naphthyl moieties proved to be straightforward, producing **2-26** and **2-27** in yields comparable to those observed for **2-1** and **2-2** (Figure 2-9).[52] Fortuitously, **2-26** proved to be only sparingly soluble in CH_2Cl_2, allowing for a simplified isolation procedure compared to other dispiro-porphodimethenes. Following the alumina filtration and solvent removal described for **2-1** and **2-2**, the resulting solid is triturated with CH_2Cl_2, and the insoluble material is collected on a fritted funnel and washed with CH_2Cl_2, providing **2-26** as a bright-orange, analytically pure powder.

Metallation of dispiro-porphodimethenes

Although the dispiro-porphodimethenes contain carbonyl groups as potential peripheral ligands, only minor coordinative interactions between the oxygen donors and metal ions are to be expected due to their distance and orientation relative to the four pyrrolic nitrogens. Consequently, the deprotonated dispiro-porphodimethenes can, in principle, be viewed as dianionic tetradentate macrocycles. With two aliphatic carbon

linkers, porphodimethene macrocycles adopt bent, roof-like structures, and the disruption of the aromaticity within the macrocyclic ring significantly alters the electronic properties relative to fully conjugated porphyrins.[12,13,18,43,59,60] In view of these changes in structural and donor attributes, metal centers ligated by dispiro-porphodimethenes should exhibit divergent physical properties and reactivity in comparison to analogous metalloporphyrins. The ability to metallate the porphodimethenes is thus an important issue in the study of these ligand systems relative to their well-studied porphyrin analogues.

With respect to the utilization of these compounds as precursors for the preparation of porphyrins, the incorporation of metals into the porphodimethenes prior to porphyrin formation may allow for the isolation of metalloporphyrins that might be otherwise inaccessible due to steric and/ or electronic changes upon oxidation to porphyrin products, which may preclude the coordination of metal cations. Furthermore, by analogy to porphyrins, the potentials for the oxidation of metalloporphodimethenes should be lower in comparison to their unmetallated derivatives, and considering that the conversion from porphodimethene to porphyrin is typically an oxidation, the coordination of metal cations may enhance the proclivity of the porphodimethenes for porphyrin forming reactions.

As an initial entry into reactivity studies of these macrocycles, several different transition metal ions were incorporated into the *syn*- and *anti*-porphodimethenes. Owing to the flexibility along the line joining the *trans meso*-carbons of the porphodimethenes, these macrocycles easily accommodate transition metal dications with a wide range of ionic radii. Dispiro-porphodimethenes have been metallated with Co,[53,56] Ni, Cu,[45,52,53,56]

Zn,[45,54,56] Ru, and Pd.[52,58] Reaction of **2-1** with an excess of either $Zn(OAc)_2 \cdot 2H_2O$, $Cu(OAc) \cdot H_2O$, or $NiCl_2 \cdot 6H_2O$ in refluxing $CHCl_3$ /MeOH yields **2-28, 2-29**, or **2-30**, respectively; treatment of **2-26** under the same conditions provides the analogous butylated metalloporphodimethene complexes of Zn (**2-32**), Cu (**2-33**), or Ni (**2-34**), as depicted in Figure 2-10. Due to the difficulties in interpreting the ^{1}H-NMR spectra of **2-30** and **2-34**, the less sterically hindered nickel complex, **2-40**, was prepared under the conditions employed for the synthesis of **2-30** and **2-34**. Reaction of **2-1** or **2-26** with one equivalent of $(C_6H_5CN)_2PdCl_2$ in refluxing THF provides **2-31** or **2-35**. The choice of a reducing solvent and the stoichiometric limitation of Pd(II) were employed to prevent oxidative rearrangement processes described in Chapter 5.

Treatment of **2-3** with $Ru(CO)_5$ afforded the mono-carbonyl complex, **2-39**, in reasonable yield (Figure 2-11). Although no further reactivity studies on **2-39** were undertaken, this compound is the only example of a ruthenium porphodimethene reported thus far. Given the success of ruthenium porphyrins as oxidation catalysts, porphyrin products derived from **2-39** or other ruthenium dispiro-porphodimethenes may provide interesting catalytic compounds.

Although attempts to grow single crystals for structural studies of **2-31** and **2-35** were undertaken, these efforts failed to produce suitable samples. In order to provide a structurally characterized example analogous to these compounds, the more soluble dispiro-porphodimethene, **2-5**, was treated with $(C_6H_5CN)_2PdCl_2$ in refluxing THF, affording **2-40**. Slow diffusion of Et_2O into a saturated $CHCl_3$ solution of **2-40** provided bright-red single crystals, which were suitable for X-ray diffraction.

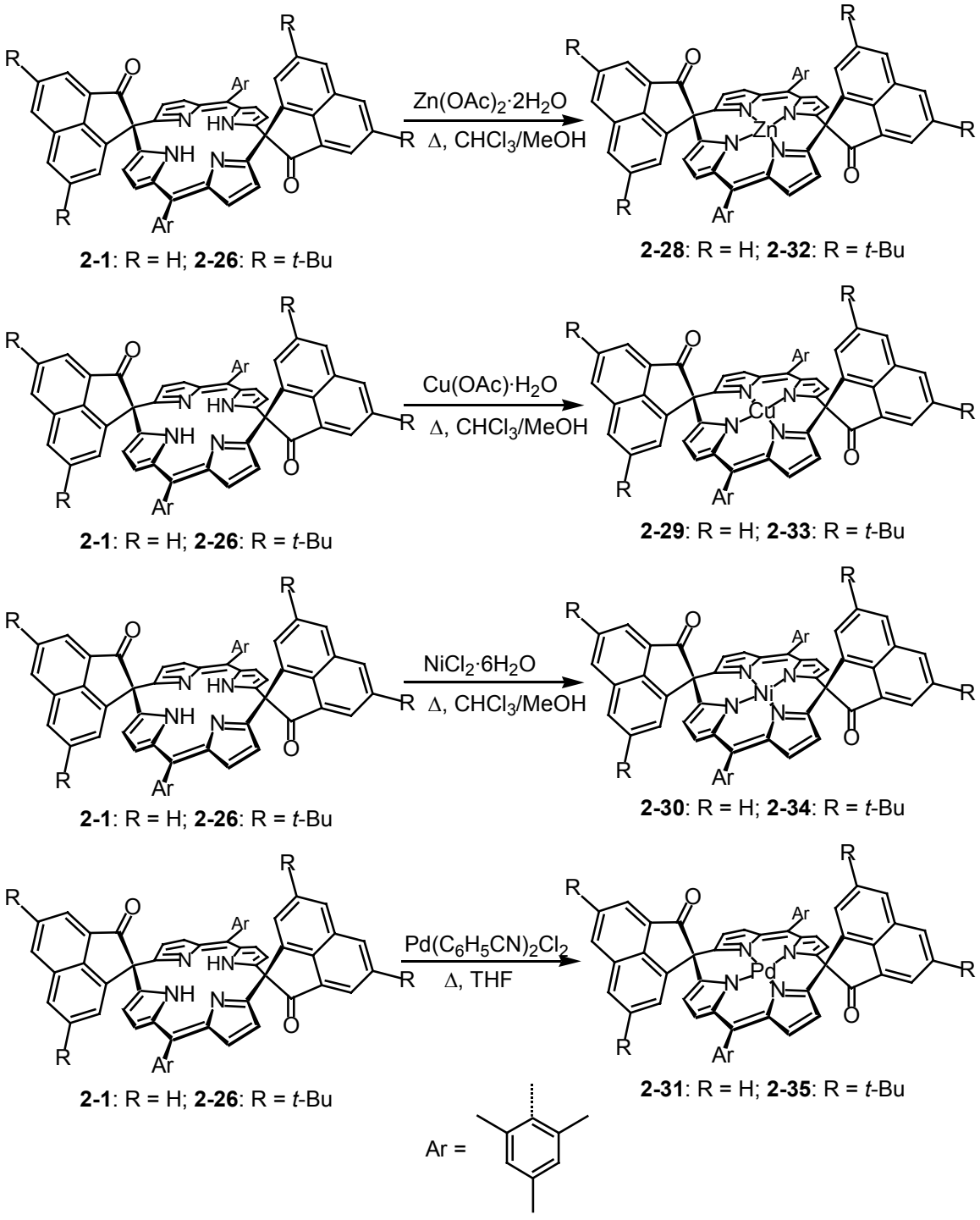

Figure 2-10. Illustration of some metallation reactions of dispiro-porphodimethenes.

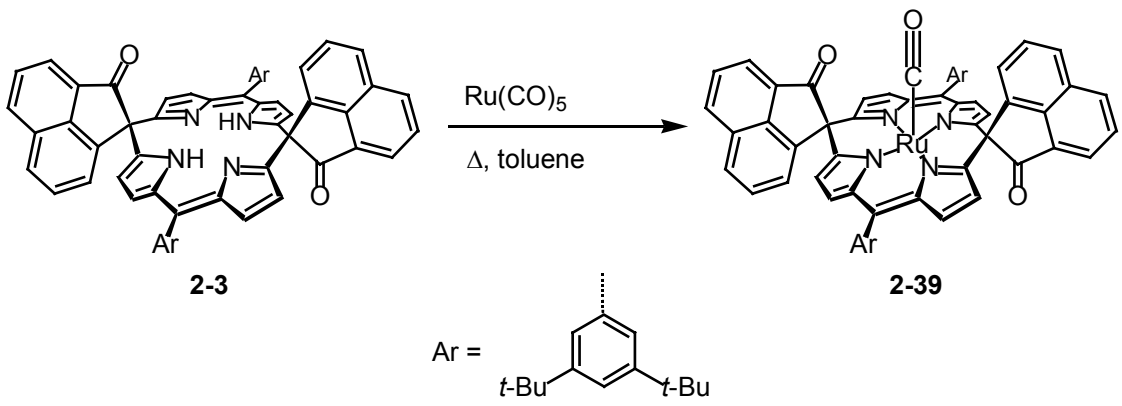

Figure 2-11. Illustration of the synthesis of **2-39**.

Physical Properties of Dispiro-porphodimethenes

Electronic absorption spectra

All free-base dispiro-porphodimethene isomers bearing acenaphthenone substituents are bright orange solids and exhibit characteristic absorption maxima in the visible region [437 nm (**2-26**) - 446 nm (**2-8**)]. The molar absorptivities are higher for the *syn*-isomers, [93,000, (**2-2**, **2-7**, **2-16**, **2-21**, **2-27**) $M^{-1}cm^{-1}$] compared to the corresponding *anti*-derivatives [66,000 (**2-3**, **2-13**) $M^{-1}cm^{-1}$]. Although they have similar extinction coefficients, the main absorption band in the aryl-substituted porphodimethenes appear at lower energies in comparison to *meso*-alkyl porphodimethenes (417–426 nm).[10,47,61-63]

As exemplified by the treatment of **2-26** with $Zn(OAc)_2 \cdot 2H_2O$ in refluxing $CHCl_3$/ MeOH to produce **2-32**, metallation of dispiro-porphodimethenes typically induces a bathochromic shift for the absorption maxima of the porphodimethenes and an increase in their molar absorptivities, allowing for the use of UV-visible spectroscopy to monitor the reaction progress (Figure 2-12). Interestingly, some exceptions to these trends are observed for porphodimethenes with transition metals from the second row. Within experimental error, the absorption maximum of **2-3** does not shift to lower energy upon

metallation with ruthenium, and the extinction coefficient of **2-1** is unchanged after metallation with palladium.

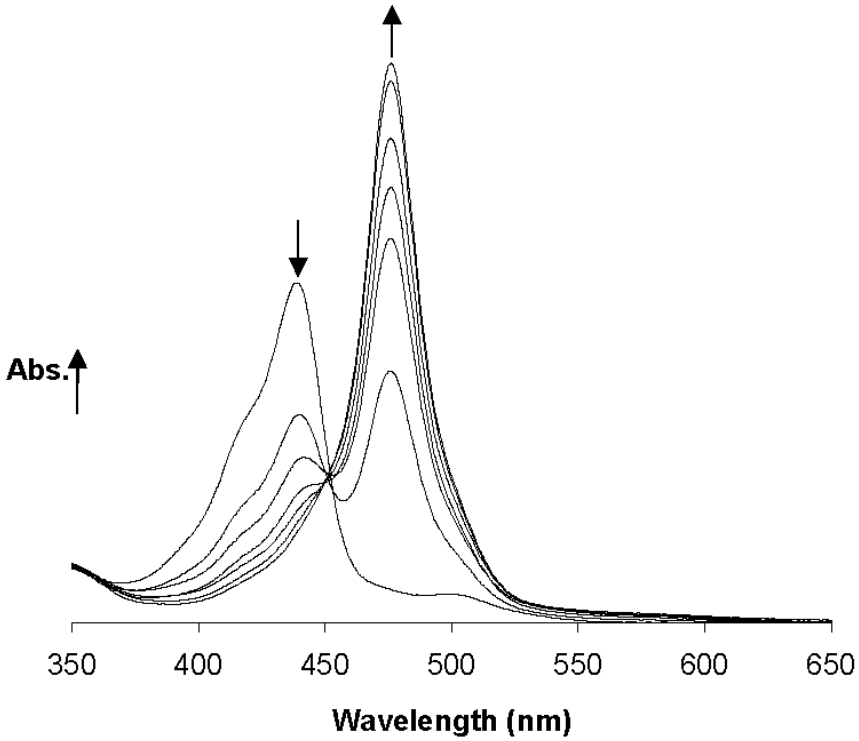

Figure 2-12. Depiction of the time-course UV-visible spectra of **2-26** upon treatment with $Zn(OAc)_2$ in refluxing $CHCl_3$/ MeOH to form **2-32**.

The most extreme example of the bathochromic shift observed upon metallation of dispiro-porphodimethenes is for the palladium derivative, **2-31**, with its strongest electronic transition being 54 nm lower in energy than the free-ligand, **2-1**; this change is in sharp contrast with the blue-shift observed for palladium tetraphenylporphyrin in comparison to the metal-free derivative. Among the dispiro-metalloporphodimethenes studied thus far, the zinc derivatives display the most dramatic increase in molar absorptivities in comparison to their free-base ligands. For example, the extinction coefficient for **2-28** (150,000 $M^{-1}cm^{-1}$) is nearly double that of **2-1** (85,000 $M^{-1}cm^{-1}$). This change is a considerably larger increase than that observed upon metallation of tetraarylporphyrins with zinc.

Table 2-1. Yields and spectrophotometric data for various dispiro-porphodimethenes (*syn* and *anti*) and some metallated derivatives (*anti* only). Refer to Figure 2-13 for structural representations. An asterisk denotes compounds prepared for this work.

Entry	M	Isomer	R	Ar	Reagents	Yield	λ_{max}(log ε)nm	Ref.
2-1	H_2	*anti*	1	Mes	$BF_3{\cdot}OEt_2$/ DDQ	15%	438 (4.93)	**56**
2-2	H_2	*syn*	1	Mes	$BF_3{\cdot}OEt_2$/ DDQ	11%	440 (4.97)	**56**
2-1	H_2	*anti*	1	Mes	TFA/ DDQ	16%	438 (4.93)	*
2-2	H_2	*syn*	1	Mes	TFA/ DDQ	8%	440 (4.97)	*
2-3	H_2	*anti*	1	*m*-(*t*-Bu)$_2$	TFA/ DDQ	12%	440 (4.82)	**56***
2-4	H_2	*syn*	1	*m*-(*t*-Bu)$_2$	TFA/ DDQ	8%	442 (4.92)	**56***
2-5	H_2	*anti*	1	*p*-Me	TFA/ DDQ	12%	440 (4.83)	**56***
2-6	H_2	*syn*	1	*p*-Me	TFA/ DDQ	3%	442 (4.92)	**56***
2-7	H_2	*anti*	1	$(OMe)_3$	$BF_3{\cdot}OEt_2$/ DDQ	15%	443 (4.97)	**56**
2-8	H_2	*syn*	1	$(OMe)_3$	$BF_3{\cdot}OEt_2$/ DDQ	9%	446 (4.90)	**56**
2-9	H_2	*anti*	1	*p*-Br	$BF_3{\cdot}OEt_2$/ DDQ	6%	441 (4.88)	**56**
2-10	H_2	*syn*	1	*p*-Br	$BF_3{\cdot}OEt_2$/ DDQ	8%	442 (4.93)	**56**
2-11	H_2	*anti*	1	COOMe	$BF_3{\cdot}OEt_2$/ DDQ	4%	440 (4.84)	**56**
2-12	H_2	*syn*	1	COOMe	$BF_3{\cdot}OEt_2$/ DDQ	4%	442 (4.95)	**56**
2-13	H_2	*anti*	1	*o*-Cl_2	TFA/ DDQ	12%	440 (4.82)	**56**
2-14	H_2	*syn*	1	*o*-Cl_2	TFA/ DDQ	11%	442 (4.86)	**56**
2-15	H_2	*anti*	1	*o*-F_2	TFA/ DDQ	5%	439 (4.90)	**56**
2-16	H_2	*syn*	1	*o*-F_2	TFA/ DDQ	2%	441 (4.97)	**56**
2-17	H_2	*anti*	2	Mes	TFA/ DDQ	18%	448 (4.94)	**55**
2-18	H_2	*syn*	2	Mes	TFA/ DDQ	4%	452 (4.92)	**55**
2-19	H_2	*anti*	3	Mes	TFA/ DDQ	11%	432 (4.89)	**55**
2-20	H_2	*anti*	4	Mes	TFA/ DDQ	4%	440 (4.94)	**55**
2-21	H_2	*syn*	4	Mes	TFA/ DDQ	1%	442 (4.97)	**55**
2-26	H_2	*anti*	5	Mes	TFA/ DDQ	15%	437 (4.95)	**52***
2-27	H_2	*syn*	5	Mes	TFA/ DDQ	11%	441 (4.97)	**52***
2-28	Zn	*anti*	1	Mes	$Zn(OAc)_2{\cdot}2H_2O$	91%	475 (5.17)	**56**
2-29	Cu	*anti*	1	Mes	$Cu(OAc)_2{\cdot}H_2O$	98%	483 (5.09)	**56**
2-30	Ni	*anti*	1	Mes	$NiCl_2{\cdot}6H_2O$	84%	440 (4.45)	*
2-31	Pd	*anti*	1	Mes	$(C_6H_5CN)_2PdCl_2$	81%	492 (4.93)	**52***
2-32	Zn	*anti*	5	Mes	$Zn(OAc)_2{\cdot}2H_2O$	97%	476 (5.14)	*
2-33	Cu	*anti*	5	Mes	$Cu(OAc)_2{\cdot}H_2O$	98%	482 (5.16)	**52***
2-34	Ni	*anti*	5	Mes	$NiCl_2{\cdot}6H_2O$	78%	442 (4.51)	*
2-35	Pd	*anti*	5	Mes	$(C_6H_5CN)_2PdCl_2$	81%	491 (4.95)	**52***
2-37	Cu	*anti*	1	$(OMe)_3$	$Cu(OAc)_2{\cdot}H_2O$	95%	483 (5.08)	**56**
2-38	Co	*anti*	1	$(OMe)_3$	$Co(OAc)_2{\cdot}4H_2O$	94%	482 (4.51)	**56**
2-39	Ru	*anti*	1	*m*-(*t*-Bu)$_2$	$Ru(CO)_5$	71%	440 (5.02)	*

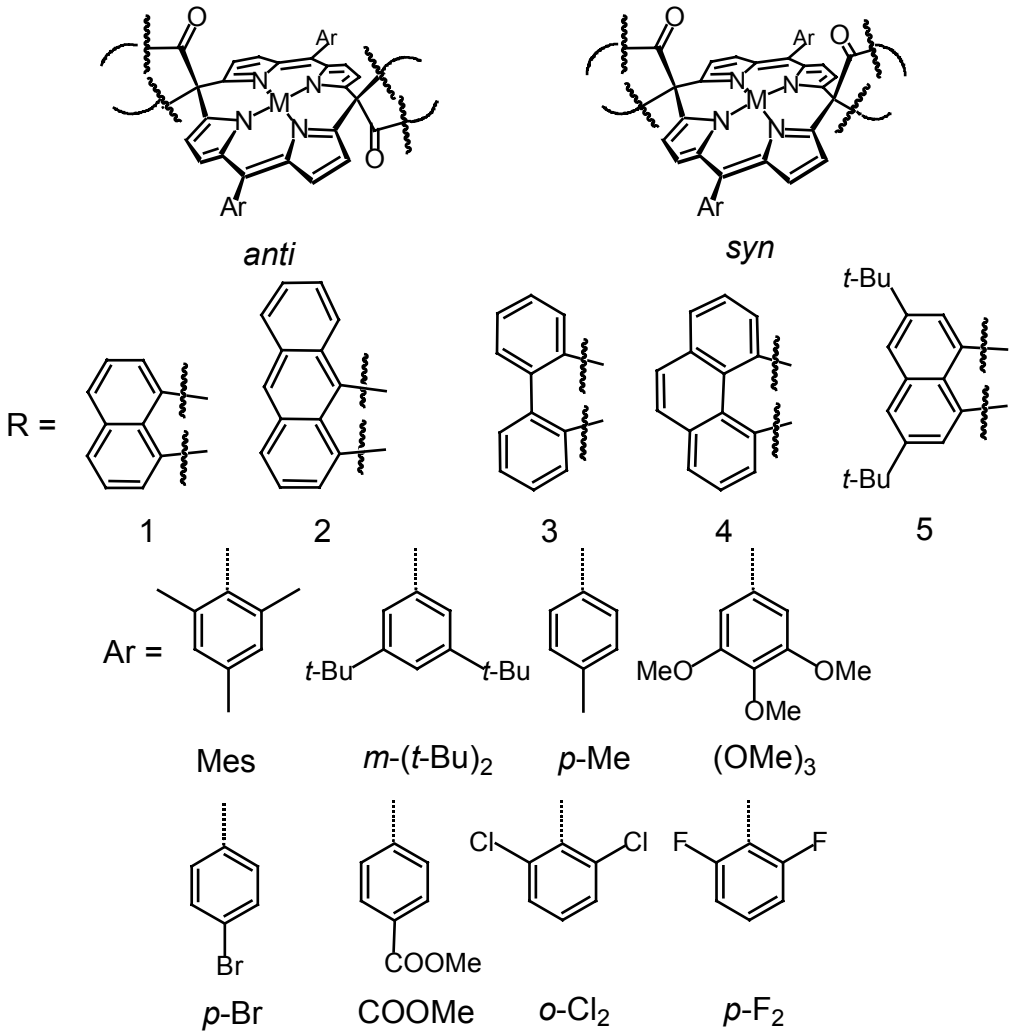

Figure 2-13. Illustration of the porphodimethenes referred to in Table 2-1.

Structural characterization

All of the porphodimethenes exhibit two sets of doublets for the pyrrolic C-H protons, typically between 6.0 and 6.5 ppm, in sharp contrast to the analogous signals for porphyrins normally found above 8 ppm. This behavior may be attributed to the disruption of electron delocalization within the macrocycle, increasing the shielding of the pyrrolic protons. Further highlighting the lack of aromaticity of the porphodimethenes, the resonances for the N-H protons appear far downfield shifted in the

^{1}H NMR spectra, whereas the corresponding resonances for tetraarylporphyrins have negative chemical shifts.

The two porphodimethene isomers can easily be distinguished by ^{1}H NMR spectroscopy, with the *anti*-isomers consistently displaying fewer resonances than their corresponding *syn*-isomers. The spectra of the free-base *anti*-isomers consistently display only one set of signals for the *meso*-aryl substituents, even though the roof-like folded structure with its spiro-locked acenaphthenones would implicate two sets of signals. For instance, the *tert*-butyl and the *ortho*-aromatic protons of the *anti*-3,5-tBu$_2$C$_6$H$_3$ derivative **2-3** each exhibit a single resonance in the ^{1}H NMR spectrum. Moreover, in the aromatic region, the typical two double doublets and four doublets from two indistinguishable acenaphthenone moieties are observed, and the β-pyrrolic protons of the porphodimethene exist as two doublets, rather than the four doublets expected for this molecule if it were static on the NMR time scale. While free rotation about the C_{meso}-C_{aryl} bond could arguably give rise to singlets for the aryl substituents, the presence of a single set of signals for the acenaphthenones and pyrroles insinuate a different mechanism, and on the basis of these observations, it appears that the porphodimethenes undergo a fast flexing of the two dipyrromethene units along a line joining the two saturated *meso*-carbons in solution as illustrated in Figure 2-14. The low temperature ^{1}H NMR spectrum of the *anti*-3,5-tBu$_2$C$_6$H$_3$ derivative, **2-3**, reveals significant broadening of some of the signals for the naphthalene protons as well as the signals from the pyrrolic and aromatic [3,5-tBu$_2$C$_6$H$_3$] protons. Even at –80^o C, no splitting of these broadened peaks could be detected, suggesting a fast equilibrium between these two possible conformers.

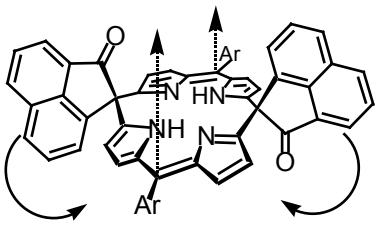

Figure 2-14. Illustration of the fast-flexing behavior observed for dispiro-porphodimethenes.

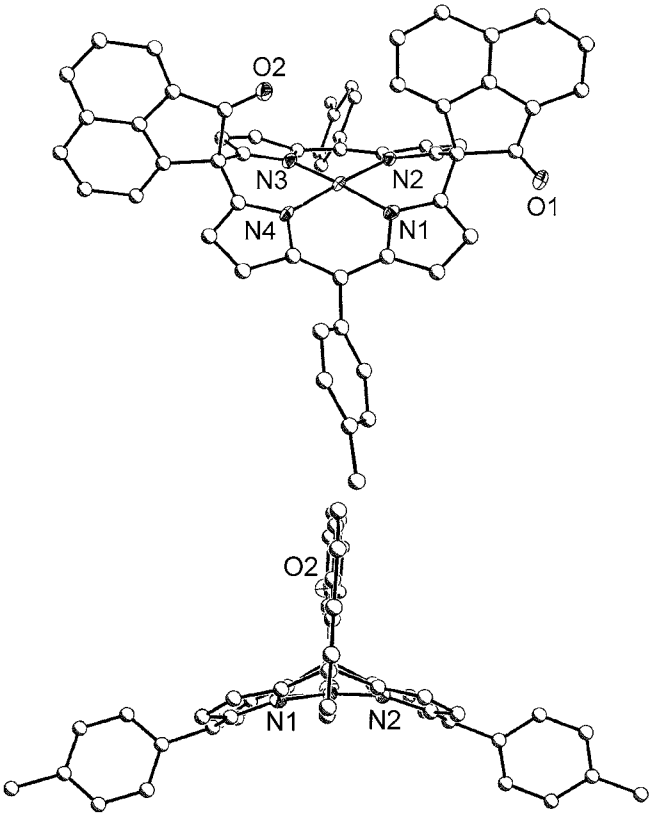

Figure 2-15. Diagram of solid-state structure of **2-40** (40% probability; carbon atoms are depicted with arbitrary radii). Hydrogen atoms are omitted for clarity.

The loss of the N-H protons singlets provides a good diagnostic for metallation reactions with diamagnetic metals. As a general trend, the separation between the two doublets arising from the pyrrolic protons in the ^{1}H NMR spectra of metallo-porphodimethenes increases in comparison to the metal-free porphodimethenes. These

changes might be due to the altered electronic situation within the dipyrromethene halves and/ or the modified structural configuration of the macrocycle upon metallation.

The solid-state structure of **2-40** is depicted in Figure 2-15. The palladium adopts a square-planar coordination geometry with bond angles ranging from 89.0(2)^{o} to 90.8(2)^{o} and bond lengths between 1.991(4) Å and 2.001(4) Å. The macrocycle adopts a roof-like folded structure, with the ridge along the line between the two *meso*-sp^3 carbons. These spiro carbons, especially C15, show significant deviations from ideal tetrahedral geometries, with angles ranging from 101.7(4)^{o} to 115.9(4)^{o}. The inter-planar angle between the two dipyrromethene halves is 135^{o}. The related compound, **2-31**, differs from **2-40** by the presence of methyl groups at the *ortho*-positions of the aryl substituents. The ^{1}H NMR spectrum of **2-31** is consistent with the fast-flexing model described above for the metal-free dispiro-porphodimethene, **2-3**, demonstrating that even the coordination of palladium does not inhibit this process on the NMR time scale at room temperature.

Conclusions

A simple, two-step synthetic approach starting from commercially available acenaphthenequinone and readily available 5-aryldipyrromethanes has been developed for the preparation of novel dispiro-porphodimethenes employing an [2 + 2] acid-catalyzed condensation reaction under Lindsey conditions. The yields for **2-1** and **2-2** using TFA as the acid catalyst were shown to be comparable to those obtained using $BF_3{\cdot}OEt_2$, allowing for a facile increase in scale for the reaction. The scope of the reaction was expanded by varying the 5-aryldipyrromethane precursors, allowing for the preparation of 16 unique dispiro-porphodimethenes with different steric and electronic properties.[56] In a related study, the vicinal diketone was varied, and dispiro-

porphodimethenes with three additional polycyclic aromatic keto- functional groups at the sp^3 *meso*-positions have been prepared.[55] Dispiro-porphodimethenes can be metallated [Zn(II), Cu(II), Ni(II), Pd(II), and Ru(II)] in good yields, and these reactions are easily monitored by UV-visible spectroscopy.

Experimental

General

The University of Florida Mass Spectrometry Services measured all mass spectral data. Atlantic Microlabs, Norcross, GA or Complete Analysis Laboratories, Parsippany, NJ performed elemental analyses. ^{1}H NMR and ^{13}C NMR spectra were recorded on Varian Mercury or VXR spectrometers at 300 MHz in $CDCl_3$ at 25^o C (unless otherwise noted), and the chemical shifts were referenced to the solvent residual peak of chloroform at 7.26 MHz. Electronic absorption spectra were collected in either $CHCl_3$ or CH_2Cl_2 on a Varian Cary 50 spectrophotometer. All reagents were used as received from Aldrich, and all solvents were used as received from Fisher, unless otherwise specified. All 5-aryldipyrromethanes required for the preparation of the porphodimethenes reported have been prepared according to modified literature procedures,[28] and they were purified by the following method: Upon removal of the excess pyrrole, the crude product mixtures were filtered through neutral alumina with either CH_2Cl_2 or a CH_2Cl_2/ hexanes mixture as the eluent. The solvents were removed in vacuo, and the residues were carefully triturated with hexanes, pentane, or cyclohexane and dried. This methodology allows for the convenient isolation of the dipyrromethanes in multi-gram quantities, and these compounds can be further purified by recrystallization.

Chromatography

Absorption column chromatography was preformed using chromatographic silica gel (Fisher, 200 – 425 mesh).

Synthesis of 2-1 and 2-2

A portion of 7.03 g of acenaphthenequinone (38.6 mmol) and 10.20 g (38.6 mmol) of 5-mesityldipyrromethane were dissolved in 2.7 L of CH_2Cl_2, and 5.28 mL (68.5 mmol) of TFA was added. After 35 min, 8.79 g of DDQ (38.7 mmol) was added to the greenish-blue solution, concurrent with a color change to deep red, and the mixture was stirred for an additional hour. The volume was reduced by 80%, and the mixture was loaded onto a plug of alumina (CH_2Cl_2, 15 × 8 cm) and slowly eluted with CH_2Cl_2. The solvent of the orange fraction was removed, and the residue was preadsorbed on silica. The *anti*-isomer was eluted from a flash silica column (20 × 5 cm) with toluene/ hexanes (5:1). The *syn*-isomer was eluted from the column with CH_2Cl_2 as the second orange fraction.

Yield **2-1**: 2.68 g (16%). The ^{1}H NMR and UV-Vis spectrum were in agreement with the published values for **2-1**.[56]

Yield **2-2**: 1.32 g (8%). The ^{1}H NMR and UV-Vis spectrum were in agreement with the published values for **2-2**.[56]

Synthesis of 2-3 and 2-4

A portion of 4.910 g (14.61 mmol) 5-(3,5-di-*tert*-butylphenyl)dipyrromethane and acenaphthenequinone (2.663 g, 14.63 mmol) were dissolved in 1.2 L of CH_2Cl_2 and 2.01 mL (26.7 mmol) of TFA was added. After 55 min, 3.324 g DDQ (11.34 mmol) was added to the greenish-blue solution, concurrent with a color change to deep red, and the mixture was stirred for an additional hour. The volume was reduced by 80 %, and the mixture was loaded onto an alumina column (CH_2Cl_2, 25 x 4 cm) and slowly eluted with

CH_2Cl_2. The solvent of the orange fraction was removed, and the two isomers were separated by silica chromatography (15 x 4 cm; toluene, followed by CH_2Cl_2). The *anti*-isomer, **2-3**, was collected by rapid elution with toluene. The *syn*-isomer, **2-4**, was collected as the second fraction from the silica column by elution with CH_2Cl_2.

Yield (**2-3**): 0.892 g, (12%). UV/ Vis [$CHCl_3$, λ_{max}(log ε)] 440(4.8) nm. ^{1}H NMR (300 MHz, $CDCl_3$): 14.03 (s, 2H), 8.87 (d, 2H, J = 5.8 Hz), 8.20 (d, 2H, J = 7.9 Hz), 8.15 (d, 2H, J = 6.8 Hz), 8.00 (m, 4H), 7.80 (dd, 2H, J_1 = 7.2 Hz, J_2 = 8.0 Hz), 7.41(t, 2H, J = 1.8 Hz), 7.24 (d, 4H, J = 1.9 Hz), 6.43 (d, 4H, J = 4.3 Hz), 6.22 (d, 4H, J = 4.3 Hz), 1.26 (s, 36H). HRMS (FAB) calculated for $[M+H]^+$ ($C_{70}H_{65}N_4O_2$): 993.5108. Found 993.5054.

Yield (**2-4**): 0.612 g (8%). UV/ Vis [$CHCl_3$, λ_{max}(log ε)] 442(4.92) nm. ^{1}H NMR (300 MHz, $CDCl_3$): 14.02 (s, 2H), 8.17 (d, 2H, J = 7.9 Hz), 8.12 (d, 2H, J = 6.6 Hz), 8.01 (d, 2H, J = 8.3 Hz), 7.99 (d, 2H, J = 7.1 Hz), 7.84 (dd, 2H, J_1 = 7.1, J_2 = 8.3 Hz) 7.78 (dd, 2H, J_1 = 7.1, J_2 = 8.1 Hz), 7.40 (t, 2H, J = 1.8 Hz), 7.30 (t, 2H, J = 1.5 Hz), 7.16 (t, 2H, J = 1.6 Hz), 6.37 (d, 4H, J = 4.3 Hz), 6.02 (d, 4H, J = 4.3 Hz), 1.31 (s, 18H), 1.22 (s, 18H). HRMS (FAB) calculated for $[M+H]^+$ ($C_{70}H_{65}N_4O_2$): 993.5108. Found 993.5101.

Synthesis of 2-5 and 2-6

A portion of 5-(*p*-toluoyl) dipyrromethane (2.000 g, 8.400 mmol) was reacted with acenaphthenequinone (1.520 g, 8.352 mmol) as described for **2-3** and **2-4**. Purification of the two isomers: 1. neutral alumina (CH_2Cl_2); 2. silica (toluene). The *anti*-isomer, **2-5**, was collected as the first orange fraction, and the *syn*-isomer, **2-6**, was collected as the second orange fraction from the silica column.

Yield (**2-5**): 0.392 g (12%). UV/ Vis [$CHCl_3$, λ_{max}(log ε)] 440 (4.83) nm. ^{1}H NMR (300 MHz, $CDCl_3$): 13.94 (s, 2H), 8.82 (d, 2H, J = 6.5 Hz), 8.19 (d, 2H, J = 8.1 Hz), 8.13 (d, 2H, J = 6.8 Hz), 7.99, (m, 4H), 7.79 (dd, 2H, J_1 = 7.0, J_2 = 8.1 Hz), 7.27 (d, 4H, J = 8.1 Hz), 7.14 (d, 4H, J = 8.1 Hz), 6.40 (d, 4H, J = 4.3 Hz), 6.19 (d, 4H, J = 4.3 Hz), 2.37 (s, 6H). HRMS (FAB) calculated for $[M+H]^+$ ($C_{56}H_{37}N_4O_2$): 797.2917. Found 797.2926.

Yield (**2-6**): 0.199 g (5%). UV/ Vis [$CHCl_3$, λ_{max}(log ε)]: 442 (4.92) nm. ^{1}H NMR (300 MHz, $CDCl_3$): 13.94 (s, 2H), 8.18 (d, 2H, J = 7.7 Hz), 8.11 (d, 2H, J = 6.6 Hz), 8.03 (d, 2H, J = 8.1 Hz), 7.96, (d, 2H, 6.4 Hz), 7.84 (dd, 2H, J_1 = 7.0, J_2 = 8.3 Hz), 7.78 (dd, 2H, J_1 = 7.2, J_2 = 8.0 Hz), 6.33 (d, 4H, J = 4.2 Hz), 5.98 (d, 4H, J = 4.3 Hz), 2.36 (s, 6H). HRMS (FAB) calculated for $[M+H]^+$ ($C_{56}H_{37}N_4O_2$): 797.2917. Found: 797.2887.

Synthesis of 2-17

Following procedures modified from the literature,[64] 17.33 g (0.130 mol) of anhydrous $AlCl_3$ was added in 2-3 g portions to a mixture of acenaphthene (100.0 g, 0.65 mol) and *t*-butyl chloride (120.4 g, 1.30 mol) in 1 L of CS_2, over the course of 1 hour. This mixture was heated at a gentle reflux for 4 hours, the solvent removed via distillation, the residue dissolved in CH_2Cl_2 (200 mL), and the $AlCl_3$ quenched by pouring the mixture over 125 g of ice. Upon the cessation of effervescence, this suspension was filtered over a 10 x 10 cm pad of silica and eluted with CH_2Cl_2 until TLC indicated no product in the eluent. The solvent was removed from this yellow solution, and the title compound was crystallized from CH_2Cl_2/ EtOH, producing thin, colorless needles of **2-17**.

Yield (**2-17**): 100.01g (58 %). ^{1}H NMR (300 MHz, $CDCl_3$): δ = 7.53 (s, 2H), 7.34 (s, 2H), 3.38 (s, 4H), 1.42 (s, 18H). ^{13}C-NMR (75 MHz, $CDCl_3$): δ = 151.52, 145.30, 136.50, 130.93, 117.68, 117.63, 35.57, 31.91, 30.78.

Synthesis of 2-18

As previously described for the analogous treatment of non-butylated acenaphthene,[65] 12.83 g (48.16 mmol) of **2-17** was added to 1 L of glacial acetic acid, and the solution was heated to 78°C. Over the course of 1h, Pb_3O_4 was added in 2-3 g portions, with subsequent additions following the discharge of the red color, until this color persisted [38.21 g (55.73 mmol) of red-lead oxide was required to reach this endpoint]. The reaction mixture was held at 75-80°C for an additional 30 min, cooled to room temperature, diluted with 1 L of water, and extracted with Et_2O (2 x). The organic portions were combined, washed with water (3 x), and dried over Na_2SO_4. This solution was filtered, and the solvents were removed to produce **2-18** as a yellow oil with a sweet odor.

Crude yield (**2-18**): 12.5 g.

An analytical sample was prepared by column chromatography (silica; hexanes/ EtOAc, 10:1).

Yield (**2-18**): 76 %. ^{1}H-NMR [major rotamer] (300 MHz, $CDCl_3$): δ = 7.72 (d, 1H, J = 1.2 Hz), 7.59 (s, 1H), 7.58 (s, 1H), 6.61 (dd, 1H, J_1 = 7.2, J_2 = 1.9 Hz), 3.83 (dd, 1H, J_1 = 17.8, J_2 = 7.4 Hz), 3.29 (d, 1H, J = 18.6 Hz), 2.11 (s, 3H), 1.42 (s, 9H), 1.41 (s, 9H). ^{13}C-NMR (75 MHz, $CDCl_3$): δ = 171.50, 151.98, 151.93, 141.41, 140.50, 135.20, 130.70, 121.01, 120.07, 118.32, 118.28, 76.50, 39.42, 35.76, 35.71, 31.95, 31.87, 21.59.

Synthesis of 2-19

From the above reaction, 12.5 g of crude **2-18** was dissolved in 250 mL of MeOH, and 400 mL of water containing 5.00 g of NaOH was added to this methanolic solution. This reaction mixture was refluxed for 6 h, cooled to room temperature, extracted with CH_2Cl_2, dried over Na_2SO_4, and the solvents were removed to provide **2-19** as a tan, amorphous solid.

Crude yield (**2-19**): 10.4 g.

Although this crude product was found to be suitable for the subsequent reaction, an analytical sample was prepared by column chromatography (silica; hexanes/ EtOAc, 5:1).

Yield (**2-19**): 75%. ^{1}H-NMR (300 MHz, $CDCl_3$): δ = 7.70 (d, 1H, J = 1.2 Hz), 7.62 (t, 1H, J = 1.2 Hz), 7.60 (d, 1H, J = 1.2 Hz), 7.37 (q, 1H, J = 1.2 Hz), 5.72 (d, 1H, J = 6.4 Hz), 3.80 (ddt, 1H, J_1 = 17.6 Hz, J_2 = 7.1 Hz, J_3 = 1.1 Hz), 3.23 (dp, 1H, J_1 = 17.6 Hz, J_2 = 1.1 Hz), 1.97 (bs, 1H), 1.43 (s, 9H), 1.42 (s, 9H). ^{13}C-NMR (75 MHz, $CDCl_3$): δ = 152.05, 151.95, 145.13, 140.83, 134.43, 130.70, 120.54, 118.61, 118.36, 118.09, 75.16, 42.55, 35.73, 35.67, 31.93, 31.83. Analysis calculated for $C_{20}H_{26}O$: C, 85.06; H, 9.28. Found: C, 84.97; H, 9.26.

Synthesis of 2-20

A portion of impure **2-19** from the above reaction (10.4 g) was treated with 55.04 g of SeO_2 in 500 mL of refluxing dioxane for 12 h. The solvent was removed by distillation, and the residue was taken up in 400 mL CH_2Cl_2. This slurry was filtered over a silica plug (10 x 5 cm) and eluted with CH_2Cl_2 until the eluent ran clear. The

solvent was removed from this orange solution, and the title compound was crystallized from hexanes, affording **2-20** as silky, yellow needles

Yield (**2-20**): 6.14 g (43 % overall from **2-17**). ^{1}H-NMR (300 MHz, $CDCl_3$): δ = 8.22 (d, 2H, J = 1.4 Hz), 8.18 (d, 2H, J = 1.4 Hz), 1.48 (s, 18H). ^{13}C-NMR (75 MHz, $CDCl_3$): δ189.16, 152.65, 143.77, 131.20, 128.31, 128.15, 120.31, 36.18, 31.69. Analysis calculated for $C_{20}H_{22}O_2$: C, 81.60; H, 7.53. Found: C, 81.53; H, 7.59.

Yield (**2-20**) from 3.5 g of pure **2-19**: 70%.

Synthesis of 2-26 and 2-27

Following the procedures described for **2-1** and **2-2**, 2.35 g (8 mmol) of **2-20** and 2.10 g (8 mmol) of 5-mesityldipyrromethane were dissolved in 1.5 L of CH_2Cl_2, and 1.1 mL (1.7 equivalents) of TFA was added. After 1 h, 1.82 g (8 mmol) of DDQ was added to the greenish-blue solution. The color of the solution rapidly turned a deep-red, and the mixture was stirred for an additional hour. The volume was reduced by 80%, and the mixture was loaded onto a neutral alumina column and slowly eluted with CH_2Cl_2. The orange fraction was collected, and the solvents were removed. The residue was placed in a fritted funnel and washed with CH_2Cl_2. The solid was dried under vacuum, providing 600 mg of the *anti*-isomer, **2-26**, in analytical purity. The filtrate, containing the *syn*-isomer and the soluble portion of the *anti*-isomer, was then preadsorbed on silica, and the isomers were separated by column chromatography (silica, 5 x 10 cm; toluene) to obtain an additional 45 mg of **2-26**. Elution with CH_2Cl_2 provided the *syn*-isomer, **2-27**, which was crystallized from CH_2Cl_2/ hexanes.

Yield **2-26**: 15% (645 mg). UV/ Vis [CH_2Cl_2, λ_{max}(log ε)]: 437(4.9) nm. ^{1}H NMR (300 MHz, $CDCl_3$): δ = 13.71 (s, 2H), 8.46 (d, 2H, *J* = 1.3 Hz), 8.16 (m, 4H), 7.85 (d,

2H, J = 1.3 Hz), 6.82 (s, 4H), 6.18 (d, 4H, J = 4.1 Hz), 5.91 (d, 4H, J = 4.1 Hz), 2.28 (s, 6H), 2.04 (s, 12H), 1.58 (s, 18H), 1.49 (s, 18H). Analysis calculated for $C_{76}H_{76}N_4O_2$: C, 84.72; H, 7.11; N, 5.20. Found C, 84.59; H, 7.02; N, 5.17.

Yield **2-27**: 10% (430 mg). UV/ Vis [CH_2Cl_2, λ_{max}(log ε)]: 441(5.0) nm. ^{1}H NMR (300 MHz, $CDCl_3$): δ = 14.09 (s, 2H), 8.23 (d, 2H, J = 1.5 Hz), 8.12 (d, 2H, J = 1.3 Hz), 8.04 (d, 2H, J = 1.3 Hz), 7.91 (d, 2H, J = 1.3 Hz), 6.87 (s, 2H), 6.80 (s, 2H), 6.17 (d, 4H, J = 4.2 Hz), 5.95 (d, 4H, J = 4.2 Hz), 2.86 (s, 6H), 2.22 (s, 6H), 1.94 (s, 6H), 1.51 (s, 18H), 1.45 (s, 18H). Analysis Calculated for $C_{76}H_{76}N_4O_2$: C, 84.72; H, 7.11; N, 5.20. Found C, 84.31; H, 7.00; N, 5.34.

Synthesis of 2-30

A saturated methanolic solution of $NiCl_2 \cdot 6H_2O$ (50 mL) was added to a solution of **2-1** (300 mg, 0.329 mmol) in 500 mL of $CHCl_3$ and brought to reflux. After 20 h, TLC and UV/ visible spectroscopy indicated the consumption of **2-1**. The reaction mixture was washed with water (3x) and dried over Na_2SO_4. Column chromatography (silica, 3 x 10 cm; CH_2Cl_2/ hexanes, 2:1) provided **2-30** as the first colored fraction. Crystallization from CH_2Cl_2/ hexanes afforded **2-30** as a microcrystalline, red-orange solid.

Yield **2-30**: 83% (265 mg). UV/ Vis [CH_2Cl_2, λ_{max}(log ε)]: 440 (4.7) nm. ^{1}H NMR (300 MHz, $CDCl_3$, 25^{o}C): δ = 12.08 (bs, 1H), 8.39 (bs, 1H), 8.16 – 8.28 (m, 4H), 8.02 (d, 2H, J = 8.8 Hz), 6.30 (dd, 2H, $J_1 = J_2$ = 7.3 Hz), 7.72 (bs, 2H), 6.84 (bs, 4H), 6.27 (bs, 4H), 6.03 (bs, 2H), 5.72 (bs, 2H), 2.45 (bs, 6H), 2.29 (s, 6H), 1.71 (bs, 6H). HRMS (EI) calculated for M^+ ($C_{60}H_{42}N_4O_2Ni$): 908.2661. Found: 908.2657.

Synthesis of 2-31

Under an inert atmosphere in a flask protected from light, 400 mg (0.469 mmol) of **2-1** and 198 mg (0.515 mmol) of $(C_6H_5CN)_2PdCl_2$ were dissolved in 200 mL of dry, degassed THF, and the solution was heated to a gentle reflux. After 2 h, UV/ visible spectroscopy indicated that the reaction progress had reached a plateau, and an additional 18 mg (0.047 mmol) of $(C_6H_5CN)_2PdCl_2$ was added based on the relative ratio of **2-1** to **2-31** observed in the electronic absorption spectrum. Reflux was continued for an additional 30 min. The solvent was removed under reduced pressure, and the title compound was purified by column chromatography (silica, 5x15 cm; hexanes/ CH_2Cl_2, 1:1). Slow removal of the solvents from the first colored fraction (red-orange) afforded **2-31** as a dark-red microcrystalline solid which was collected on a frit, washed with pentanes, and dried under vacuum.

Yield: **2-31**: 81% (364 mg). UV/ Vis [CH_2Cl_2, $\lambda_{max}(\log \varepsilon)$]: 492(4.9) nm. ^{1}H NMR (300 MHz, $CDCl_3$): δ = 8.87 (dd, 2H, J_1 = 6.5, J_2 = 1.1 Hz), 8.21 (dd, 2H, J_1 = 7.1, J_2 = 0.7 Hz), 8.14 (dd, 2H, J_1 = 7.1, J_2 = 0.7 Hz), 7.90-7.99 (m, 4H), 7.81 (dd, 2H, $J_1 = J_2$ = 7.1 Hz), 6.83 (s, 4H), 6.35 (d, 4H, J = 4.5 Hz), 5.94 (d, 4H, J = 4.5 Hz), 2.29 (s, 6H), 2.05 (s, 12H), 1.29 (s, 6H). HRMS (ESI-FTICR) calculated for $[M+H]^+$ ($C_{60}H_{43}N_4O_2Pd$): 957.2421. Found: 957.2458.

Synthesis of 2-32

A saturated methanolic solution of $Zn(OAc)_2 \cdot 2H_2O$ (12 mL) was added to a solution of **2-26** (600 mg, 0.557 mmol) in 400 mL of $CHCl_3$ and brought to reflux. After 2.5 h, TLC and UV/ visible spectroscopy indicated the near quantitative conversion of **2-**

26 to **2-32**. The reaction mixture was washed with water (3x) and dried over Na_2SO_4. Removal of the solvent allowed for the isolation of **2-32** as a red-orange solid.

Yield **2-32**: 97% (614 mg). UV/ Vis [CH_2Cl_2, λ_{max}(log ε)]: 474 (5.14) nm. ^1H NMR (300 MHz, $CDCl_3$): δ = 8.41 (d, 2H, *J* = 1.4 Hz), 8.24 (d, 2H, *J* = 1.4 Hz), 8.18 (d, 2H, *J* = 1.4 Hz), 7.85 (d, 2H, *J* = 1.2 Hz), 6.82 (s, 4H), 6.30 (d, 4H, *J* = 4.0 Hz), 6.02 (d, 4H, *J* = 4.3 Hz), 2.29 (s, 6H), 2.05 (s, 12H), 1.58 (s, 18H), 1.50 (s, 18H). Analysis calculated for $C_{76}H_{74}N_4O_2Zn$: C, 80.02; H, 6.54; N, 4.91. HRMS (FAB) calculated for M^+ ($C_{76}H_{74}N_4O_2Zn$): 1138.5103. Found: 1138.5031. Calculated for $[M+H]^+$ ($C_{76}H_{75}N_4O_2Zn$): 1138.5181. Found: 1139.5180.

Synthesis of 2-33

A saturated methanolic solution of $Cu(OAc)_2$ (5mL) was added to a solution of **2-26** (400 mg, 0.370 mmol) in $CHCl_3$/ MeOH (4:1) and brought to reflux. After 1 h, TLC and UV/ Vis spectroscopy indicated the near quantitative conversion of **2-26** to **2-33**. The reaction mixture was diluted with $CHCl_3$ (200 mL), washed with water (3x), dried over Na_2SO_4, and filtered on silica (4x4 cm; $CHCl_3$). Removal of the solvent allowed for the isolation of **2-33** as a red-orange solid.

Yield: **2-33**: 95% (402 mg). UV/ Vis [CH_2Cl_2, λ_{max}(log ε)]: 482(5.2) nm. Analysis calculated for $C_{76}H_{74}N_4O_2Cu$: C, 80.14; H, 6.55; N, 4.92. Found C, 80.14; H, 6.54; N, 4.70.

Synthesis of 2-34

A saturated methanolic solution of $NiCl_2 \cdot 6H_2O$ (20 mL) was added to a solution of **2-26** (240 mg, 0.223 mmol) in 300 mL of $CHCl_3$ /toluene (2:1) and brought to reflux. After 12 h, TLC and UV/ visible spectroscopy indicated the consumption of **2-26**. The

reaction mixture was washed with water (3x) and dried over Na_2SO_4. Column chromatography (silica, 3 x 10 cm; CH_2Cl_2/ hexanes /toluene, 1:1) provided **2-30** as the first colored fraction. Crystallization from CH_2Cl_2/ hexanes afforded **2-30** as a microcrystalline, red-orange solid.

Yield **2-32**: 78% (198 mg). UV/ Vis [CH_2Cl_2, λ_{max}(log ε)]: 442 (4.2) nm. ^{1}H NMR (300 MHz, d_8-toluene, 100^o C): δ = 9.38 (bs, 2H), 8.38 (s, 2H), 8.12 (s, 2H), 7.89 (s, 2H), 6.70 (s, 4H), 6.38 (2d, unresolved, 4H), 6.08 (2d, unresolved, 4H), 2.16 (s, 6H), 2.04 (s, 12H), 1.68 (s, 18H), 1.44 (2s, unresolved, 18H). Analysis calculated for $C_{76}H_{74}N_4O_2Ni$: C, 80.49; H, 6.58; N, 4.94. LRMS (DIOS) calculated for $[M+H]^+$ ($C_{76}H_{75}N_4O_2Ni$): 1133.5. Found: 1133.1.

Synthesis of 2-35

As described for the preparation of **2-31**, 220 mg (0.204 mmol) of **2-26** was treated with 86 mg (0.225 mmol) of $(C_6H_5CN)_2PdCl_2$ in 100 mL of dry, degassed THF under an inert atmosphere. The reaction was monitored via UV/ Vis. After 1.5 h at reflux, an additional portion of 10 mg (0.026 mmol) of $(C_6H_5CN)_2PdCl_2$ was added, and the solution was refluxed for an additional 1 h. The solvent was removed under reduced pressure, and the title compound was purified by column chromatography (silica, 5x12 cm; hexanes/ CH_2Cl_2, 1:1). Removal of the solvents from the first colored fraction (red-orange) afforded **2-35** as a dark-red solid, which was collected on a frit, washed with pentanes, and dried under vacuum.

Yield: **2-35**: 76% (182 mg). UV/ Vis [CH_2Cl_2, λ_{max}(log ε)]: 491(4.9) nm. ^{1}H NMR (300 MHz, $CDCl_3$): δ = 8.63 (d, 2H, *J* = 1.2 Hz), 8.16 (d, 2H, *J* = 1.4 Hz), 8.13 (d, 2H, *J* = 1.2 Hz), 7.84 (d, 2H, *J* = 1.4 Hz), 6.82 (s, 4H), 6.34 (d, 4H, *J* = 4.5 Hz), 5.91 (d, 4H, *J*

= 4.3 Hz), 2.28 (s, 6H), 2.02 (s, 12H), 1.54 (s, 18H), 1.49 (s, 18H). Analysis calculated for $C_{76}H_{74}N_4O_2Pd \cdot CH_2Cl_2$: C, 73.01; H, 6.05; N, 4.42. Found: C, 73.48; H, 5.98; N, 4.51. HRMS (ESI-FTICR) calculated for M^+ ($C_{76}H_{74}N_4O_2Pd$): 1180.4865. Found: 1180.4784.

Synthesis of 2-39

A sample of the porphodimethene **2-3** (100 mg, 0.100 mmol) and $Ru(CO)_5$ (26 mg, 0.110 mmol) were dissolved in 50 mL of toluene. The reaction mixture was heated to reflux, and after 1.5 h an additional portion of $Ru(CO)_5$ (13 mg, 0.055 mmol) was added. The reaction was allowed to proceed for an additional 3.5 h. The solvent was removed, and the brown residue was redissolved in a minimal volume of CH_2Cl_2/ hexanes (1:2). Filtration through a small pad of silica followed by elution with CH_2Cl_2/ hexanes (1:2) yielded a dark brown solution. Recrystallization from CH_2Cl_2/ hexanes provided **2-39** as a dark green-brown solid.

Yield: 80 mg (71%). ^{1}H NMR (300 MHz, $CDCl_3$): 8.25 (d, 1H, J = 8.1 Hz), 8.20 (d, 1H, J = 8.1 Hz), 8.10 (d, 1H, J = 6.9 Hz), 8.01 (m, 2H), 7.94 (d, 1H, J = 8.1 Hz), 7.81 (m, 4H), 7.78 (m, 1H, J_1 = 7.6, J_2 = 15.2 Hz), 7.61 (d, 1H, J = 6.9 Hz), 7.38 (s, 2H), 7.32 (s, 2H), 7.24 (s, 2H), 6.50 (d, 2H, J = 4.4 Hz), 6.44 (d, 2H, J = 4.4 Hz), 5.58 (d, 2H, J = 4.4 Hz), 5.49 (d, 2H, J = 4.4 Hz), 4.78 (bs, 2H), 1.31 (s, 18H), 1.26 (s, 18H). UV/ Vis [CH_2Cl_2, λ_{max} (log ε)]: 440 (5.02). HRMS (FAB) calculated for M^+ ($C_{71}H_{62}N_4O_3Ru$): 1120.3865. Found: 1120.3637. Calculated for M^+ ($C_{70}H_{62}N_4O_2Ru$) (**2-39** with loss of CO): 1092.3910. Found: 1092.3872.

X-ray Crystallography

Unit cell dimensions were obtained (Table 3-1) and intensity data collected by Prof. Michael Scott on a Siemens CCD SMART diffractometer at low temperature, with

monochromatic Mo-Kα X-rays (λ = 0.71073 Å). The data collections nominally covered over a hemisphere of reciprocal space, by a combination of three sets of exposures; each set had a different ϕ angle for the crystal and each exposure covered 0.3° in ω. The crystal to detector distance was 5.0 cm. The data sets were corrected empirically for absorption using SADABS.[66] The structure was solved using the Bruker SHELXTL software package for the PC, by direct method option of SHELXS. The space group was determined from an examination of the systematic absences in the data, and the successful solution and refinement of the structure confirmed these assignments. All hydrogen atoms were assigned idealized locations and were given a thermal parameter equivalent to 1.2 or 1.5 times the thermal parameter of the carbon atom to which it were attached. For the methyl groups, where the location of the hydrogen atoms was uncertain, the AFIX 137 card was used to allow the hydrogen atoms to rotate to the maximum area of residual density, while fixing their geometry.

Table 2-2. Crystallographic data for compound **2-40**.

	2-40·Et_2O·$CHCl_3$
Formula	$C_{61}H_{45}Cl_3PdN_4O_3$
Formula weight	1094.83
Crystal system	Triclinic
Space group	*P*-1
Z	2
Temp, K	193(2)
D_{calc} gcm^{-3}	1.025
a Å	11.673(3)
b Å	14.571(4)
c Å	15.375(4)
α, deg	76.995(4)
β, deg	84.400(4)
γ, deg	76.741(5)
V $Å^3$	2477(1)
μ, mm^{-1}	0.59
Uniq. data coll./obs.	8629/6645
$R_1[I \geq 2\sigma(I)data]$[a]	0.0660
$wR_2[I \geq 2\sigma(I)data]$[b]	0.1788

[a] $R_1 = \Sigma||F_o| - |F_c||/ \Sigma| F_o|$
[b] $wR_2 = \{ \Sigma[w (F_o^2 - F_c^2)^2 / \Sigma[w (F_o^2)^2$

CHAPTER 3
SYNTHESES OF PORPHYRINS BEARING 8-NAPHTHYL FUNCTIONAL GROUPS

Introduction

In most biological systems containing tetrapyrrolic macrocycles, the orientation of the prosthetic groups with respect to substrates, amino acid residues, or each other greatly influences their biological function.[3] One example of the importance of the local environment in a natural porphyrin system is provided by the cytochrome P450 superfamily of enzymes, which play an essential role in both the transformations of xenobiotic substances, such as pharmaceuticals and toxins,[67,68] and the metabolism of endogenous compounds, including steroids[69-71] and fatty acids.[72,73] In cooperation with P450 reductase and various physiological reducing agents, these enzymes activate dioxygen for the oxidation of substrates that are often rather inert. When organic molecules are oxidized in these systems, the protein matrix helps direct the substrate into the active site of the enzyme, often in a specific orientation. The hydrogen-bonding interactions in the area surrounding the active site have a profound effect on the product of the oxidation reaction, often providing for regiochemical and/ or stereochemical control. For example, different forms of cytochrome P450 produce different oxidation products from the same substrate depending on the local environment about the catalytic center.[68]

In view of the influence of the structure about the active site for this and other numerous biological systems of interest, the preparation of *meso*-substituted porphyrins with anthracene, biphenylene or naphthalene spacers has attracted much attention over

the past two decades. These rigid aromatic groups provide a useful spacer to anchor different groups at precise locations and orientations near the porphyrin backbone. This ability offers many exciting opportunities in the area of molecular recognition and catalysis. For instance, the reactivity of the metal catalyst towards substrates can be adjusted by the addition of groups adept at forming hydrogen bonds. These interactions can help hold an incoming substrate in a specific location with respect to the porphyrin catalyst and thus influence the action of the oxidant on the substrate.

Porphyrins bearing rigid aromatic moieties attached to one or more *meso*-position have been used to determine the distance dependence of photoinduced electron-transfer reactions,[74,75] to prepare and examine cofacial diporphyrins,[76-83] and to synthesize bridged porphyrins with well-defined separations.[84-86] Various functional groups have been incorporated onto anthracene or naphthalene substituted porphyrins for the preparation of molecular receptors,[87] for the construction of heteronuclear one-dimensional arrays,[53] and for the design of dinuclear complexes.[44,88]

The incorporation of a symmetrically or asymmetrically functionalized linker into the porphyrin backbone is among the most important steps in these synthetic approaches. In general, multi-step procedures are required, and new synthetic strategies are often needed in order to vary the type of functional group on the aromatic spacer. Thus far, no general concept has been devised to allow for the facile synthesis of porphyrins bearing rigid aromatic spacers with diverse functional groups in one step from a common precursor. The ability to vary the type of functional group on these rigid spacers offers many exciting opportunities for the engineering of porphyrin platforms with divergent recognition motifs and reactivity.

Porphyrins joined at the 1-position of an 8-substituted naphthalene spacer can be regarded as superior precursors for the design of artificial receptors, sophisticated oxidation catalysts or models for biological, porphyrin-based enzymes due to the proximity of the functional groups to the macrocyclic ring. Porphyrins containing a single 8-functionalized naphthalene moiety have been prepared and utilized for diverse purposes, including molecular recognition[89] and the examination of electronic porphyrin-quinone interactions,[90] but prior to the work presented herein, no general concept had been devised to allow for the facile synthesis of porphyrins with diverse functional groups attached to two rigid aromatic spacers. With these issues in mind, we have designed and constructed a series of porphyrins with two functionalized arms located above or above and below the porphyrin plane as depicted in Figure 3-1.

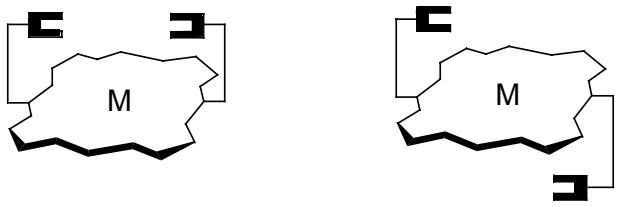

Figure 3-1. Illustration of porphyrins bearing two functionalized arms.

Results and Discussion

In sharp contrast to traditional pathways for the preparation of porphyrins, the dispiro-porphodimethenes presented in Chapter 2 were used as precursors for the preparation of porphyrins bearing two 8-functionalized naphthyl moieties (Figure 3-2). These dispiro-porphodimethenes bearing 5-membered, α-keto-functionalized rings at their spiro-locks are ideal synthons for porphyrin-forming reactions. To generate a porphyrin from these porphodimethenes, the bonds joining the sp^3 *meso*-carbons to the carbonyl carbons must be broken, and oxidation of the tetrapyrrolic ring must occur.

Given the susceptibility of ketones to nucleophilic attack and the considerable driving force for the formation of the large aromatic porphyrin ring system, these requirements may be met under a number of conditions. Nucleophiles as poor as the hydroxide ion are adequate to cause ring opening, and even the use of a large excess of $NaBH_4$ does not prevent oxidation of the ring-opened intermediate to the porphyrin product by dioxygen alone.

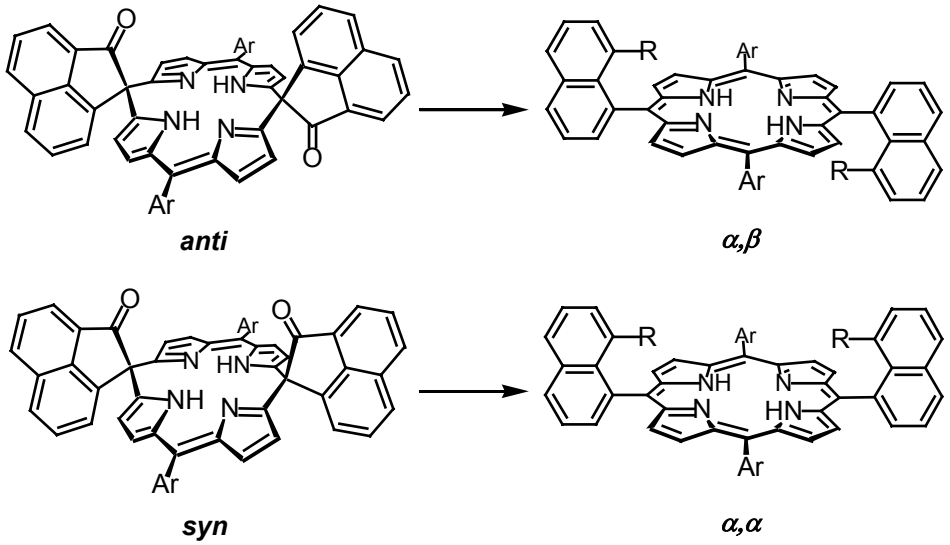

Figure 3-2. Illustration of general ring-opening strategy to provide bis-naphthyl porphyrins.

Functional groups such as alcohols and carboxylic acids are incompatible with the condensation conditions employed for conventional porphyrin syntheses. If they are to be incorporated into porphyrins by traditional methodologies, these groups must be masked and later deprotected, resulting in diminished yields for already meager-yielding reactions. By varying the conditions employed for the ring-opening reaction of dispiro-porphodimethenes, alcohols, esters, carboxylic acids, or carboxylate potassium salts may be directly incorporated at the 8-positions of the naphthalene spacers. Depending on which porphodimethene isomer (*syn* or *anti*) is chosen for the porphyrin forming

reaction, these functional groups may be directed both above (α, α) or above and below (α, β) the porphyrin plane (Figure 3-2). In addition, the steric and electronic attributes of the aromatic substituents at the other *meso*-positions of these porphyrins can be readily adjusted using this simple methodology by varying the aryl groups on the porphodimethene precursor, as delineated in Chapter 2.

Ring-Opening Reactions with KOH and NaOMe

Treatment of the porphodimethenes (*syn* or *anti*) with 30% KOH in refluxing THF will induce the opening of the spiro-rings (Figure 3-3). Presumably, nucleophilic attack of the hydroxide anion at the carbonyl carbon initiates the ring-opening reaction, and the resulting species reacts with dioxygen, rapidly forming the porphyrin macrocycle. Subsequent protonation with $HCl_{(aq)}$ yields the corresponding diacids of the *trans*-8-carboxynaphthyl-functionalized porphyrins; in the absence of acid, the dipotassium salts can be isolated. Despite these rather harsh reaction conditions, no interconversion between α, α- and α, β-atropisomers has been detected. The isolation and purification of the α, β-free acids have been severely hampered by the poor solubility of these compounds in common organic solvents. Fortunately, these materials can be isolated directly by precipitation from the reaction mixture as the dipotassium salts, and they can be further purified by recrystallization from methanol/ ether solutions. In sharp contrast, the α, α-atropisomers are quite soluble as the free-acids. The insolubility of the α, β-acids has been attributed to intermolecular hydrogen bonding interactions between the acid groups, which are aligned above and below the porphyrin plane.[53] On the basis of the rigidly predefined positions of the functional groups, these compounds have the strong tendency to form infinite single-stranded porphyrin arrays.[53]

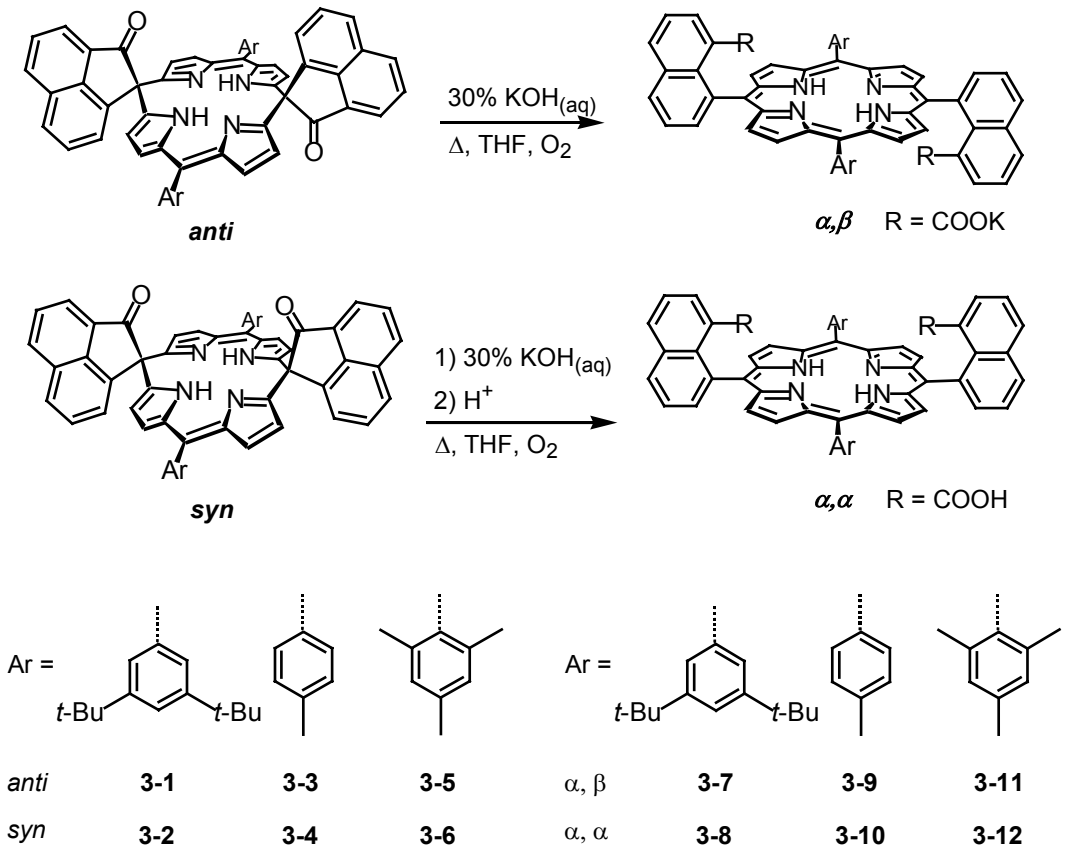

anti	**3-1**	**3-3**	**3-5**	α, β	**3-7**	**3-9**	**3-11**
syn	**3-2**	**3-4**	**3-6**	α, α	**3-8**	**3-10**	**3-12**

Figure 3-3. Depiction of ring-opening with KOH to form porphyrin dicarboxylates.

Some dispiro-metalloporphodimethene derivatives have been treated similarly with KOH to yield the corresponding metalloporphyrin species (Figure 3-4).[56] The overall yields for this ring-opening reaction are highly dependent on the identity of the *meso*-aryl substituent, the isomer (*syn* or *anti*), as well as the absence or presence and nature of the metal ion incorporated into the macrocycle (Table 3-1). Yields between 46% for the zinc derivative **3-13** and 92% for the free-base porphyrin **3-12** have been found. In general, higher yields were obtained for the unmetallated derivatives, since the metallated compounds are more prone to undergo ring closure by oxidative lactonization and formation of *meso*-C/ O bound dispiro-porphodimethenes, as presented in Chapter 4.

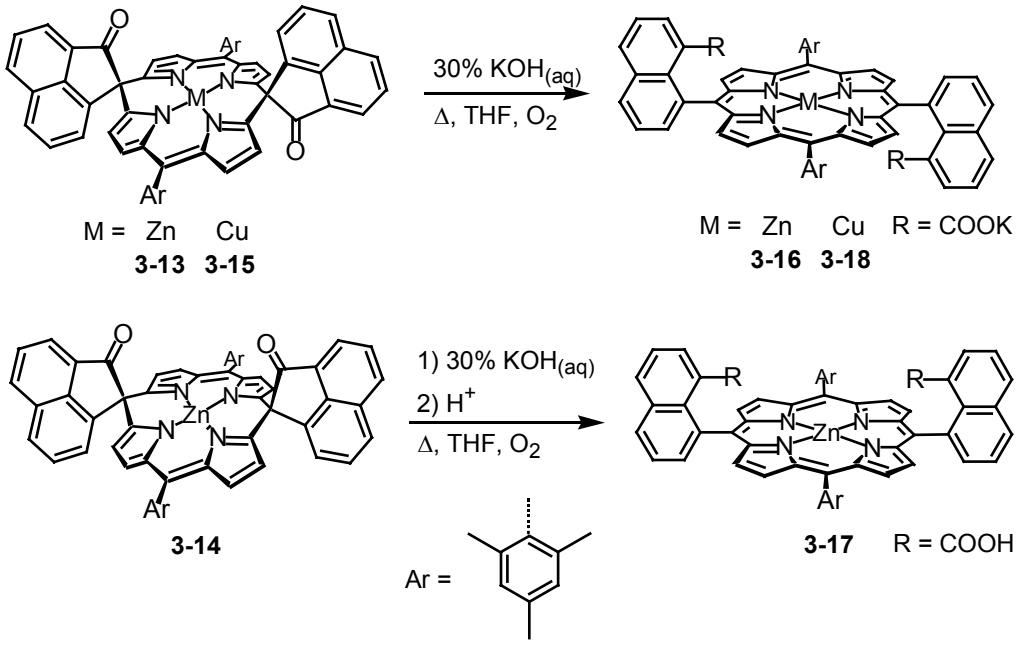

Figure 3-4. Depiction of ring-opening to form metalloporphyrin dicarboxylates.

Inasmuch as the main absorption bands (Soret bands) of the porphyrins appear at higher energy with considerably higher intensity as compared to porphodimethenes, thus the progress of the porphyrin formation reactions can be easily monitored by UV-visible spectroscopy. Figure 3-5 depicts the UV-visible spectra of **3-13** upon reaction with KOH in refluxing THF forming **3-16**. Besides the aforementioned alteration of the main absorption band, the formation of the characteristic Q-bands in the low energy region of the visible spectrum is evident, concomitant with a color change of the reaction mixture from dark orange to dark purple.

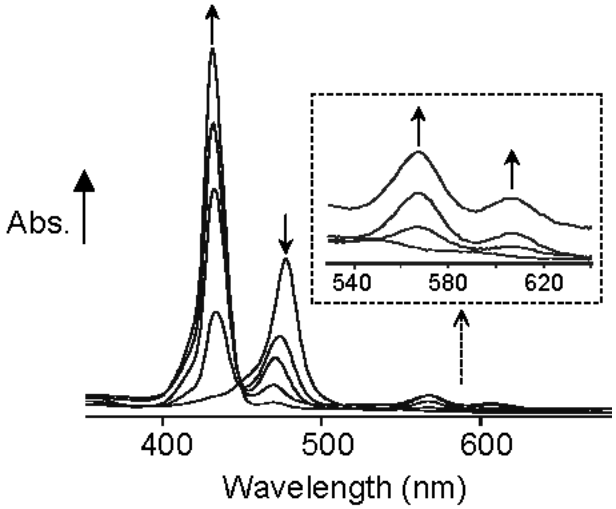

Figure 3-5. UV-visible spectra of **3-13** upon reaction with 30% KOH in refluxing THF, forming **3-16**. The arrows indicate the direction of change in the peaks during porphyrin formation.

Other nucleophiles will react with the porphodimethenes, and the ring-opening can be accomplished with freshly prepared NaOMe in an air- and water-free THF/ methanol mixture to yield the corresponding 8-methoxycarbonylnaphthyl functionalized porphyrins (Figure 3-6). To avoid formation of the favored diacids, water must be rigorously excluded from the reaction mixtures, and in contrast to the hydroxide reactions, the transformation readily occurs at room temperature. To provide an oxidant, dry dioxygen is bubbled through the initially dark green solution, concurrent with a color change to purple. Water or an aqueous NH_4Cl solution is then added to the reaction mixture to quench the unreacted NaOMe. The diesters can be obtained in yields ranging from 60% (**3-19** and **3-21**) to 81% (**3-23**) after column chromatography (silica gel, CH_2Cl_2/ hexane mixtures as eluents) (Table 3-1).

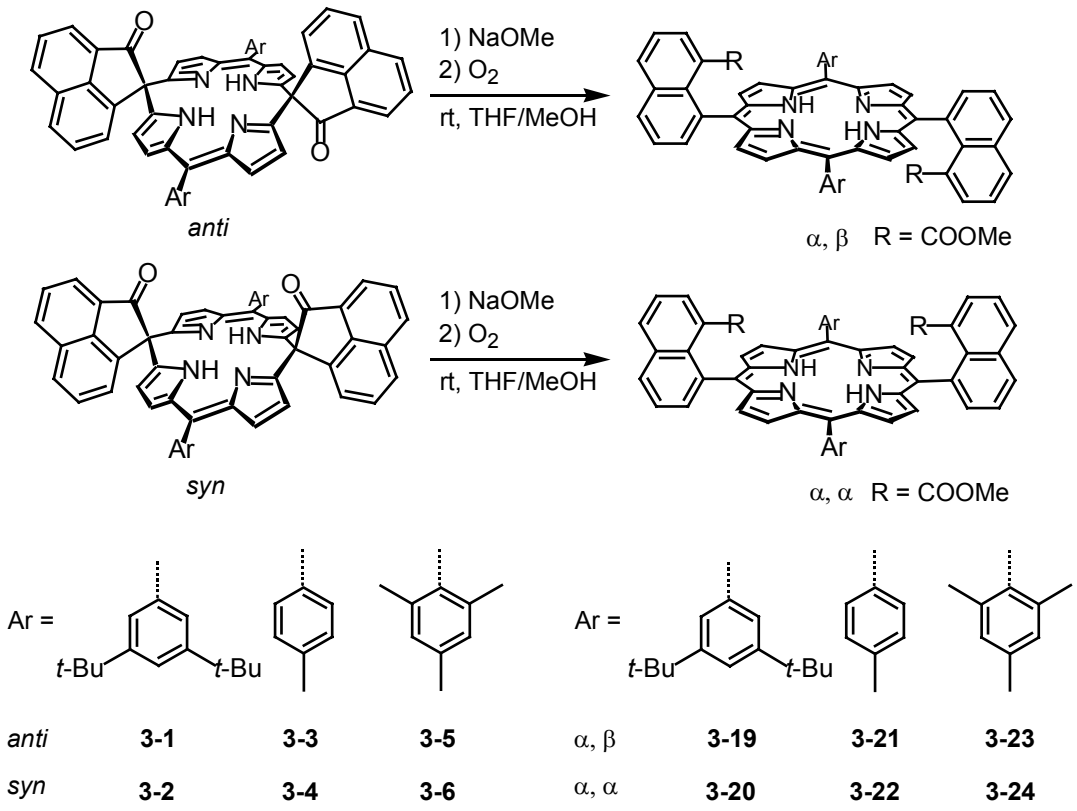

Figure 3-6. Depiction of the formation of porphyrin diesters using NaOMe.

Ring-Opening Reactions with $NaBH_4$

For numerous reasons, including their hydrogen bond donor/ acceptor sites for molecular recognition and the existing methodology and general ease by which benzylic alcohols may be further derivatized, porphyrins bearing hydroxymethyl groups at the 8-position of two naphthalene spacers are desirable building blocks for the preparation of novel organic and inorganic compounds. In view of the sensitivity of the porphodimethenes to strong bases or acids and the considerable driving force toward porphyrin formation, the ring opening of the porphodimethenes seemed plausible with simple reducing agents. Reaction of the porphodimethenes with an excess of $NaBH_4$ in THF/ methanol open to air produces the desired porphyrins in almost quantitative yields (Figure 3-7, Table 3-1).

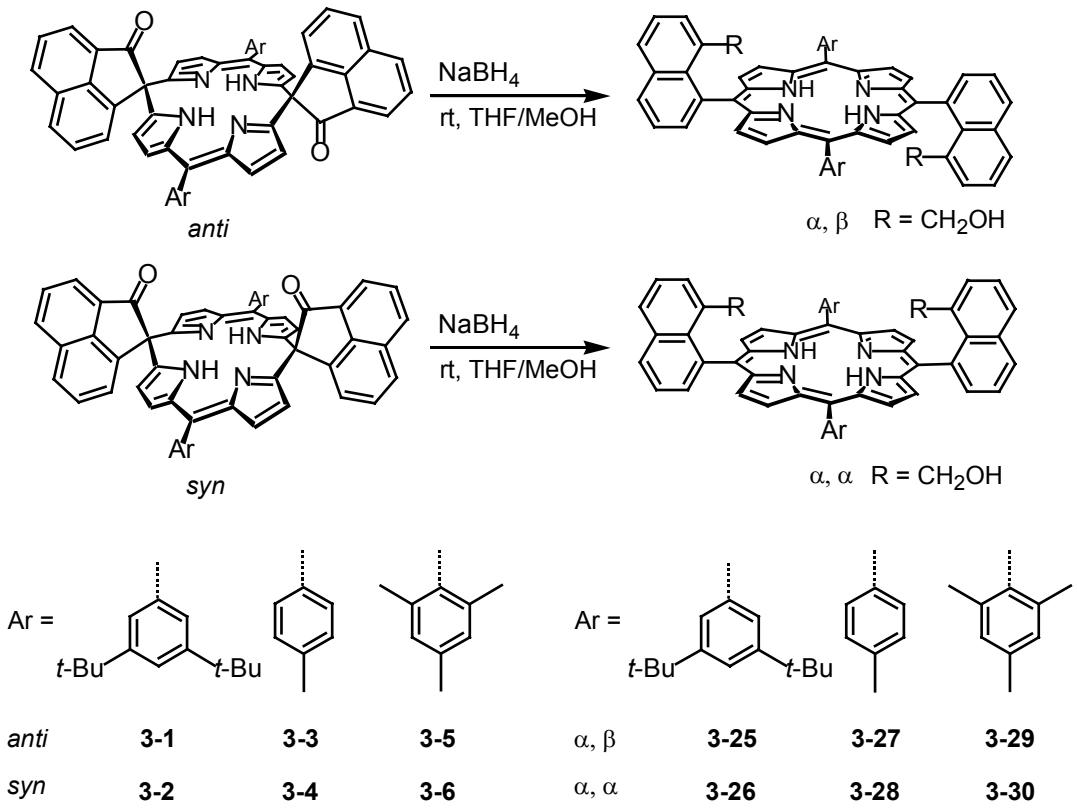

anti	**3-1**	**3-3**	**3-5**	α, β	**3-25**	**3-27**	**3-29**
syn	**3-2**	**3-4**	**3-6**	α, α	**3-26**	**3-28**	**3-30**

Figure 3-7. Diagram of the reductive ring-opening of dispiro-porphodimethenes to form porphyrin dialcohols.

If the reaction is carried out under rigorous air- and water-free conditions, a brilliant green solution forms, which turns dark brown-green after a few minutes. The UV-visible spectrum of the solution exhibits an absorption band at 433 nm with a shoulder at 447 nm, and it also displays an unusual broad band at 820 nm. Although this spectrum is not consistent with that of a two-electron-reduced metallated porphyrin species such as $[Zn(TPP)]^{-2}$, the absence of a metal in the macrocycle may allow for the formation of the disodium salt of the porphyrin dianion, which would be expected to have electronic transitions distinct from those of $[Zn(TPP)]^{-2}$. When the green solution is exposed to air, the broad band at 820 nm slowly decreases while the Soret band at 425 nm and the characteristic Q-bands grow in, indicating the formation of the porphyrin. Relative to the 8-carboxynaphthylporphyrins (**3-7** – **3-12** and **3-16** – **3-18**), the dialcohols

(**3-20** – **3-22**) exhibit enhanced stability in air; but, in the presence of strong oxidants, they also undergo ring-closing reactions to form cyclic ether porphodimethenes, as addressed in Chapter 4.

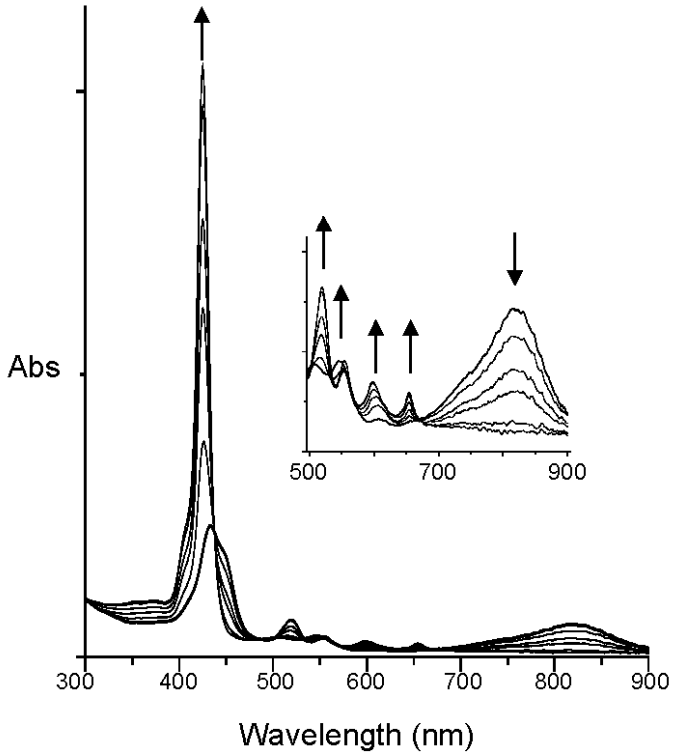

Figure 3-8. Diagram of the UV-visible spectrum upon reductive ring-opening of dispiro-porphodimethenes to form porphyrin dialcohols.

Acid-induced ring opening of the spiro-linked acenaphthenones also affords porphyrin macrocycles. The addition of strong acids such as HCl or H_2SO_4 to a solution of the porphodimethenes will cause ring opening at room temperature. If the reactions are undertaken in the presence of water, the protonated porphyrin diacid is obtained, and the free-base porphyrin is generated after washing the product with water. Prior to ring opening, the N-protonated macrocycle is formed, as demonstrated by UV-visible spectroscopy of the protonated porphodimethene **3-2** (Figure 3-9). Protonation of the porphodimethene **3-2** induces a split in the primary absorption band of (442 nm) into two

bands at 411 nm and 478 nm. Although the mechanistic details of the transformation are not clear, the drive to develop a flat, fully aromatic macrocycle likely induces the ring-opening reaction and subsequent porphyrin formation upon oxidation by molecular oxygen.

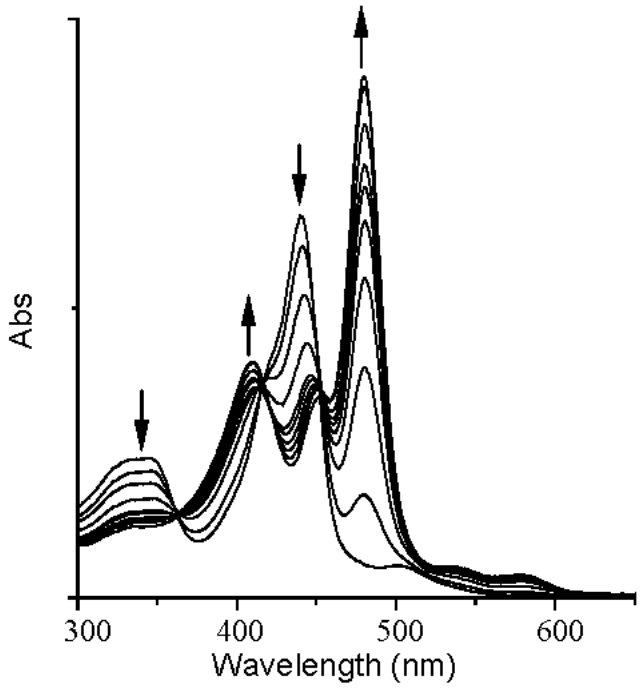

Figure 3-9. Depiction of the UV-visible spectra of the titration of **3-1** with TFA to form the protonated porphodimethene.

Preparations of the α, α-porphyrin diacids using acids result in substantially lower yields of the desired porphyrin products under all conditions attempted in comparison to reactions with KOH, and the isolation of the α, β-atropisomers by this method are inherently problematic due to solubility issues previously delineated. Due to these limitations, the pursuit of this methodology for the preparation of porphyrin diacids was abandoned, but the preparative reaction for porphyrin diesters using acid-induced ring opening was found to be quite useful. If methanol is added to the acid-catalyzed reactions with the rigorous exclusion of water, the diester porphyrins are obtained in high

yields (Figure 3-10, Table 3-1). These reactions were carried out under a dry O_2 atmosphere with freshly distilled solvents, and concentrated sulfuric acid was employed as the proton source. No interconversion of the α-α and α-β atropisomers was observed for these reactions. Although reaction times are longer in comparison to the NaOMe reactions, the yields for the diesters synthesized by the acid-induced route are higher relative to the NaOMe method, and this procedure is implicitly better suited for the conversion of base-sensitive porphodimethene precursors to porphyrin diesters.

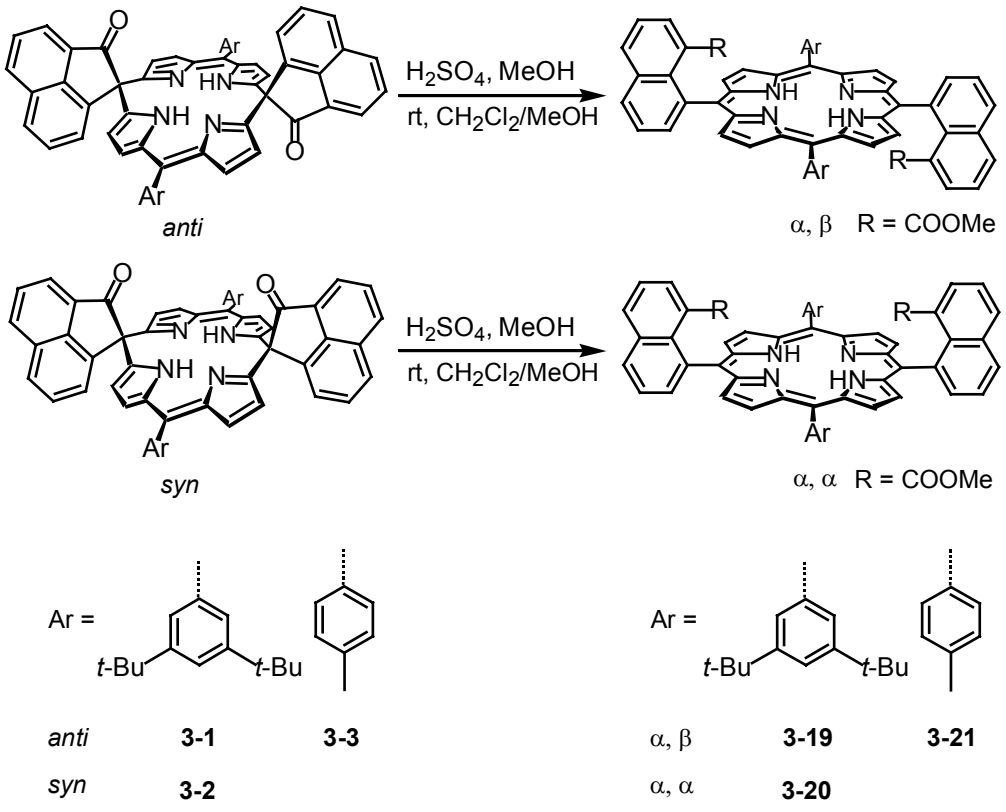

Figure 3-10. Illustration of the acid-induced ring opening of dispiro-porphodimethenes to generate porphyrin diesters.

Table 3-1. Summary of the yields and spectrophotometric data of porphyrins bearing 8-naphthyl functional groups at *trans-meso* positions (refer to Figure 3-9 for structural depiction of porphodimethenes). * => This work. † => not reported.

Entry	R	Atrop-isomer	Ar	M	Reagent	Yield	λ_{max}(log ε)	Ref.
3-7	COOK	α, β	*m*-(*t*-Bu)$_2$	2H	KOH	90 %	427(5.4)	56*
3-8	COOH	α, α	*m*-(*t*-Bu)$_2$	2H	KOH/ HCl	78 %	426(5.6)	56*
3-9	COOK	α, β	*p*-Me	2H	KOH	75 %	432(5.6)	56*
3-10	COOH	α, α	*p*-Me	2H	KOH/ HCl	80 %	426(5.6)	56*
3-11	COOK	α, β	Mes	2H	KOH	65 %	431(†)	56
3-12	COOH	α, α	Mes	2H	KOH/ HCl	92 %	432(†)	56
3-16	COOK	α, β	Mes	Zn	KOH	46 %	430(5.6)	56
3-17	COOH	α, α	Mes	Zn	KOH/ HCl	75 %	431(5.6)	56
3-18	COOK	α, β	Mes	Cu	KOH	61 %	421(5.2)	56
3-19	COOMe	α, β	*m*-(*t*-Bu)$_2$	2H	NaOMe	60 %	426(5.6)	56*
3-19	COOMe	α, β	*m*-(*t*-Bu)$_2$	2H	H_2SO_4/ MeOH	94 %	426(5.6)	56*
3-20	COOMe	α, α	*m*-(*t*-Bu)$_2$	2H	NaOMe	71 %	426(5.7)	56*
3-20	COOMe	α, α	*m*-(*t*-Bu)$_2$	2H	H_2SO_4/ MeOH	87 %	426(5.7)	56*
3-21	COOMe	α, β	*p*-Me	2H	NaOMe	73 %	425(5.8)	56*
3-21	COOMe	α, β	*p*-Me	2H	H_2SO_4/ MeOH	85 %	425(5.8)	56*
3-22	COOMe	α, α	*p*-Me	2H	NaOMe	68 %	426(5.7)	56*
3-23	COOMe	α, β	Mes	2H	NaOMe	81 %	425(5.5)	56
3-24	COOMe	α, α	Mes	2H	NaOMe	69 %	425(5.7)	56
3-25	CH_2OH	α, β	*m*-(*t*-Bu)$_2$	2H	$NaBH_4$/ HCl	98 %	424(5.7)	56*
3-26	CH_2OH	α, α	*m*-(*t*-Bu)$_2$	2H	$NaBH_4$/ HCl	95 %	426(5.5)	56*
3-27	CH_2OH	α, β	*p*-Me	2H	$NaBH_4$/ HCl	97 %	424(5.6)	56*
3-28	CH_2OH	α, α	*p*-Me	2H	$NaBH_4$/ HCl	95 %	424(5.8)	56*
3-29	CH_2OH	α, β	Mes	2H	$NaBH_4$/ HCl	98 %	424(5.6)	56
3-30	CH_2OH	α, α	Mes	2H	$NaBH_4$/ HCl	98 %	424(5.6)	56

Conclusions

Dispiro-porphodimethenes with 5-membered, α-keto-functionalized rings at their spiro-locks were shown to be excellent precursors for the preparation of porphyrins bearing two 8-naphthyl functionalized substituents at *trans*-*meso*-positions in high yields. Ring opening and subsequent porphyrin formation can be induced by KOH to generate the carboxylates or their potassium salts, NaOMe or H_2SO_4 with MeOH to form the methyl esters, or $NaBH_4$ to produce the alcohols. Through the rational selection of the aryl groups at the *meso*-positions of the porphodimethene precursors, this general pathway allows for the preparation of 8-naphthyl functionalized porphyrins with different steric, electronic, and solubility properties.

Experimental

General

The University of Florida Mass Spectrometry Services measured all mass spectral data. Atlantic Microlabs, Norcross, GA performed elemental analyses. ^{1}H NMR spectra were recorded on a Varian Mercury or VXR spectrometers at 300 MHz in $CDCl_3$ at 25^o C (unless otherwise noted), and the chemical shifts were referenced to the solvent residual peak of chloroform at 7.26 MHz. Electronic absorption spectra were collected in either $CHCl_3$ or MeOH on a Varian Cary 50 spectrophotometer. All reagents were used as received from Aldrich, and all solvents were used as received from Fisher, unless otherwise specified. Procedures for the preparation of porphodimethenes **3-1** - **3-6** are described in Chapter 2. The reaction of the porphodimethenes (**3-1** – **3-4**) with NaOMe for the preparation of the diesters **3-19** - **3-22** and the acid-catalyzed ring-opening reactions for the synthesis of **3-19** - **3-21** were performed under Schlenk conditions, with dried and degassed solvents. Porphyrin diacids, dialcohols, and dipotassium salts have

been found to undergo oxidative ring-closing reactions over time in the presence of air, and these compounds should be stored under an inert atmosphere.

Chromatography

Absorption column chromatography was preformed using chromatographic silica gel (Fisher, 200 – 425 mesh).

Synthesis of 3-7

A portion of 0.200 g (0.201 mmol) of **3-1** was dissolved in 12 mL of hot THF. The solution was allowed to cool, and 1 mL of 30% $KOH_{(aq)}$ was added. The reaction mixture was refluxed for 3 h, cooled to room temperature, and the product was collected on a fine frit. The filtrate was concentrated to one sixth of its original volume, and the residue was redissolved in minimal hot THF. Slow diffusion of pentane into the THF solution afforded additional crystalline material

Yield (**3-7**): 196 mg, (90% from the combined fractions). UV/ Vis [MeOH, $\lambda_{max}(\log \varepsilon)$]: 427 (5.4). ^{1}H NMR (CD_3OD) δ = 8.62 (8H, s), 8.30 (2H, d, J = 8.3 Hz), 8.14 (2H, d, J = 8.4 Hz), 8.10 (2H, d, J = 7.0 Hz), 8.04 (4H, d, J = 1.7 Hz), 7.82 (4H, m), 7.53 (2H, dd, J_1 = 7.0, J_2 = 8.1 Hz), 7.27 (2H, d, J = 7.0 Hz), 1.49 (36H, s). HRMS (FAB) calculated for $[M+H]^+$ ($C_{70}H_{65}N_4O_4K_2$): 1103.4280. Found: 1103.4252.

Synthesis of 3-8

A portion of 0.300 g (0.301 mmol) of **3-2** was dissolved in 35 mL of THF and 1.3 mL of a 30% aqueous KOH solution was added. The reaction mixture was refluxed for 3 h and then acidified with 10 mL 6 N HCl. After stirring for an additional 5 min, a mixture of 10 mL H_2O and 30 mL CH_2Cl_2 was added. The dark green organic layer was washed with water (3 x) and dried over $NaSO_4$. The solvent was removed and the

residue was redissolved in a mixture of 15 mL CH_2Cl_2 and 10 mL hexane. Slow removal of the solvents under vacuum afforded **3-8** as a purple microcrystalline solid.

Yield (**3-8**): 0.242 g (78 %). UV/ Vis [$CHCl_3$, λ_{max}(log ε)] 426(5.59) nm. ^{1}H NMR (300 MHz, $CDCl_3$): δ = 8.52 (bs, 4H), 8.46 (bs, 4H), 8.16 (d, 4H, J = 8.11 Hz), 7.92-8.05 (m, 6H), 7.82 (t, 2H, 7.6 Hz), 7.71 (t, 2H, J = 1.7 Hz), 7.53 (s, 2H), 7.21 (t, 2H, J = 7.6 Hz), 1.40 (bs, 18H), 1.38 (bs, 18H). HRMS (FAB) calculated for $[M+H]^+$ ($C_{70}H_{66}N_4O_4$): 1027.5162. Found: 1027.5164.

Synthesis of 3-9

As described for **3-7**, a THF solution containing 0.080 g (0.10 mmol) of **3-3** was treated with excess $KOH_{(aq)}$ in the presence of O_2.

Yield (**3-9**): 0.070 g (75%). UV/ Vis [$CHCl_3$, λ_{max}(log ε)] 432 (5.61) nm. ^{1}H NMR (300 MHz, $CDCl_3$): 8.65 (bs, 8H), 8.34 (d, 2H, J = 8.1 Hz), 8.17 (d, 2H, J = 8.1 Hz), 8.08-8.14 (m, 6H), 7.82 (dd, 2H, $J_1 = J_2$ = 7.7 Hz), 7.53-7.60 (m, 6H), 7.33 (dd, 2H, J_1 = 1.2, J_2 = 6.9 Hz), 2.67 (s, 6H). HRMS (FAB) calculated for $[M+H]^+$ ($C_{56}H_{37}N_4O_4K_2$): 907.2089. Found: 907.2047.

Synthesis of 3-10

As described for **3-8**, 0.054 g (0.068 mmol) of **3-4** was treated with 30 % weight/ volume KOH, followed by acidic workup.

Yield (**3-10**): 0.045 g (80%). UV/ Vis [$CHCl_3$, λ_{max}(log ε)] 426 (5.64) nm. ^{1}H NMR (300 MHz, $CDCl_3$): δ = 8.50 (d, 8H, J = 4.8 Hz), 8.31 (d, 4H, J = 4.8 Hz), 8.22 (d, 2H, J = 8.2 Hz), 8.10 (d, 2H, J = 8.2 Hz), 7.94 (bs, 2H), 7.87 (dd, 2H, $J_1 = J_2$ = 7.6 Hz), 7.62 (bs, 2H), 7.39 (bs, 4H), 7.32 (dd, 2H, $J_1 = J_2$ = 7.6 Hz), 6.00 (bs, 2H), 2.65 (s, 6H),

1.38 (bs, 18H). HRMS (FAB) calculated for $[M+H]^+$ ($C_{56}H_{39}N_4O_4$): 831.2971. Found: 831.2944.

Synthesis of 3-19

A portion of 5 mg (0.22 mmol) of Na was added to a mixture of 15 mL THF/ MeOH (2:1). After the sodium had completely reacted, 80 mg (0.081 mmol) of **3-1** was added. The solution was stirred for 2 h before oxygen was bubbled through the reaction mixture. After 5 min, 15 mL of water and 35 mL of CH_2Cl_2 was added. The organic layer was separated and immediately washed with water (3x). The organic layer was dried ($NaSO_4$) and the solvents removed under reduced pressure. Purification was achieved by column chromatography (Silica, CH_2Cl_2/ hexanes, 2:1).

Yield (**3-19**): 51 mg (60%).

An alternative synthesis of **3-19** utilizing the acid cleavage route was also carried out with a portion of 0.025 g (0.025 mmol) of **3-1** in 20 mL of CH_2Cl_2 and 5 mL of MeOH, both solvents being freshly distilled under nitrogen. The flask was then charged with dry oxygen, and 0.1 mL of concentrated H_2SO_4 was added slowly. After stirring the reaction under dry oxygen at room temperature overnight, the crude mixture was washed three times with water, dried with Na_2SO_4, and concentrated to 3 mL under reduced pressure. This concentrate was then filtered through a short (5 cm x 25 mm) silica plug with CH_2Cl_2 as the eluent.

Yield (**3-19**): 24 mg (94%). UV/ Vis [$CHCl_3$, $\lambda_{max}(\log \varepsilon)$] 426(5.6) nm. ^{1}H NMR (300 MHz, $CDCl_3$): δ = 8.80 (d, 4H, J = 4.9 Hz), 860 (d, 4H, 4.9 Hz), 8.36 (d, 2H, J = 7.1 Hz), 8.32 (d, 2H, J = 8.3 Hz), 8.26 (d, 2H, J = 8.3 Hz), 8.05 (d, 4H, J = 1.9 Hz), 7.90 (dd, 2H, J_1 = 7.1 Hz, J_2 = 8.3 Hz), 7.75 (t, 2H, J = 1.8 Hz), 7.56 (dd, 2H, J_1 = 7.1 Hz, J_2 = 8.3

Hz), 7.33 (d, 2H, J = 7.0 Hz), 1.49 (s, 36H), 0.31 (s, 6H), -2.42 (s, 2H). HRMS (FAB) calculated for $[M+H]^+$ ($C_{72}H_{71}N_4O_4$): 1055.5475. Found: 1055.5413.

Synthesis of 3-20

Following the procedures described for **3-19**, a portion of **3-2** (0.080 g, 0.081 mmol) was treated with 5 mg Na in 4 mL MeOH and 15 mL THF.

Yield (**3-20**): 0.061 g (71%).

This derivative was also prepared from 0.025 g (0.025 mmol) of **3-19** via acid catalyzed ring opening in the presence of MeOH, as described for **3-19**.

Yield (**3-20**): 0.023 g (87%). UV/ Vis [$CHCl_3$, λ_{max}(log ε)] 426(5.69) nm. ^{1}H NMR (300 MHz, $CDCl_3$): δ = 8.77 (d, 4H, J = 4.9 Hz), 8.57 (d, 4H, 4.7 Hz), 8.36 (d, 2H, J = 8.4 Hz), 8.32 (d, 2H, J = 8.4 Hz), 8.26 (d, 2H, J = 8.4 Hz), 8.18 (t, 2H, J = 1.5 Hz), 7.89 (dd, 2H, J_1 = 7.2 Hz, J_2 = 8.0 Hz), 7.88 (t, 2H, J = 1.5 Hz), 7.75 (t, 2H, J = 1.8 Hz), 7.56 (dd, 2H, J_1 = 7.2 Hz, J_2 = 8.1 Hz), 7.32 (d, 2H, J = 7.0 Hz), 1.53 (s, 18H), 1.45 (s, 18H), 0.28 (s, 6H), -2.43 (s, 2H). HRMS (FAB) calculated for $[M+H]^+$ ($C_{72}H_{71}N_4O_4$): 1055.5475. Found: 1055.5494.

Synthesis of 3-21

Following the methodology described for **3-19**, 0.060 g (0.075 mmol) of **3-3** was reacted with sodium methoxide to form the methyl ester.

Yield (**3-21**): 0.047 g (73%).

This product was also prepared from 0.025 g (0.030 mmol) of **3-3** from the reaction with concentrated sulfuric acid as described for **3-19**.

Yield (**3-21**): 0.023 g (85%). UV/ Vis [$CHCl_3$, λ_{max}(log ε)] 425 (5.81) nm. ^{1}H NMR (300 MHz, $CDCl_3$): δ = 8.77 (d, 4H, J = 4.9 Hz), 8.58 (d, 4H, 4.9 Hz), 8.34 (m,

2H), 8.32 (s, 2H), 8.27 (dd, 2H, J_1 = 1.5, J_2 = 8.3 Hz), 8.09 (d, 4H, J=8.1 Hz), 7.90 (dd, 2H, $J_1 = J_2$ = 7.7 Hz), 7.57 (dd, 2H, J_1 = 7.0, J_2 = 8.1 Hz), 7.50 (d, 4H, J = 7.9 Hz), 7.35 (dd, 2H, J_1 = 1.3 Hz, J_2 =7.0 Hz), 2.66 (s, 6H), 0.29 (s, 6H), -2.50 (bs, 2H). HRMS (FAB) calculated for $[M+H]^+$ ($C_{58}H_{43}N_4O_4$): 859.3284. Found: 859.3298.

Synthesis of 3-22

As described for **3-19**, 0.060 g (0.075 mmol) of compound **3-4** was treated with freshly prepared sodium methoxide under air and water free conditions.

Yield (**3-22**): 0.044 g (68%). UV/ Vis [$CHCl_3$, λ_{max}(log ε)] 426 (5.71) nm. ^{1}H NMR (300 MHz, $CDCl_3$): δ = 8.77 (d, 4H, J = 4.7 Hz), 8.58 (d, 4H, 4.9 Hz), 8.38 (d, 2H, J = 7.0 Hz), 8.33 (d, 2H, J = 8.3 Hz), 8.26 (d, 2H, J = 8.3 Hz), 8.22 (d, 2H, J = 7.9 Hz), 7.97 (d, 2H, J = 7.9 Hz), 7.91 (dd, 2H, J_1 = 7.0, J_2 = 8.1 Hz), 7.56 (dd, 2H, J_1 = 7.0, J_2 = 8.3 Hz) 7.51 (t, 2H, J = 8.33 Hz), 7.75 (t, 2H, J = 1.8 Hz), 7.56 (dd, 2H, J_1 = 7.2 Hz, J_2 = 8.1 Hz), 7.32 (d, 2H, J = 7.0 Hz), 1.53 (s, 18H), 1.45 (s, 18H), 0.28 (s, 6H), -2.43 (s, 2H). HRMS (FAB) calculated for $[M+H]^+$ ($C_{58}H_{43}N_4O_4$): 859.3284. Found: 859.3298.

Synthesis of 3-25

A portion of **3-1** (54 mg, 0.054 mmol) was dissolved in 10 mL of THF and 30 mg $NaBH_4$ (0.79 mmol) dissolved in 2 mL of MeOH was added. After 3 min, another sample of $NaBH_4$ (30 mg, 0.79 mmol) was added to the reaction mixture and the solution stirred for 1 h. The mixture was treated with 20 mL of 2N HCl followed by 30 mL of CH_2Cl_2. The organic phase was separated, washed with water (3 x) and subsequently dried over anhydrous $NaSO_4$. The solvents were removed under reduced pressure and the purple residue was redissolved in 20 mL of CH_2Cl_2. After addition of 5 mL of hexanes, the CH_2Cl_2 was slowly distilled off and the remaining slight brown hexane solution

decanted from the microcrystalline material. Drying under vacuum yielded analytically pure **3-25**.

Yield (**3-25**): 53 mg (98%). UV/ Vis [$CHCl_3$, λ_{max}(log ε)] 424 (5.7) nm. ^{1}H NMR: δ = (300 MHz, $CDCl_3$): δ = 8.77 8.79 (d, 4H, J = 4.8 Hz), 8.56 (d, 4H, J = 4.8 Hz), 8.33 (dd, 2H, J_1 = 1.4, J_2 = 8.3 Hz), 8.13-8.19 (m, 4H), 8.05 (d, 4H, J = 1.8 Hz), 7.73-7.80 (m, 4H), 7.63 (d, 4H, J = 5.6 Hz), 3.02 (d, 4H, J = 5.6 Hz), 1.49 (s, 36H), 0.30 (t, 2H, J = 5.8 Hz), -2.37 (s, 2H). HRMS (FAB) calculated for $[M+H]^+$ ($C_{70}H_{71}N_4O_2$): 999.5577. Found: 999.5549.

Synthesis of 3-26

Following the procedures described for **3-25**, a portion of 25 mg (0.025 mmol) of **3-2** was treated with 0.030 g (0.793 mmol) of $NaBH_4$.

Yield (**3-26**): 24 mg (95%). UV/ Vis [$CHCl_3$, λ_{max}(log ε)] 426(5.54) nm. ^{1}H NMR (300 MHz, $CDCl_3$): δ = 8.80 (d, 4H, J = 4.9 Hz), 8.57 (d, 4H, J = 4.9 Hz), 8.33 (dd, 2H, J_1 = 1.3 Hz, J_2 = 8.3 Hz), 8.12-8.20 (m, 6H), 7.97 (dd, 2H, J_1 = J_2 = 1.7 Hz), 7.73-7.86 (m, 4H), 7.59-7.67 (m, 4H), 3.07 (s, 4H), 1.51 (s, 18H), 1.47 (s, 18H), 0.39 (bs, 2H), -2.37 (s, 2H). HRMS (FAB) calculated for $[M+H]^+$ ($C_{70}H_{70}N_4O_2$): 999.5577. Found: 999.5604.

Synthesis of 3-27

As outlined for **3-25**, 0.050 g (0.063 mmol) of **3-3** was treated with 0.060 g (1.586 mmol) $NaBH_4$.

Yield (**3-27**): 0.049 g (97%). UV/ Vis [$CHCl_3$, λ_{max}(log ε)] 424 (5.64) nm. ^{1}H NMR (300 MHz, $CDCl_3$): δ = 8.78 (d, 4H, J = 4.8 Hz), 8.56 (d, 4H, J = 4.8 Hz), 8.34 (dd, 2H, J_1 = 1.3 Hz, J_2 = 8.3 Hz), 8.12-8.21 (m, 4H), 8.06 (d, 4H, J = 7.9 Hz), 7.77 (dd, 2H,

J_1 = 7.0 Hz, J_2 = 8.1 Hz), 7.59-7.67 (m, 4H), 7.52 (d, 4H, J = 7.7 Hz), 2.99 (s, 4H), 2.67 (s, 6H), 0.22 (bs, 2H), -2.42 (s, 2H). HRMS (FAB) calculated for $[M+H]^+$ ($C_{56}H_{43}N_4O_2$): 803.3386. Found: 803.3367.

Synthesis of 3-28

As outlined for **3-25**, 0.025 g (0.031 mmol) of **3-4** was reacted with 0.030 g (0.793 mmol) $NaBH_4$.

Yield (**3-28**): 0.024 g (95%). UV/ Vis [$CHCl_3$, $\lambda_{max}(\log \varepsilon)$] 424 (5.8) nm. ^{1}H NMR (300 MHz, $CDCl_3$): δ = 8.77 (d, 4H, J = 4.8 Hz), 8.55 (d, 4H, J = 4.8 Hz), 8.34 (dd, 2H, J_1 = 1.4 Hz, J_2 = 8.2 Hz), 8.06-8.20 (m, 6H), 8.00 (d, 2H, 7.58), 7.76 (dd, 2H, J_1 = 7.1, J_2 = 8.1 Hz), 7.64 (d, 4H, J = 5.45), 7.51 (J_1 = J_2 = 6.8 Hz), 3.07 (s, 4H), 2.66 (s, 6H), 0.38 (bs, 2H), -2.41 (s, 2H). HRMS (FAB) calculated for $[M+H]^+$ ($C_{56}H_{43}N_4O_2$): 803.3386. Found: 803.3385.

CHAPTER 4
REDOX-SWITCHABLE PORPHYRIN-PORPHODIMETHENE INTERCONVERSIONS

Introduction

Nucleophilic substituents placed in proximity to the *meso*-carbon positions of a porphyrin ring influence the electronics of the macrocycle, and these interactions can be detected by both electrochemical and EPR measurements.[91-93] For example, the NH group in *meso*-(*o*-anilido)porphyrins are located close enough to the macrocycle to significantly alter the electrochemistry of the ring.[93] This interplay between nucleophiles and the *meso*-carbon positions of the porphyrin macrocycle may have many broad implications, including porphyrin degradation in metal assisted oxidation reactions and natural heme catabolism.[94,95] In addition, the decomposition of mono-functionalized naphthoic acid porphyrins to afford oxaporphyrins reported by Chang appears to be initially induced by the intramolecular attack of the pendent carboxylic acid on the *meso*-carbon to form an isoporphyrin. Subsequent oxidation to the oxaporphyrin is likely caused by molecular oxygen (Figure 4-1).[95] Isolation and characterization of the intermediates involved in this degradative processes has likely been hampered by the presence of only one functional group since the postulated isoporphyrin intermediates are quite unstable. The simultaneous interaction of two functional groups fixed at the 5- and 15- positions of a porphyrin presents the opportunity to form a more stable porphodimethene product as opposed to the isoporphyrin intermediate proposed by Chang. With this in mind, we examined the oxidative behavior of porphyrins with

nucleophilic substituents proximal to two *trans meso*-carbons electrochemically and chemically.

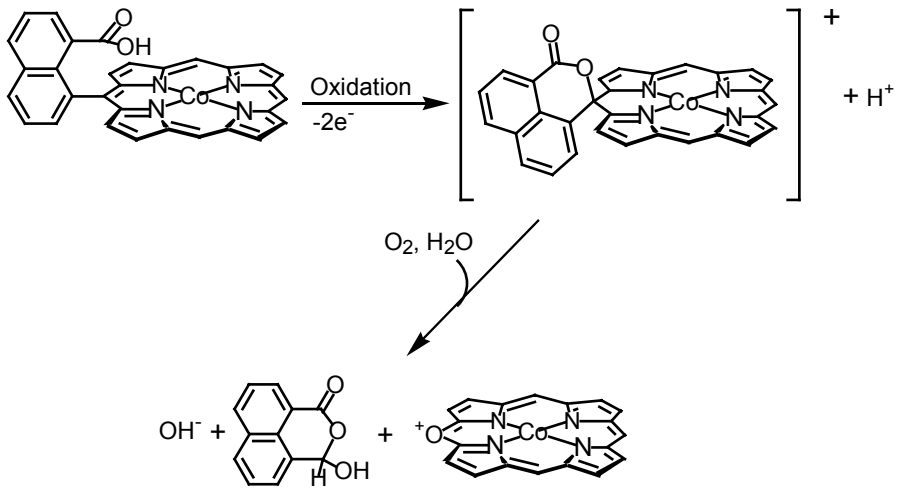

Figure 4-1. Illustration of the degradation of a naphthoic acid porphyrin to generate an oxaporphyrin.

Results and Discussion

The syntheses of *trans*-porphyrins bearing two 8-carboxy functionalized naphthalene spacers were described in Chapter 3. When these compounds are exposed to air for prolonged periods or treated with oxidizing agents such as DDQ or $[Fe(Cp)_2]PF_6$, a decay of both the metallated and unmetallated porphyrins is observed. The stability of these porphyrins is strongly dependent on several factors including the electronic and steric nature of the *meso*-aryl substituents in addition to the identity of the metal ion incorporated into the macrocycle. Degradation of the porphyrins can be attributed to the proximity of the carboxylate groups to the porphyrin plane allowing a direct interaction between the carboxylate oxygens and respective *meso* sp^2-carbon atoms.

Accordingly, the electrochemical attributes of some selected derivatives were examined (Table 4-1). In sharp contrast to the both *meso*-(*o*-anilido) and *meso*-carboxynaphthalene derivatives, compounds **4-1** - **4-7** do not exhibit a reversible $2e^-$

oxidation, even at higher scan rates (400 mV/ s). Instead, an irreversible oxidation wave is observed, and compared to the reversible oxidation waves normally found for tetraarylporphyrins, and the oxidation is shifted to significantly lower potentials. Nevertheless, in analogy to the tetraarylporphyrins, the oxidation potentials of these macrocycles are profoundly influenced by the electronic properties of both the aryl substituents and the central metal ion, and their unusual redox behavior with regards to tetraarylporphyrins is undoubtedly governed by the carboxylate groups bound at 8-position of the naphthalene spacer.

Table 4-1. Electrochemical Oxidation Potentials of **4-1 – 4-9**.[a]

Entry	Ar	R	M	atropisomer	$E_{p(ox)}$[b]	solvent
4-1	3,4,5-$(OMe)_3C_6H_2$	COOK	H_2	α, β	491	MeOH
4-2	2,4,6-$Me_3C_6H_2$	COOK	H_2	α, β	455	MeOH
4-3*	3,5-$(Bu^t)_2C_6H_3$	COOK	H_2	α, β	516	MeOH
4-4	2,4,6-$Me_3C_6H_2$	COOK	Cu	α, β	443	MeOH
4-5	2,4,6-$Me_3C_6H_2$	COOK	Zn	α, β	286	MeOH
4-6*	3,5-$(Bu^t)_2C_6H_3$	COOH	H_2	α, α	842	CH_2Cl_2
4-7	2,4,6-$Me_3C_6H_2$	COOH	Zn	α, α	736	CH_2Cl_2
4-8	2,4,6-$Me_3C_6H_2$	COOMe	H_2	α, β	978/ 1340 [c]	CH_2Cl_2
4-9*	2,4,6-$Me_3C_6H_2$	CH_2OH	H_2	α, β	996	CH_2Cl_2

[a.] Refer to Figure 4-2 for structural depiction of porphyrins. [b.] Potentials (mV vs SCE) were measured with a Pt disk working electrode, a Pt wire counter electrode, an electrolyte concentration of 0.1 M, and a scan rate of 100 mV/ s. [c.] [$E_{1/2}$(ox1)/ $E_{1/2}$(ox2)]. * => This work.

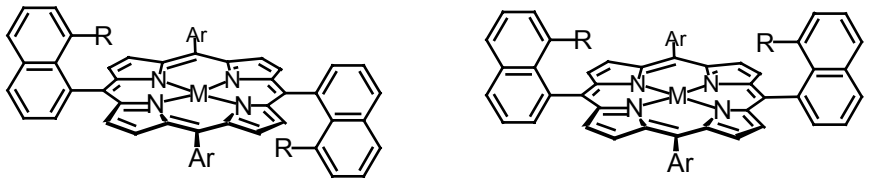

α, β α, α

Figure 4-2. Depiction of 8-naphthyl substituted porphyrins investigated.

Hence, if the reactive carboxylate is protected as the ester as exemplified in **4-8**, the cyclic voltammogram of the porphyrin shifts to higher potentials and exhibits two

reversible oxidation waves. Although the ester groups in **4-8** are in proximity to the porphyrin plane, the increased steric strain and reduced nucleophilicity of the carbonyl oxygen does not allow for extensive oxygen-porphyrin interactions. Even without the ester protection, a reduction in the nucleophilicity of the carboxylate oxygen induces a shift to higher potential for the first oxidation, as highlighted by the 450 mV increase for the α, α-free acid **4-7** relative to the α, β-dipotassium salt **4-5** (R = mesityl, M = Zn for both). Unfortunately, due to the insolubility of the free acid α, β-atropisomers in common solvents,[53] no data is available for these derivatives.

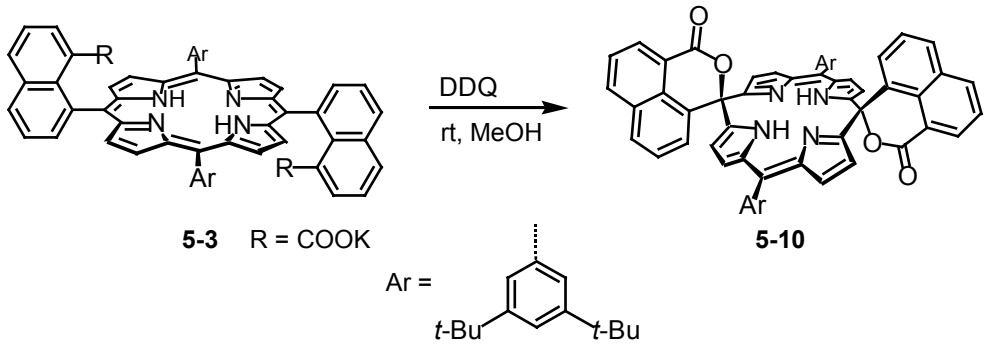

Figure 4-3. Depiction of the oxidative lactonization of **4-3**.

Given the exceptionally low oxidation potential of these porphyrins, simple reagents should be capable of oxidizing the macrocycles and reaction of the α, β-dipotassium salt **4-3** in MeOH with an excess of DDQ instantly affords the precipitation of a bright orange material, **4-10**, in 95% yield (Figure 4-3). In comparison to the porphyrin **4-3** (427 nm), the UV-visible spectrum of the oxidation product displays a significant bathochromic shift (473 nm) of the primary absorption band accompanied by a decrease in intensity [log ε: 5.4 (**4-3**); 5.2 (**4-10**)] and loss of the Q-bands. On the basis of the ^{1}H NMR spectrum of the oxidized product, the tetrapyrrolic macrocycle remains intact, but the pyrrolic protons shift upfield [δ: 8.54, 8.42 ppm (**4-3**); 6.32, 6.03 ppm (**4-**

10)], intimating a disruption of the electron delocalization within the macrocyclic ring system. In sharp contrast to typical porphyrins, the resonances for the N-H protons in ^{1}H NMR of the unmetallated derivative **4-10** are drastically shifted downfield to 14.3 ppm, characteristic for porphodimethenes. Using similar procedures, the α, α-free acid **4-6** was also chemically oxidized, and the orange product, **4-11**, was isolated and fully characterized. Evidently, the irreversible oxidation wave in the cyclic voltammograms of **4-1** – **4-7** can be attributed to an initial attack of the carboxy-oxygen at the *meso*-carbons and subsequent intramolecular lactonization and formation of the corresponding porphodimethenes. While intermolecular nucleophilic *meso*-substitution and -addition reactions of oxidative activated and unactivated porphyrins have been widely examined, to the best of our knowledge, an analogous intramolecular reaction has not been reported.

As illustrated by the solid-state structure of **4-10** depicted in Figure 4-4, the oxidative process leads to the formation of a six-membered lactone ring whereby the two 1*H*,3*H*-naphtho[1,8-*cd*]pyrane-1-one groups are aligned in the expected *anti* position. Due to the sp^3-hybridized *meso*-carbon atoms, the tetrapyrrolic skeleton adopts a strong roof-like conformation with an inter-planar angle between the two dipyrromethene moieties of 124.8^o, comparable to the angles found for other unmetallated porphodimethenes.

In an effort to reestablish the aromatic porphyrin system, we investigated the electrochemical behavior of the porphodimethenes. As an example, the *anti*-derivative **4-10** undergoes an irreversible reduction at -1010 mV and re-oxidation at 451 mV (SCE). The reduction of the metallated (Zn) *syn*-porphodimethene **4-7** has also been achieved by chemical means through the addition of stoichiometric amounts of cobaltocene.[54] The

resulting porphyrin immediately precipitated out of the THF reaction mixture, affording α, α-*trans*-8-carboxynaphthylporphyrin as the dicobaltocenium salt in high yield.

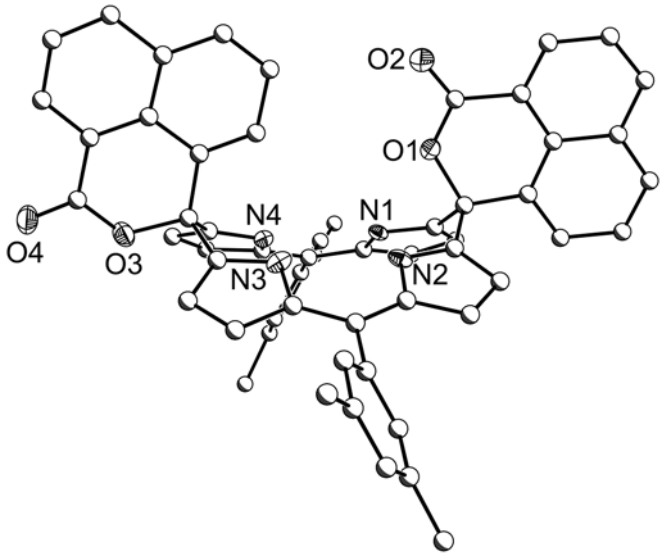

Figure 4-4. Diagram of **4-10** (30% ellipsoids, carbons arbitrary radii). Hydrogen atoms and Bu^t-methyl-groups omitted for clarity.

The porphyrin dialcohol, **4-9** was also found to be susceptible to oxidative ring-closing reactions, generating the cyclic ether porphodimethene **4-12** (Figure 4-5). As anticipated based on the relatively high pK_a for benzylic alcohols in comparison to carboxylates**,** the potential required to oxidize **4-9** to **4-12** (996 mV) is considerably higher than that needed to oxidize the corresponding dipotassium salt, **4-3**, to the lactone, **4-10** (516 mV).

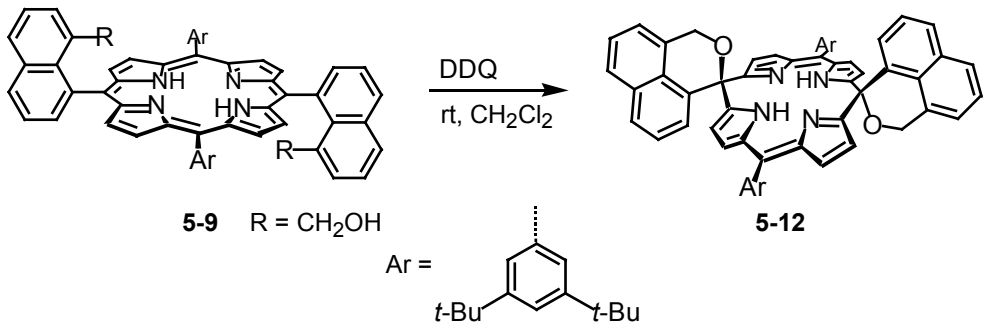

Figure 4-5. Diagram of the transformation of **4-9** to **4-12**.

Conclusion

In summary, the first examples of reversible, redox-controlled porphyrin-porphodimethene interconversions via sequential intramolecular ring opening and closing reactions at the *meso* positions have been described. The respective oxidation potentials can be easily manipulated by the judicious choice of the aromatic residues as well as by the metal ion incorporated into the macrocycles. With regard to the functional groups at the naphthalene spacer, these potential recognition sites can be electrochemically and chemically activated and deactivated, offering many exciting possibilities for the design of novel redox-switchable sensors or photosensitizers.

Experimental

General procedures

The University of Florida Mass Spectrometry Services measured all mass spectral data. Atlantic Microlabs, Norcross, GA performed elemental analyses. ^{1}H NMR spectra were recorded on a Varian Mercury spectrometer at 300 MHz in $CDCl_3$ at 25^{o} C, and the chemical shifts were referenced to the solvent residual peak of chloroform at 7.26 MHz. Electronic absorption spectra were collected in CH_2Cl_2 on a Varian Cary 50 spectrophotometer. All reagents were used as received from Aldrich, and all solvents were used as received from Fisher, unless otherwise specified.

Chromatography

Absorption column chromatography was preformed using chromatographic silica gel (Fisher, 200 – 425 mesh).

Synthesis of 4-10

A portion of 500 mg (0.450 mmol) of **4-3** was dissolved in 75 mL warm methanol, and 230 mg (1.00 mmol) of DDQ was added. A bright red-orange precipitate formed

immediately, and the reaction mixture was allowed to stir for 90 min. The product was collected by filtration, washed with pentane, and dried to afford **4-10** as a red-orange powder. X-ray quality single crystals were grown by diffusion of pentane into a saturated THF solution of the product.

Yield (**4-10**): 95% (440 mg). UV/ Vis [CH_2Cl_2, λ (log ε)]: 473 (5.0), 414 (4.64). ^{1}H NMR (300 MHz, $CDCl_3$): 14.25 (s, 2H), 8.73 (d, 2H, J = 7.3 Hz), 8.54 (d, 2H, J = 7.3 Hz), 8.22 (d, 2H, J = 8.1 Hz), 8.19 (d, 2H, J_1 = 7.7 Hz), 8.07 (d, 2H, J_1 = 8.3 Hz), 7.72 (d, 2H, J = 7.3 Hz), 7.69 (d, 2H, J = 8.1 Hz), 7.45 (d, 2H, J = 1.7 Hz), 7.24 (d, 2H, J = 1.9 Hz), 6.41 (d, 4H, J = 4.3 Hz), 6.30 (d, 4H, J = 4.3 Hz), 1.28 (s, 36H). Analysis Calculated for $C_{70}H_{68}N_4O_5$ (**4-10**·THF): C, 81.29; H, 6.27; N, 5.12. Found: C, 81.26; H, 6.27; N, 5.36.

Synthesis of 4-11

A portion of 400 mg (0.389 mmol) of **4-6** was dissolved in 65 mL CH_2Cl_2, and 207 mg (0.900 mmol) of DDQ was added. The reaction mixture changed color from a deep purple to bright orange, and was allowed to stir for 90 min. The product was collected by filtration through neutral alumina with CH_2Cl_2 as eluent, and precipitated with hexanes to afford 390 mg of **4-11** as a yellow-orange powder.

Yield (**4-11**): 95% (390 mg). UV/ Vis [CH_2Cl_2, λ_{max}(log ε)]: 464 (5.0). ^{1}H NMR (300 MHz, $CDCl_3$): 13.09 (s, 2H), 8.72 (d, 2H, J = 7.2 Hz), 8.61 (d, 2H, J = 7.0 Hz), 8.23 (d, 2H, J = 8.2 Hz), 8.05 (d, 2H, J_1 = 8.1 Hz), 7.84 (dd, 2H, J_1 = J_2 = 7.8 Hz), 7.75 (dd, 2H, J = 7.7 Hz), 7.46 (s, 2H), 7.23 (bs, 4H), 6.74 (d, 4H, J = 4.3 Hz), 6.53 (d, 4H, J = 4.3 Hz), 1.28 (s, 36H). HRMS (FAB) calculated for $[M+H]^+$ ($C_{70}H_{67}N_4O_4$): 1025.5006. Found 1025.4959.

Synthesis of 4-12

A portion of 35 mg (0.035 mmol) of **4-9** was dissolved in 10 mL warm methanol/ $CHCl_3$ (2:1), and 18 mg (0.080 mmol) of DDQ was added. After stirring at room temperature for 2 h, the solution changed from purple to red-orange, and the reaction was allowed to continue for an additional 90 min. The product was filtered over a short plug of silica with CH_2Cl_2 as the eluent, and dried under vacuum to afford **4-12** as an amorphous solid.

Yield (**4-12**): 94% (33 mg). UV/ Vis [CH_2Cl_2, λ_{max}(log ε)]: 452 (4.9). ^{1}H NMR (300 MHz, $CDCl_3$): 14.36 (bs, 2H), 8.71 (d, 2H, J = 7.1 Hz), 7.94 (d, 2H, J = 8.1 Hz), 7.80 (m, 4H), 7.47 (m, 4H), 7.29 (m, 6H), 6.40 (d, 4H, J = 4.1 Hz), 6.33 (d, 4H, J = 4.1 Hz), 5.46 (s, 4H), 1.29 (s, 36H). HRMS (FAB) calculated for $[M+H]^+$ ($C_{70}H_{69}N_4O_2$): 997.5421. Found: 997.5388.

X-ray Crystallography

Unit cell dimensions were obtained (Table 4-2) and intensity data collected by Prof. Michael Scott on a Siemens CCD SMART diffractometer at low temperature, with monochromatic Mo-Kα X-rays (λ = 0.71073 Å). The data collections nominally covered over a hemisphere of reciprocal space, by a combination of three sets of exposures; each set had a different ϕ angle for the crystal and each exposure covered 0.3° in ω. The crystal to detector distance was 5.0 cm. The data sets were corrected empirically for absorption using SADABS.[66] The structure was solved using the Bruker SHELXTL software package for the PC, by direct method option of SHELXS. The space group was determined from an examination of the systematic absences in the data, and the successful solution and refinement of the structure confirmed these assignments. All

hydrogen atoms were assigned idealized locations and were given a thermal parameter equivalent to 1.2 or 1.5 times the thermal parameter of the carbon atom to which it were attached. For the methyl groups, where the location of the hydrogen atoms was uncertain, the AFIX 137 card was used to allow the hydrogen atoms to rotate to the maximum area of residual density, while fixing their geometry.

Table 5-8. Crystallographic data for **5-23**.

	4-10·1.5THF
Formula	$C_{76}H_{76}N_4O_{5.5}$
Formula weight	1133.41
Crystal system	Monoclinic
Space group	$P2_1/n$
Z	4
Temp, K	193(2)
D_{calc} gcm^{-3}	1.181
a Å	15.2507(7)
b Å	16.5894(8)
c Å	25.851(1)
α, deg	
β, deg	102.923(1)
γ, deg	
V Å^3	6374.7(5)
μ, mm^{-1}	0.074
Uniq. data coll./obs.	8862/6536
$R_1[I \geq 2\sigma(I)\text{data}]$[a]	0.0804
$wR_2[I \geq 2\sigma(I)\text{data}]$[b]	0.2182

[a] $R_1 = \Sigma||F_o| - |F_c||/ \Sigma| F_o|$
[b] $wR_2 = \{ \Sigma[w (F_o^2 - F_c^2)^2 / \Sigma[w (F_o^2)^2$

Electrochemistry

Electrochemical measurements were made using an EG&G PAR Versa Stat II potentiostat with a Pt disc working electrode, a Pt wire counter electrode, and an aqueous SCE reference electrode (NaCl, 3M) fitted with a Vicor frit as a salt bridge. In all cases, dry, degassed MeOH or CH_2Cl_2 was the solvent, and tetra-n-butylammoniumhexafluorophosphate, at a concentration of 0.10 M, was used for the supporting electrolyte. Ferrocene was added to the cell after each series of measurements to confirm the potential of the reference electrode. The analyte concentration was 2.5(2) mM. All measurements were made at room temperature.

CHAPTER 5
OXIDATIVE TRANSFORMATIONS OF DISPIRO-PORPHODIMETHENES TO NON-PLANAR PORPHYRINS AND SHEET-LIKE PORPHYRINS BEARING LARGE, FUSED EXOCYCLIC RING SYSTEMS

Introduction

The spectroscopy, redox potentials, spin states, electronic spectra, and axial coordination chemistry of metalloporphyrins, chlorins, and related compounds can be modulated through subtle distortions in planarity or the presence of exocyclic ring systems fused to the periphery of the macrocycle. In biological systems, the reactivity and properties of tetrapyrrolic macrocycles are often tuned through combinations of these two factors.[78,96-108] Photosynthetic proteins provide biological examples of tetrapyrroles with both non-planar deformations and exocyclic rings. As illustrated in Figure 5-1, chlorophylls feature a *meso*-, β-fused cyclopentenone ring, which is known to alter the optical and redox properties of the aromatic dihydroporphyrin core. Crystal structures of photosynthetic proteins reveal that almost invariably the macrocycles exhibit non-planar conformations. It has been suggested that these microenvironment-induced distortions fine-tune the redox and photophysical properties of the chromophores, affecting electron-transfer rates within the photosynthetic apparatus.

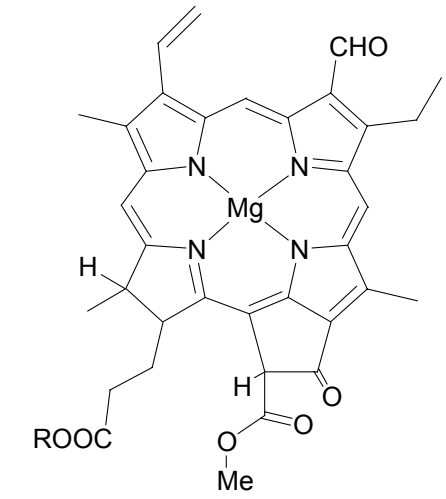

Chlorophyll b

Figure 5-1. Depiction of the structure of chlorophyll b.

An example of the influence of deviations from planarity on the reactivity of heme enzymes is illustrated by the cytochromes P450, which were introduced in Chapter 2 as a paradigm for the impact of local environment about catalytic active sites. In these systems, the binding of the substrate in close proximity to the axial coordination site induces a conformational change in the protein matrix, inducing a distortion from planarity for the heme group (Figure 5-2). This deformation, in conjunction with the concerted loss of water from the axial coordination site, causes the Fe(III) to undergo a transition from 6-coordinate low-spin to 5-coordinate high-spin. Reduction of this complex by 1 e^- generates a 5-coordinate high spin Fe(II) heme, which is predisposed to the binding and activation of $^3O_2$ due to its S = 2 spin state and out-of-plane coordination mode. Subsequent reduction to the peroxo complex and cleavage of the O-O bond by the addition of two protons and loss of water provides the reactive complex, which oxidizes the substrate. Without the conformational change upon substrate binding, the crucial

high-spin Fe(II) species could not be generated, and the rapid binding of $^3O_2$ would not occur due to spin inhibition of the S = 1 ligand with Fe(III) or low-spin Fe(II).

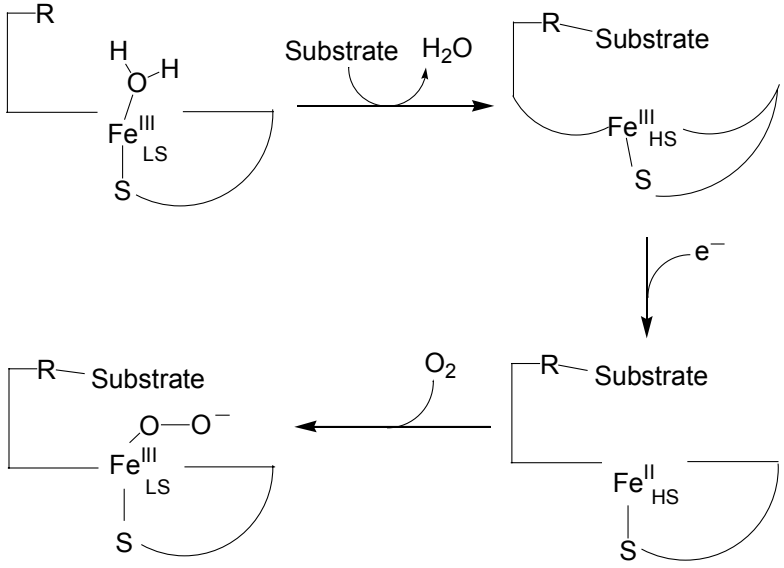

Figure 5-2. Illustration of the initial steps in the catalytic cycle of cytochrome P450 illustrating the importance of non-planar deformations of porphyrins in biological systems.

To help elucidate the origins resulting from modifications to the porphyrin frame, non-planar porphyrins with unusual symmetries as well as porphyrins exhibiting π-delocalization with extremely low-energy electronic transitions and multiple ring system interactions continue to be desirable synthetic targets.[109-113] Along with providing theoretical insight into these biologically relevant but still poorly understood phenomena,[98,114-116] synthetic porphyrins with small energy gaps may find practical utility as novel optical, electronic, or therapeutic materials,[117-119] while non-planar porphyrins with engineered deformations exhibit enhanced properties for a variety of applications such as catalysis[120] and host-guest chemistry.[121] For numerous reasons, dispiro-metalloporphodimethenes are ideal precursors for the preparation of intrinsically non-planar porphyrins with two exocyclic naphthocycloheptenone ring systems via

oxidative rearrangement reaction. Further oxidative dehydrogenation generates exceedingly large, almost perfectly planar porphyrins bearing bis-naphthoazulenone ring systems in high yield, and to the best of our knowledge, these compounds exhibit the longest absorption wavelength reported for monomeric metalloporphyrins.

Results and Discussion

Synthesis Guided by Electrochemistry and Photochemistry

Oxidations of dispiro-porphodimethenes

Reasoning that the conversion from porphodimethenes to porphyrins is a 2e-, 2H+ process and given the considerable driving force for forming the aromatic macrocycle, the electrochemical investigation of **5-1** was undertaken. In this experiment, an irreversible oxidation was observed at 1.41 V vs. Ag/ AgCl. Porphyrins with redox-inactive, late transition metals are known to have less positive first oxidation potentials than their free-base analogues, and in order to lower the potential for the irreversible process observed for **5-1**, the cyclic voltammograms of some metallated derivatives of this ligand were also measured (Figure 5-3 and Table 5-1). These derivatives exhibited lower potential for this process by 0.30(2) – 0.50(2) V. For instance, **5-2** undergoes an irreversible oxidation at 1.08 V vs. Ag/ AgCl. For purposes of comparison, the Cu complex of the tetramethyl porphodimethene, **5-6**, was prepared,[47] and its oxidative electrochemistry was examined (Figure 5-4). In contrast to the irreversible oxidation found for **5-2**, **5-6** undergoes two reversible oxidations at 0.94 and 1.17 V vs. Ag/ AgCl, with potentials similar to, but slightly less positive than the reversible oxidations measured under these conditions for copper tetramesitylporphyrin [Cu(TMP)].

Table 5-1. Oxidative electrochemistry of dispiro-porphodimethenes and related reference compound. † => E ½ for reversible process. * => Not measured. Potentials in V vs. Ag/ AgCl.

Entry	M	Ox (2)	Ox (1)	Red (1)
5-1	H_2		1.41	-1.23†
5-2	Cu		1.08	-1.17†
5-3	Pd		1.05	*
5-4	Zn		0.92	*
5-5	Ni		1.12	*
5-6	Cu	1.17†	0.94†	-1.29†
Cu(TMP)	Cu	1.36†	1.18†	-1.36†

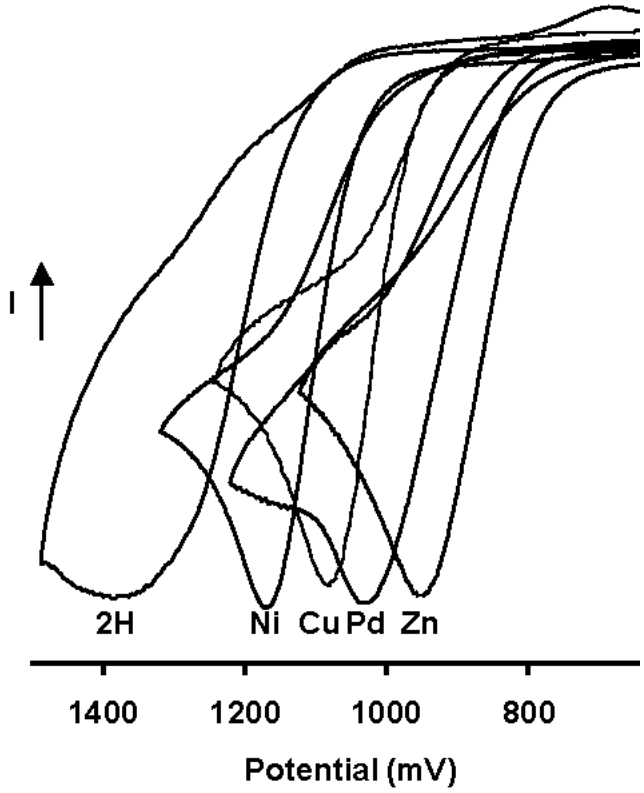

Figure 5-3. Depiction of the cyclic voltammogram of **5-2**.

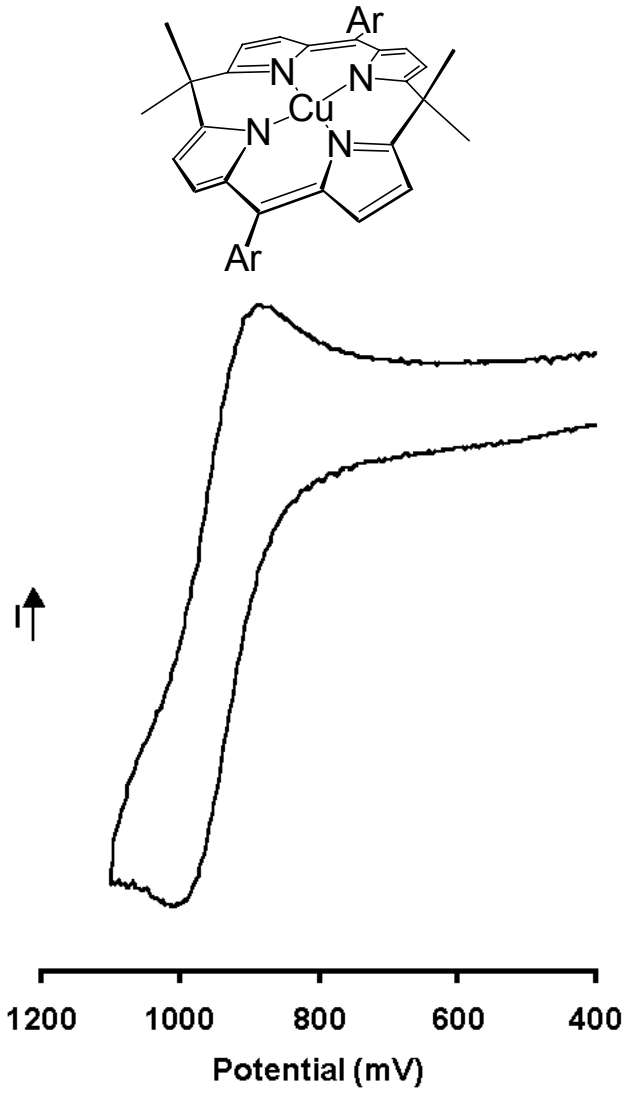

Figure 5-4. Depiction of **5-6** and its cyclic voltammogram.

Based upon the irreversible oxidations observed in the cyclic voltammograms of the dispiro-porphodimethenes and the reversible oxidations observed for the reference compound **5-6**, oxidation reactions of the free-base and metallated dispiro-porphodimethenes were undertaken. Treatment of **5-1** under various oxidative conditions resulted in either no reaction or complex mixtures of products. Reactions of the

metallated derivatives **5-2**, **5-3**, **5-4**, and **5-5** under the same sets of conditions produced mixtures of green products and/ or sparingly soluble dark red products (Figure 5-5).

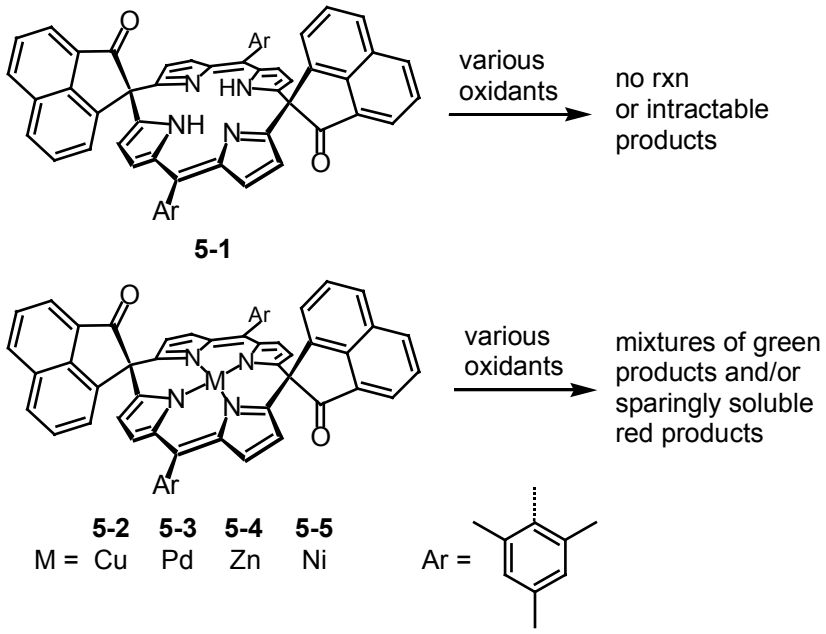

Figure 5-5. Illustration of chemical oxidations of **5-1** and its metallated derivatives.

One oxidation reaction that was attempted in the course of these investigations was the treatment of **5-5** with an ethanolic solution of $FeCl_3 \cdot 6H_2O$ in refluxing toluene (Figure 5-6). This procedure results in the production of an interesting pair of bright green porphyrin enantiomers, **5-7**, bearing naphthocycloheptenone moieties fused to *meso*- and β-positions and 8-methoxycarbonyl functionalized naphthyl groups at the *meso*-positions *trans* to the fused ring systems. The prospect of preparing porphyrins with two, fused-ring systems, such as that found in **5-7**, attracted our attention. Based on the reactivity of ethanol illustrated in Figure 5-6, the synthesis of the desired bis-naphthocycloheptenone porphyrins should require the rigorous exclusion of compounds with ROH functionalities including water.

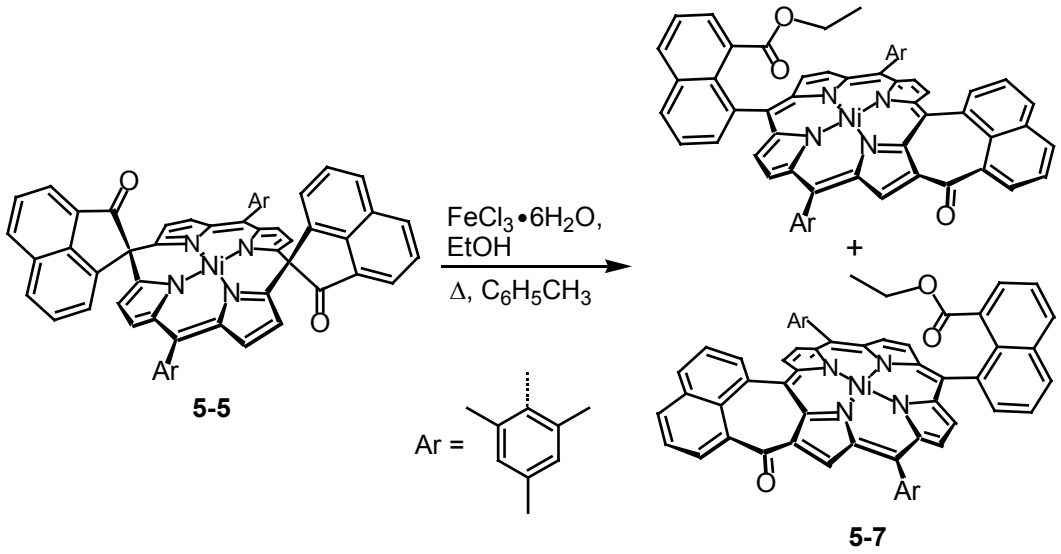

Figure 5-6. Depiction of the oxidative rearrangement and ring opening of **5-5.**

In direct light, solutions of **5-3** are observed to undergo decomposition from their original red-orange color to form compounds similar in color to **5-7**. This transformation is not observed for these solutions when they are protected from irradiation, implying a light-initiated process for the change. Cyclic ketones, especially ones with significant ring-strain, are known to undergo homolytic cleavage of the carbonyl-carbon and α-carbon bond via Norrish Type-I processes.[122] Often this bond homolysis is non-productive, and reformation of the broken bond occurs unless more stable products are accessible by radical processes. Considering the strong driving force for the formation of porphyrins, β-unsubstituted dispiro-porphodimethenes with ketone functionalities adjacent to the spiro-locks appeared to be ideal systems for such rearrangements. By analogy, consider the rearrangement of the hypothetical dispiro-cyclohexadiene depicted in Figure 5-7. Homolytic bond cleavage of this molecule at one of the spiro-locks would generate a diradical, which could then either reform the parent bond or rearrange, as illustrated, to form a more stable product. The oxidative rearrangement of this dispiro-

cyclohexadiene to generate benzene with two fused cyclohexenones is analogous to the formation of porphyrins with exocyclic keto-ring systems from the dispiro-porphodimethenes, but the greater degree of electron delocalization for porphyrins relative to benzene creates an even larger driving force for its formation.

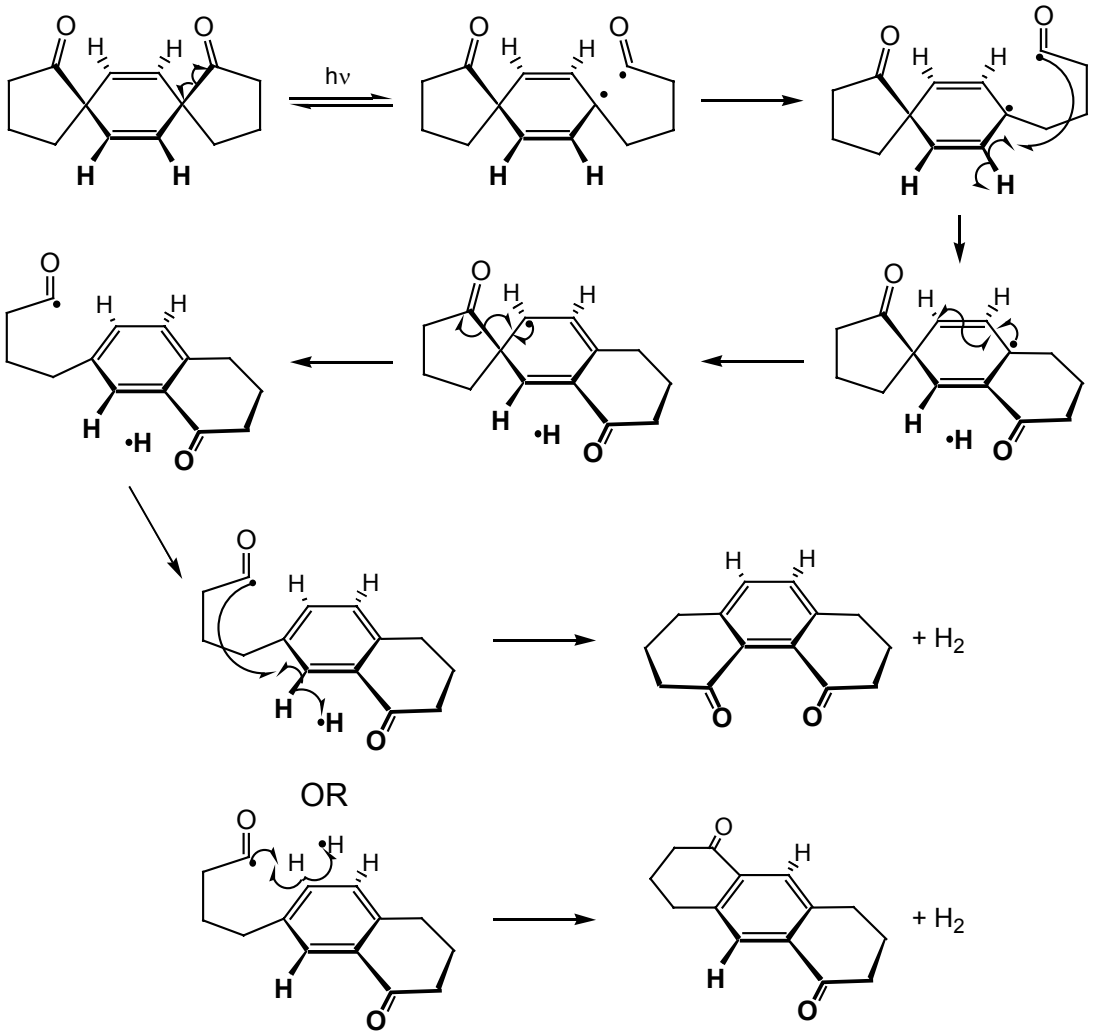

Figure 5-7. Illustration of a plausible mechanism for the oxidative rearrangements of a hypothetical dispiro-cyclohexadiene**.**

Time-course UV-visible spectra upon irradiation of dilute (~0.006 mM) solutions of **5-3** reveal the appearance of broad, rather intense electronic transitions in the low energy region of the spectra and the loss of the visible transition for the porphodimethene

coupled with the emergence of Soret-like features (Figure 5-8). Although the Soret-features have similar energies to and are thus difficult to distinguish from the band observed for **5-3**, the isosbestic points in the UV-region and the evolution of features from 550 – 750 nm clearly imply a transformation, and based upon the low-energy electronic transitions, these reactions produce porphyrin products.

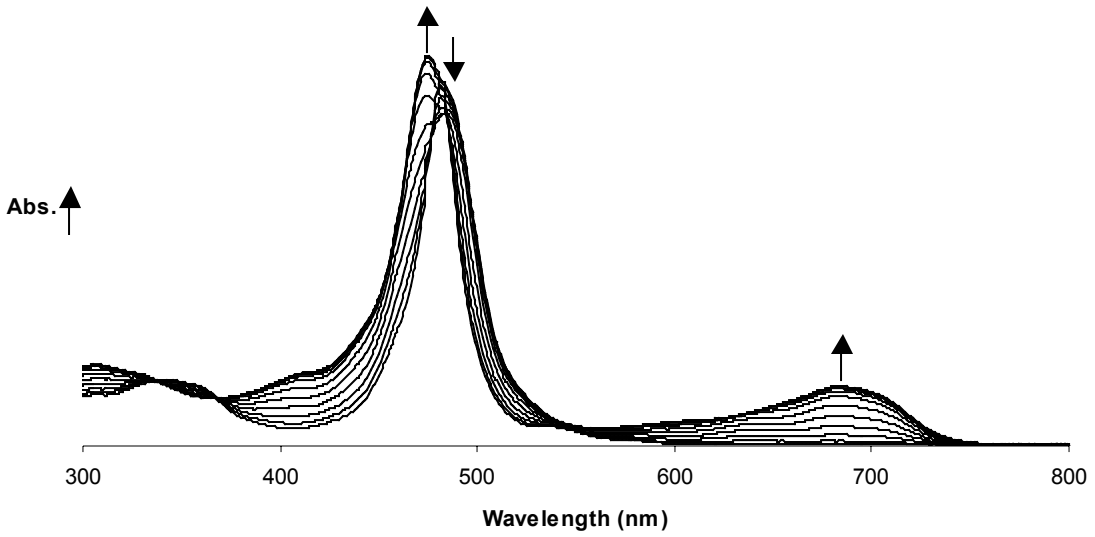

Figure 5-8. Depiction of time-course UV-visible spectra of **5-3** upon measured exposure to a halogen lamp fitted with UV-filter. Measurements recorded after sequential 30 s exposures to the light source.

To further examine this process, photophysical investigations of this and the analogous palladium porphodimethene with two 6-membered rings at the sp^3 *meso*-carbons, **5-3a**, depicted in Figure 5-9 were undertaken.[58] Transient absorption spectra of **5-3** reveal a rapid disappearance of the transient with respect to increasing temperature, and these data were best fitted to a two-component decay, with the decays having lifetimes of 2.2 μs and 360 ns. This situation is in sharp contrast to the temperature-dependant transient absorption measurements for **5-3a**, which were best fit by a one-

component decay with a 2.7 μs lifetime. The additional rapid decay observed for **5-3** has been attributed to the degradative process observed in the exposure-dependant UV-visible spectra. With respect to light reactivity for these two otherwise quite similar complexes, this disparity likely results from the increased ring-strain for the five-membered ketones in comparison to the six-membered ketones in **5-3b**.

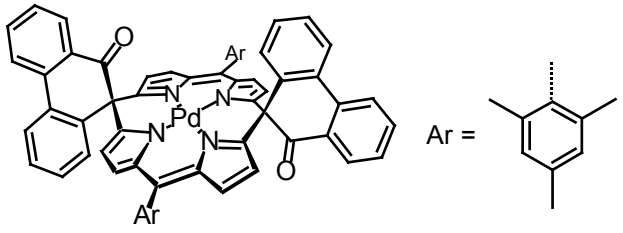

5-3a

Figure 5-9. Depiction of palladium dispiro-porphodimethene bearing 6-membered ketone rings α to the sp^3 *meso*-carbons.

Rearrangement processes that require dehydrogenation should be promoted by oxidants adept at accepting protons and electrons sequentially, such as DDQ, as the formation of DDHQ is more favorable than the formation of H_2 by approximately 0.74 V.[19,123] With this and the other aforementioned issues in mind, reaction conditions employing light activation and an excess of DDQ under anhydrous conditions were envisioned to effect the conversions of dispiro-metalloporphodimethenes to bis-naphthocycloheptenone porphyrins. Treatment of **5-2**, and **5-3** under these conditions generates the *cis*- and *trans*-isomer pairs of porphyrins **5-8**, **5-9**, **5-10**, and **5-11** in high combined yields (Figure 5-10).

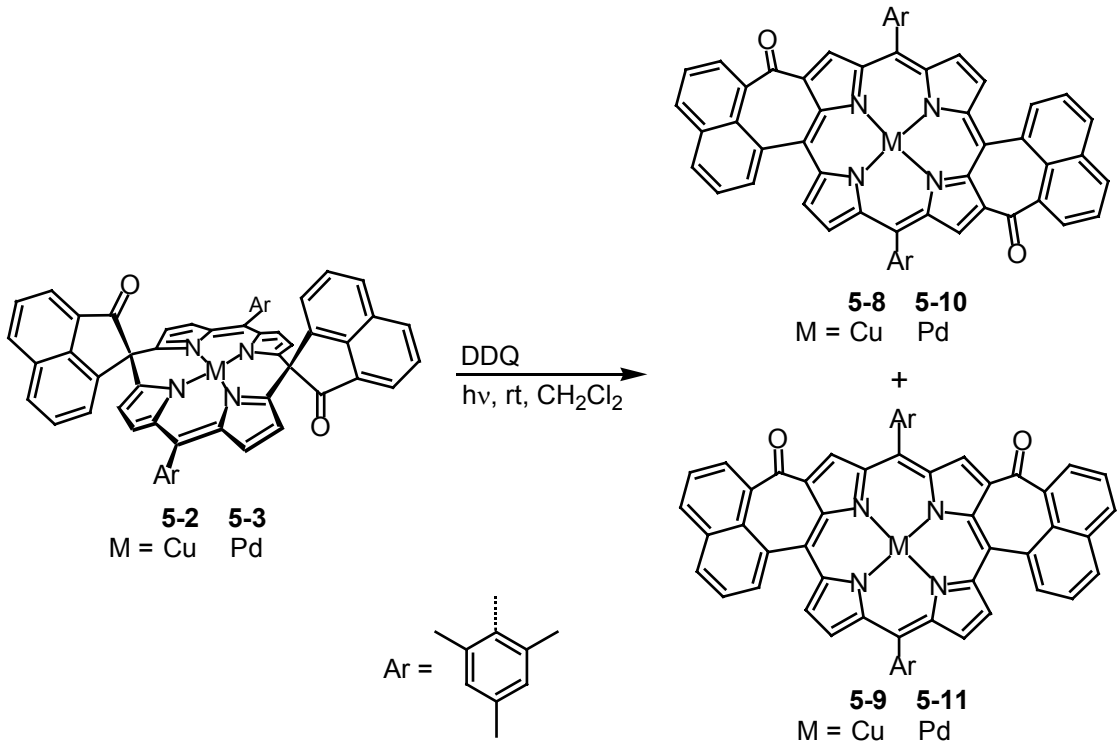

Figure 5-10. Depiction of the light-initiated oxidative rearrangements of metalloporphodimethenes to bis-naphthocycloheptenone metalloporphyrins.

Oxidative dehydrogenations of bis-naphthocycloheptenone metalloporphyrins

In contrast to the two reversible oxidations typical for Cu porphyrin complexes, the cyclic voltammograms of **5-8** and **5-9** each show one reversible oxidation, but at higher potentials these compounds exhibit irreversible oxidations, and the reversibility of the first oxidations diminish, implying that they likely are undergoing chemical transformations. Treatment of **5-8**, **5-9**, **5-10**, and **5-11** with chemical oxidants produces poorly soluble porphyrin products, similar to those obtained from the reactions of **5-2** and **5-3** with oxidants as described in Figure 5-5. In order to enhance the solubility of the porphyrin products, the metalloporphodimethene precursors **5-12**, **5-13**, **5-14**, and **5-15** bearing *t*-butyl groups were prepared as described in Chapter 2.

Treatment of **5-12**, **5-13**, **5-14**, and **5-15** with light and DDQ produces the butylated metalloporphyrins (Figure 5-11), as expected based on the corresponding reactions for **5-**

2 and **5-3**. Chromatographic separation of the isomers results in the *cis*- and *trans*-bis-naphthocycloheptenone porphyrin isomers in high combined yields, ranging from 89 % (**5-16** and **5-17**) to 97 % (**5-22** and **5-23**) (Table 5-2).

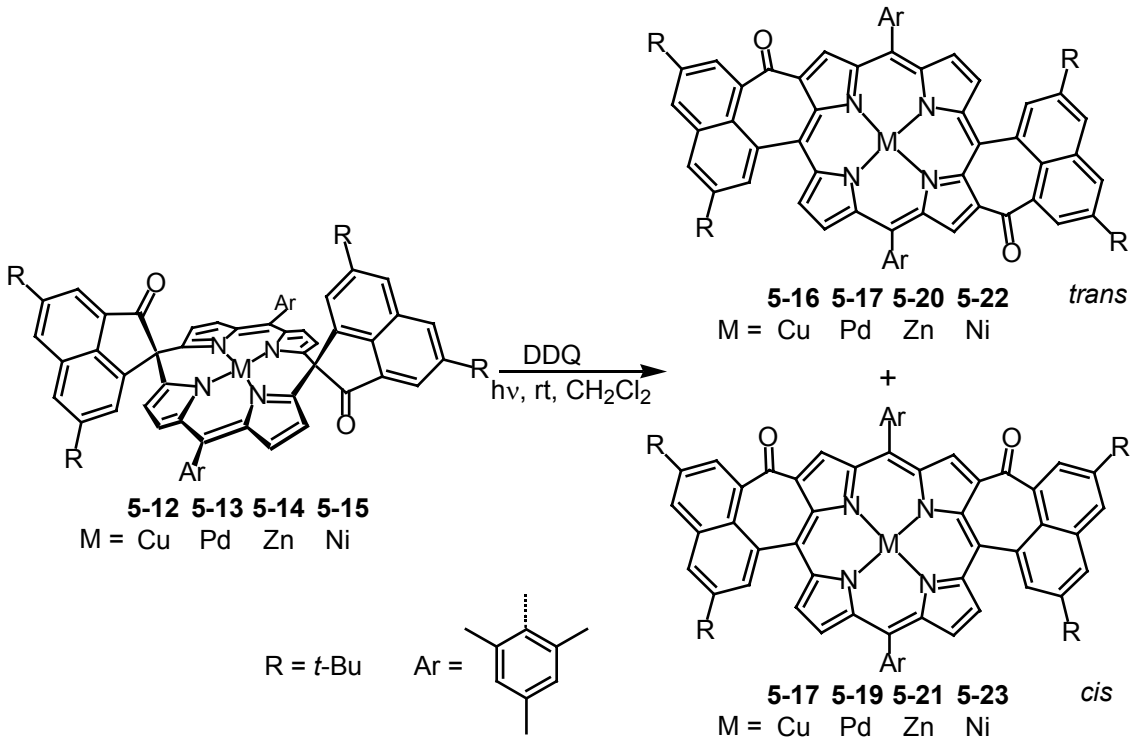

Figure 5-11. Illustration of the synthesis of bis-naphthocycloheptenone metalloporphyrins bearing *t*-butyl groups for enhanced solubility of subsequent products.

As illustrated in Figure 5-12, treatment of **5-17**, **5-19**, **5-21**, or **5-23** with an excess of both DDQ and $FeCl_3 \cdot 6H_2O$ in refluxing CH_2Cl_2, produces the corresponding *cis*-bis-naphthoazulenone porphyrin. Isolation of these porphyrins requires only aqueous work-up, filtration over silica, and recrystallization. The *trans*-isomers can similarly be generated from the corresponding *trans*-bis-naphthocycloheptenone porphyrins. Compared to the conversion of the *cis*- isomers, reaction times are longer for the *trans*-isomers, and the procedure requires additional equivalents of the oxidants. The excess of oxidants coupled with the exceptionally low first oxidation potential for these porphyrins

necessitates the use of a reductive work-up procedure, and aqueous $NaBH_4$ works well for this purpose.

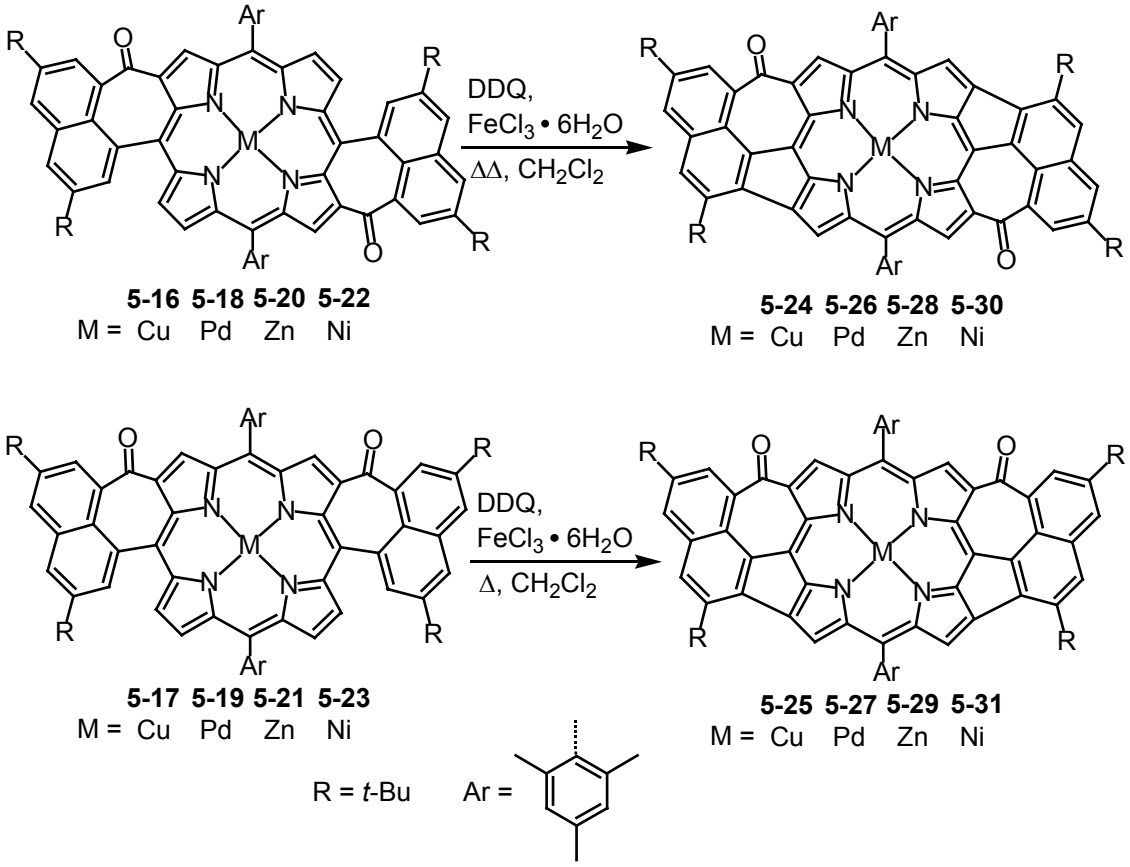

Figure 5-12. Depiction of the oxidative dehydrogenation of bis-naphthocycloheptenone metalloporphyrins to generate large sheet-like porphyrins.

If the *trans*-isomers are treated under the conditions described for the *cis*-isomers, partially oxidized porphyrins bearing both naphthocycloheptenone and naphthoazulenone fused ring systems are isolated. The palladium complex of this asymmetric porphyrin, **5-32**, was isolated in good yield (Figure 5-13). Further oxidation of this intermediate to **5-26** does not occur to an appreciable extent until all of the starting material has been converted to **5-32**, likely due to the higher oxidation potential for this intermediate in comparison to the starting material, **5-16**.

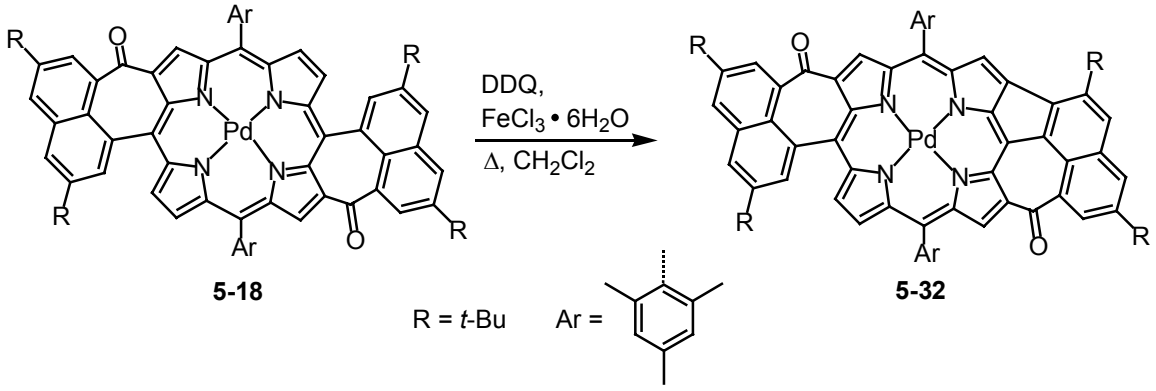

Figure 5-13. Depiction of the oxidative dehydrogenation of bis-naphthocycloheptenone metalloporphyrins to generate large sheet-like porphyrins.

The two oxidative processes depicted in Figures 5-11 and 5-12 can be performed in one pot, generating a mixture of porphyrin isomers directly from the metalloporphodimethenes. Likely owing to the degradation of the *cis*- bis-naphthoazulenone porphyrins under the more severe conditions required to effect the complete transformation of the *trans*-isomers, the combined yields for the two-step, one-pot procedure were lower than for the step-wise approach. Furthermore, chromatographic resolution of the isomer pairs is considerably more facile for the bis-naphthocycloheptenone porphyrins in comparison to the bis-naphthoazulenone porphyrins, making the two-step procedure the preferred method with respect to isolating these compounds.

An initial attempt to oxidatively dehydrogenate **5-19** using $FeCl_3 \cdot 6H_2O$ in refluxing benzonitrile was successful with respect to the two cyclizations (Figure 5-14), but these harsh reaction conditions result in the chlorination of one of the naphthyl carbons, as demonstrated by the solid-state structure of **5-27a** (Figure 5-15). Treatment with $FeCl_3 \cdot 6H_2O$ in other solvents at lower reaction temperatures did not afford the desired products, and DDQ alone under various reaction conditions was also found to be

ineffective. While oxidative biaryl-coupling reactions utilizing $FeCl_3$ or DDQ as an oxidant are common,[124] it seems the only report of their use in combination involved the deprotection of methoxy phenyl methyl esters using catalytic amounts of DDQ with excess $FeCl_3$.[125] In this system, Fe(III) regenerates the active oxidant from its reduced form (DDHQ). DDQ in conjunction with other metal salts such as $Sc(OTf)_3$ will induce the oxidative coupling of triarylporphyrins to generate coplanar diporphyrins,[126] and although the $Sc(OTf)_3$/ DDQ procedure was not attempted for the oxidation of bis-naphthocycloheptenone metalloporphyrins, numerous other reagents and conditions were tested. None of these trials produced the desired products in yields as high as the $FeCl_3$/ DDQ procedures described herein, and isolation of the porphyrins was often more problematic.

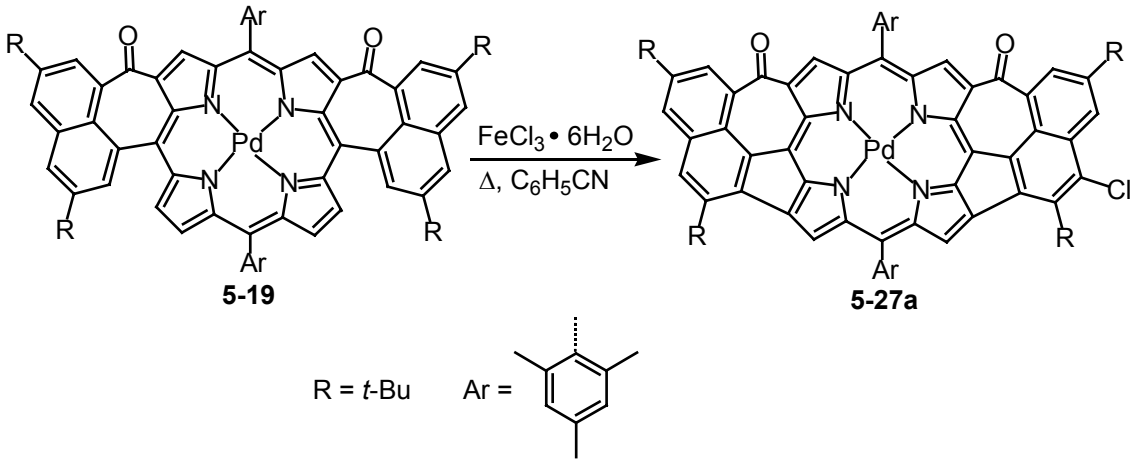

Figure 5-14. Depiction of the over-oxidation of **5-19** to producing the undesired chlorinated compound **5-27a**.

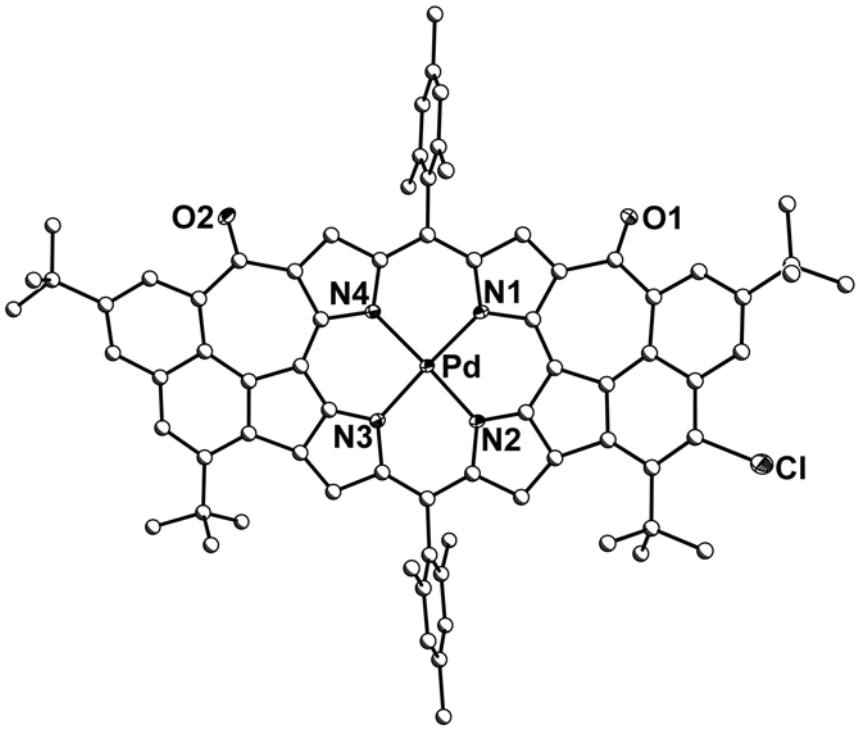

Figure 5-15. Diagram of the solid-state structure of **5-27a**. Carbon atoms depicted with arbitrary radii, all other atoms represented as 30 % ellipsoids. Hydrogen atoms omitted for clarity.

Demetallation of the *cis*-zinc derivative, **5-29**, was accomplished by treatment with concentrated HCl in $CHCl_3$ at room temperature overnight (Figure 5-16). Standard aqueous workup and column chromatography afforded **5-33** in reasonable yield. Demetallation of the related *trans*-isomer **5-28** was achieved via treatment with TFA, producing **5-34** in good yield, without the need for column chromatography.

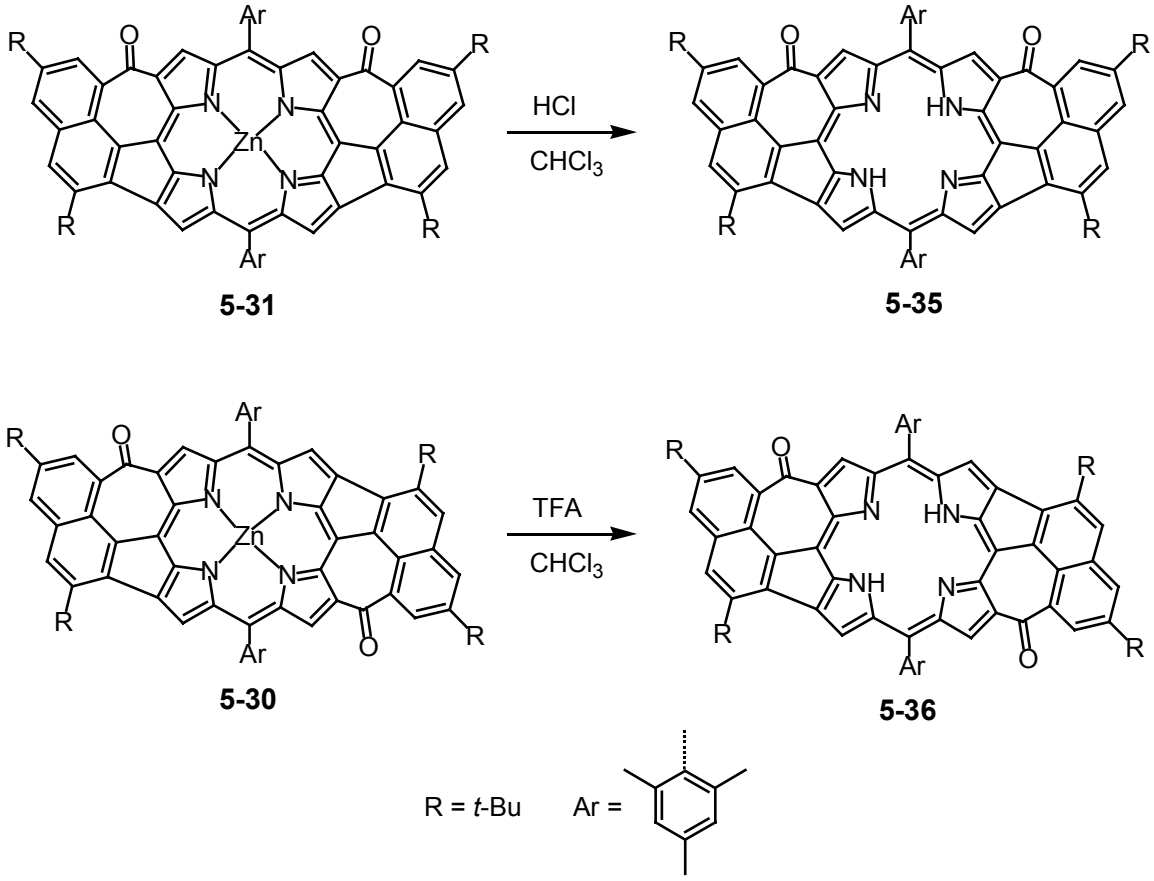

Figure 5-16. Illustration of the demetallation reactions to provide the metal-free bis-naphthoazulenone porphyrins **5-35** and **5-36**.

Characterization of Porphyrins with Exocyclic Ring-Systems

Electronic absorption spectra

The Soret bands in the UV/ visible spectra of the bis-naphthocycloheptenone porphyrins are bathochromically shifted in comparison to metal complexes of tetraphenylporphyrin, ranging from 466 nm (**5-10**) to 490 nm (**5-17**). The low energy electronic transitions for these porphyrins are also red-shifted (652 nm for **5-11** - 705 nm for **5-24**) as well as broad and intense (log ε = 4.6) in comparison to the Q-bands found for typical metalloporphyrins (Figure 5-17). For all isomer pairs studied thus far, the *trans*-isomer has a higher energy Soret-band and lower energy Q-bands than the related *cis*-isomer (Table 5-2).

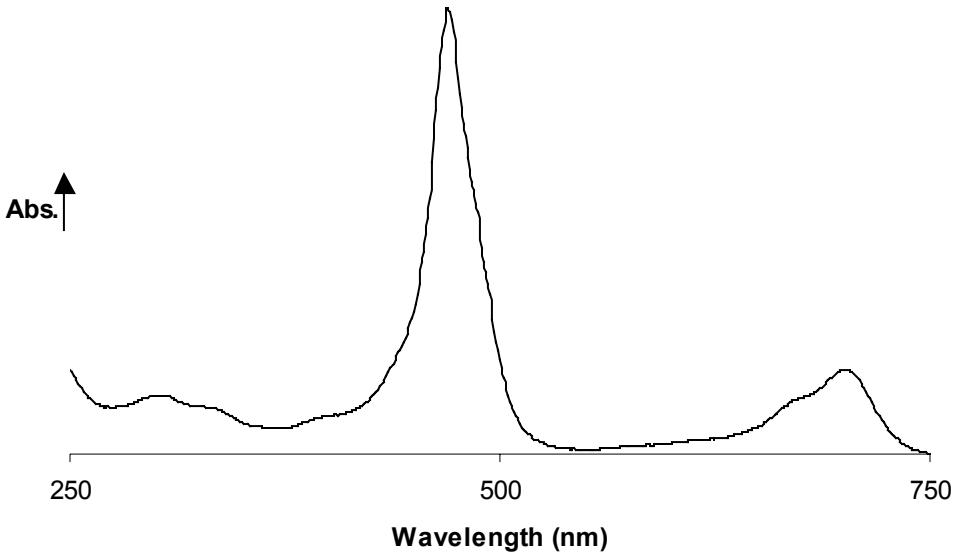

Figure 5-17. Depiction of the UV/ visible spectrum of **5-10**.

Table 5-2. Summary of the yields and spectrophotometric data of porphyrins bearing naphthocycloheptenone ring systems (refer to Figures 5-6, 5-10, and 5-11 for structural depictions).

Entry	R	M	Isomer	Yield	Combined Yield	λ (log ε)	λ (log ε)
5-7	H	Ni	n/a	74 %	n/a	468 (5.4)	678 (4.5)
5-8	H	Cu	*trans*	36 %	95 %	470 (5.2)	700 (4.5)
5-9	H	Cu	*cis*	59 %		488 (5.2)	678 (4.5)
5-10	H	Pd	*trans*	37 %	96 %	466 (5.3)	674 (4.6)
5-11	H	Pd	*cis*	59 %		483 (5.4)	652 (4.6)
5-16	*t*-Bu	Cu	*trans*	32 %	89 %	473 (5.3)	705 (4.6)
5-17	*t*-Bu	Cu	*cis*	57 %		490 (5.3)	681 (4.6)
5-18	*t*-Bu	Pd	*trans*	32 %	94 %	470 (5.4)	678 (4.7)
5-19	*t*-Bu	Pd	*cis*	62 %		486 (5.4)	656 (4.6)
5-20	*t*-Bu	Zn	*trans*	35 %	94 %	473 (5.4)	715 (4.7)
5-21	*t*-Bu	Zn	*cis*	59 %		489 (5.4)	688 (4.6)
5-22	*t*-Bu	Ni	*trans*	32 %	97 %	476 (5.2)	692 (4.7)
5-23	*t*-Bu	Ni	*cis*	65 %		494 (5.1)	672 (4.5)

The UV/ visible/ near-IR spectra of the bis-naphthoazulenone porphyrins reveal numerous exceptional features, including low energy (Q-type) absorptions with dramatic bathochromic shifts in comparison to typical metalloporphyrins. All of these porphyrins have a band at ~ 450 nm, while the location of the other transitions are metal dependant, with copper species having spectra further red-shifted than their palladium analogs. Otherwise, the shapes of the spectra are very similar for each isomer, regardless of the metal incorporated. For both the *cis*- and *trans*- isomers, the most intense absorption band (log ε = 4.9) occurs in the visible region [540-579 nm (Figure 5-18, Table 5-3)], and these bands approach the record low energy Soret absorption of 625 nm noted by Lash and coworkers.[115] In addition to the aforementioned high-energy bands, the *cis*-isomers exhibit rather intense (log ε = 4.2) Q-like features from 846 nm for **5-31** to 923 nm for **5-29** (Figure 5-19, Table 5-3).

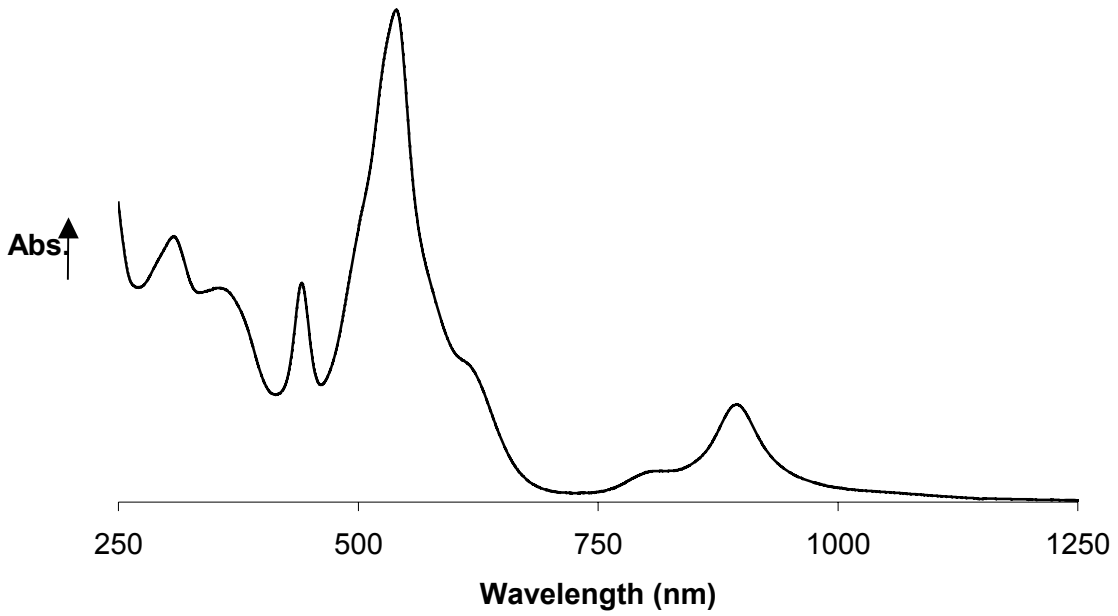

Figure 5-18. Depiction of the UV/ visible spectrum of **5-29**.

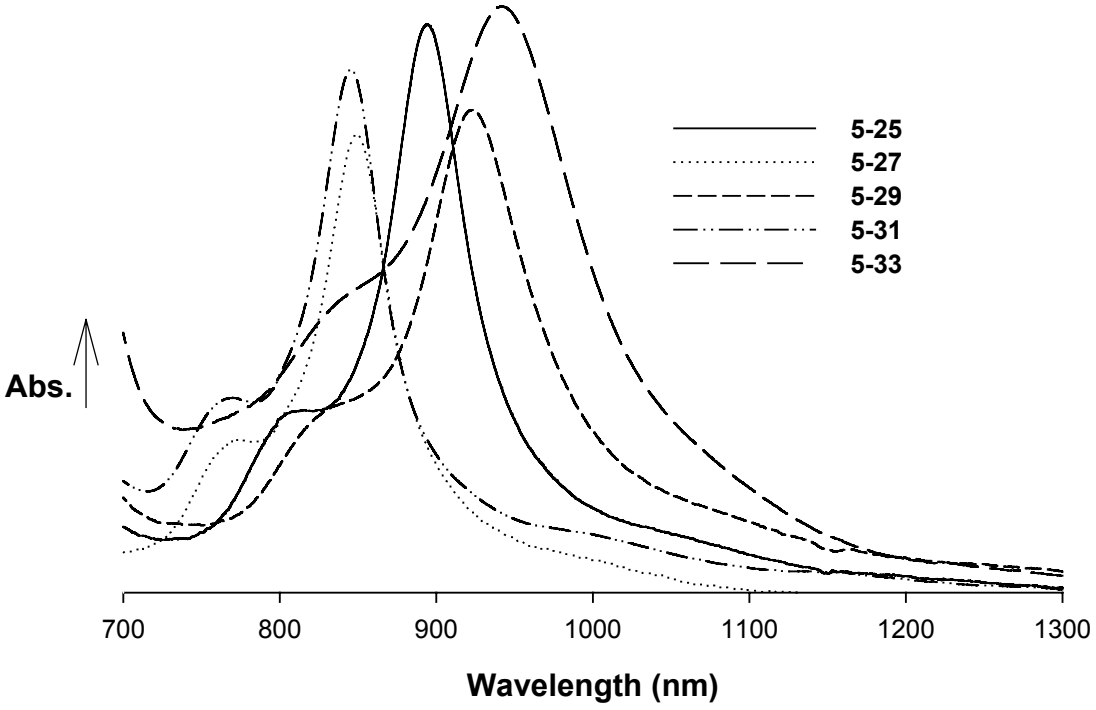

Figure 5-19. Illustration of the metal dependence for the near-IR transitions of the *cis*-naphthoazulenone porphyrins. Absorptions not normalized for concentrations.

The *trans*-isomers have visible regions that are red-shifted and have more features in comparison to their *cis* counterparts, and their Q-like bands exhibit extreme bathochromic shifts and they are split into two less intense transitions in the near-IR region. The low-energy bands for **5-28** are found at 1060 nm and 1228 nm (Figure 5-20). As observed for the *cis*-isomers, the energies of the near-IR transitions are metal-dependant (Table 5-3). Although triply-fused, multi-porphyrin tapes have been shown to reach further into the IR,[126-128] the extremely red-shifted transitions observed for **5-28** are, to the best of our knowledge, the lowest energy electronic transitions ever observed for a monomeric porphyrin species by at least 200 nm.

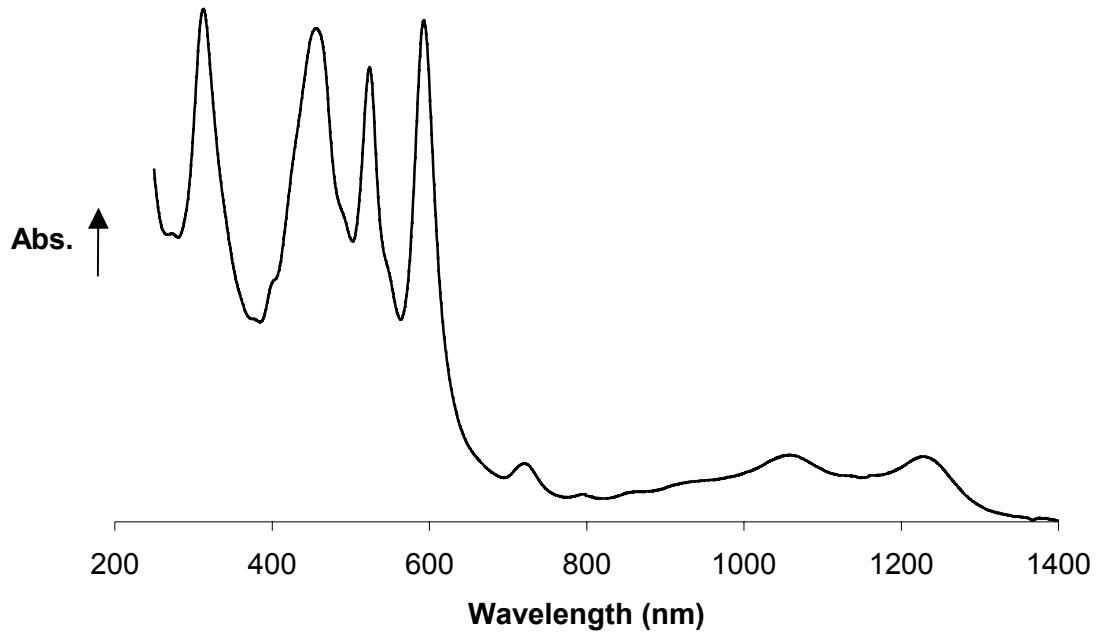

Figure 5-20. Depiction of the UV/ visible/ near-IR spectrum of **5-28**.

Table 5-3. Summary of the yields and selected spectrophotometric data of porphyrins bearing naphthoazulenone ring systems. λ given in nm, sh => shoulder.

Entry	M	Isomer	Yield	λ (log ε)	λ (log ε)	λ (log ε)	λ (log ε)	λ (log ε)
5-24	Cu	*trans*	90 %	449 (4.8)	519 (4.7)	579 (4.9)	1038 (3.9)	1204 (3.9)
5-25	Cu	*cis*	98 %	441 (4.8)		540 (4.9)	804 (sh)	894 (4.2)
5-26	Pd	*trans*	92 %	445 (4.7)	522 (4.5)	567 (4.9)	994 (3.8)	1145 (3.8)
5-27	Pd	*cis*	96 %	445 (4.8)	524 (sh)	553(4.9)	768 (sh)	850 (4.2)
5-28	Zn	*trans*	74 %	456 (4.9)	524 (4.9)	593 (4.9)	1060(4.0)	1228 (4.0)
5-29	Zn	*cis*	89 %	445 (4.7)		546 (5.1)	833 (sh)	923 (4.3)
5-30	Ni	*trans*	74 %	447 (4.8)	507 (4.7)	564 (4.9)	1038 (4.2)	1147 (3.9)
5-31	Ni	*cis*	89 %	454 (4.8)	513 (4.8)	558 (4.8)	763 (sh)	846 (4.2)
5-32	Pd	*trans*	82 %	464 (5.0)	515 (4.8)	577 (4.7)	646 (4.0)	825 (4.0)
5-33	2H	*cis*	85 %	437 (4.7)		541 (5.0)	879 (sh)	923 (4.2)
5-34	2H	*trans*	87 %	430 (4.8)		582 (4.5)	856 (3.8)	1101 (3.9)

Structural characterization

^{1}H NMR spectra of the naphthocycloheptenone and naphthoazulenone porphyrins provide substantial insight into the structures of these porphyrin products. The two

carbonyl moieties on the periphery of these macrocycles profoundly alters the electron distribution about the conjugated fused-ring systems, potentiating the shielding for the protons in the aromatic region. The mesityl methyl and naphthyl *t*-butyl groups act as convenient handles for removing the complex coupling patterns typically observed for such complex aromatic systems. Other than the pairs of β-pyrrole positions in the naphthocycloheptenone porphyrins, no hydrogen atoms in **5-16** –**5-34** have any hydrogens on neighboring carbons, allowing for only *meta*-coupling. The small *J* values for the coupling typically observed for the naphthyl resonances actually aids in their identification, while not causing complexity in their spectra. The degeneracies observed for the mesityl methyl resonances imply the symmetries of the macrocycles, and their chemical shifts provide insight into the degree of non-planarity for the ring system, due to the strong influence of the ring currents on these resonances, which cause dramatic changes for their chemical shifts based upon their proximity to the macrocyclic core (Figure 5-21).

In the solid-state, the *trans*, non-planar porphyrin, **5-10**, adopts an *anti* configuration with respect to the carbonyl groups of the cycloheptanone moieties (Figure 5-22). Steric clash of naphthyl [C22, C33] and pyrrolic [C7, C17] hydrogens induces a distortion in the macrocycle, resulting in a mean deviation of 0.32 Å for the 20 carbon atoms in the porphyrin core from the average plane defined by the four nitrogen atoms. As depicted by the histogram in Figure 5-23, the macrocycle exhibits a classic, ruffled $B1_u$ deformation with the *meso*-carbon atoms displaced alternately above and below this N-normal plane.

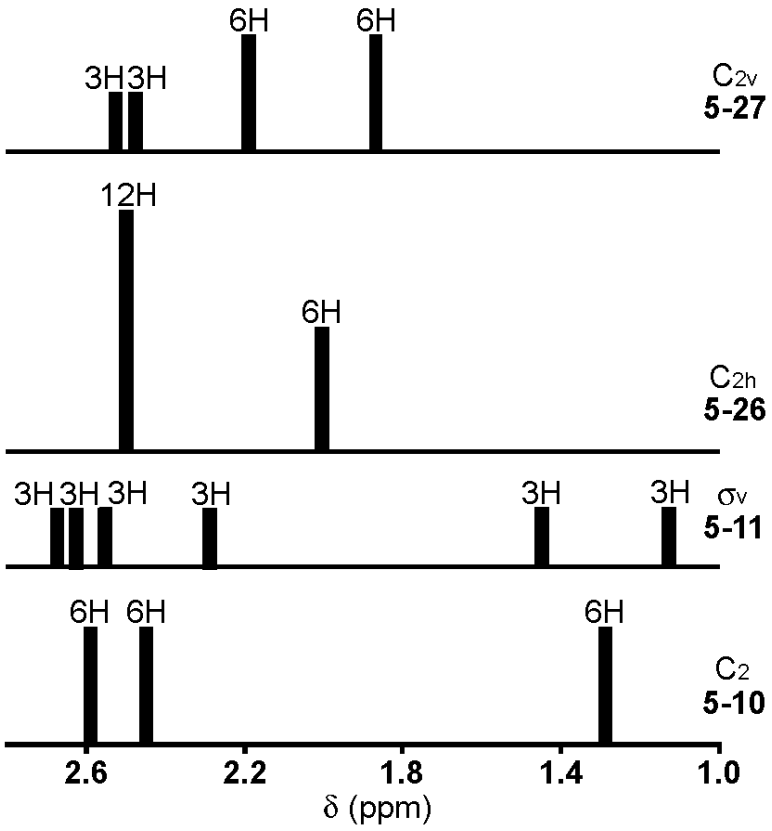

Figure 5-21. Illustration of the symmetry-based changes observed for the mesityl methyl resonances in the ^{1}H NMR spectra of palladium porphyrins with bis-exocyclic ring systems (highest plausible symmetry implied by spectrum indicated above compound number).

As illustrated by Figure 5-24, **5-11** adopts a non-planar conformation in the solid-state, consistent with the asymmetry observed in the ^{1}H NMR spectrum of this compound at room temperature. While the mode of distortion for **5-11** is similar to that observed for **5-10**, it is not truly ruffled by the classical definition. Although the *meso*-carbons are located alternately above and below the plane containing the four nitrogens, the angles of the bonds joining the two β-carbon atoms on opposite pyrroles (for example C7-C8 and C17-C18) and the N-normal plane do not have a C_2-operation, eliminating the $B1_u$ symmetry classification. This deformation is actually quite atypical for the porphyrin

ring system, and is not consistent with the symmetry equivalent, $B2_u$, saddle deformation either, as this mode places the *meso*-carbon atoms in the N-normal plane with the pyrrole moieties alternating above and below this plane.

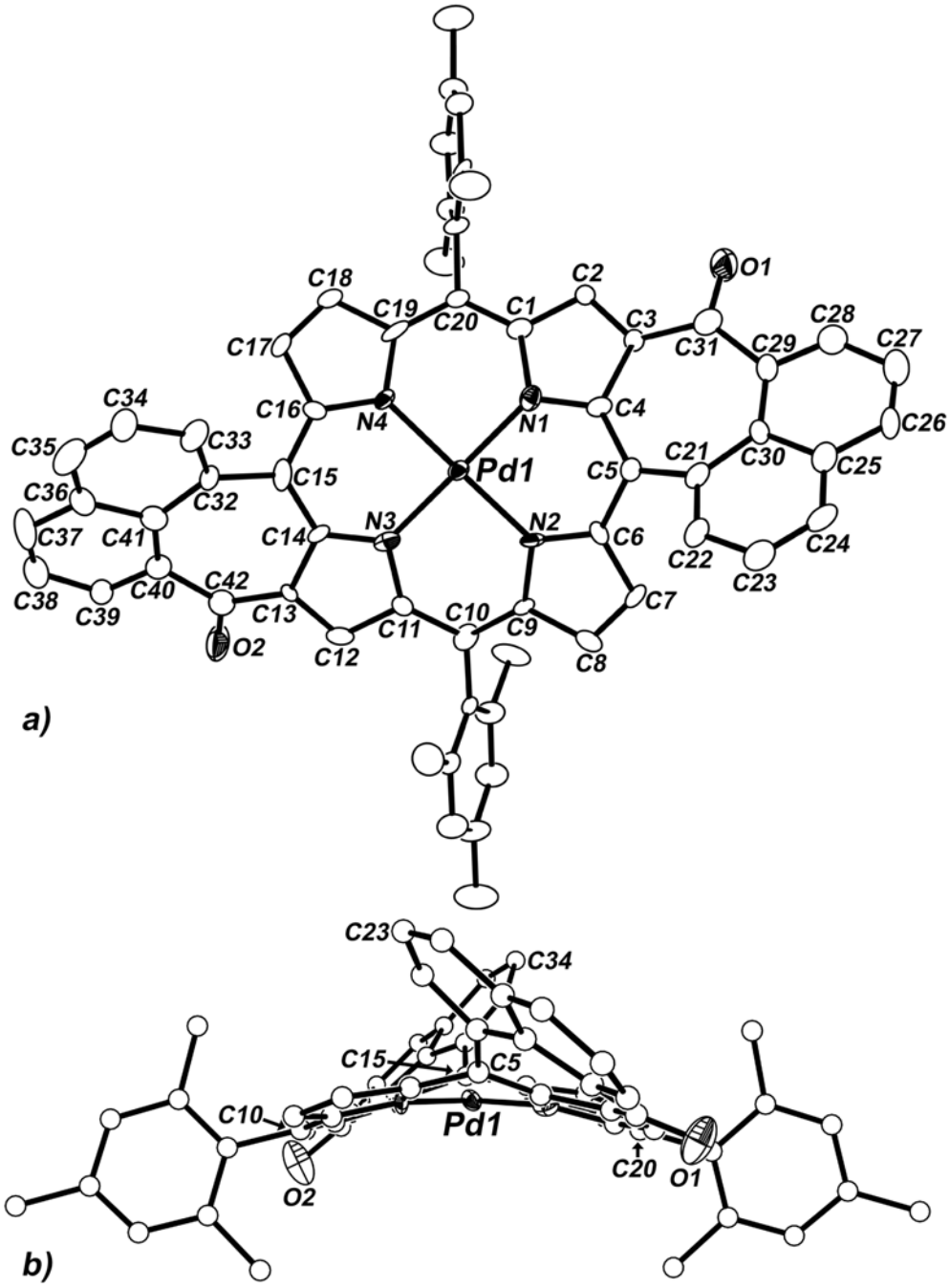

Figure 5-22. Diagram of the X-ray structure of **5-10**. a) Top view (ellipsoids at 30 % probability). Hydrogen atoms have been omitted for clarity. b) Side view of **5-10** (arbitrary radii for carbon atoms).

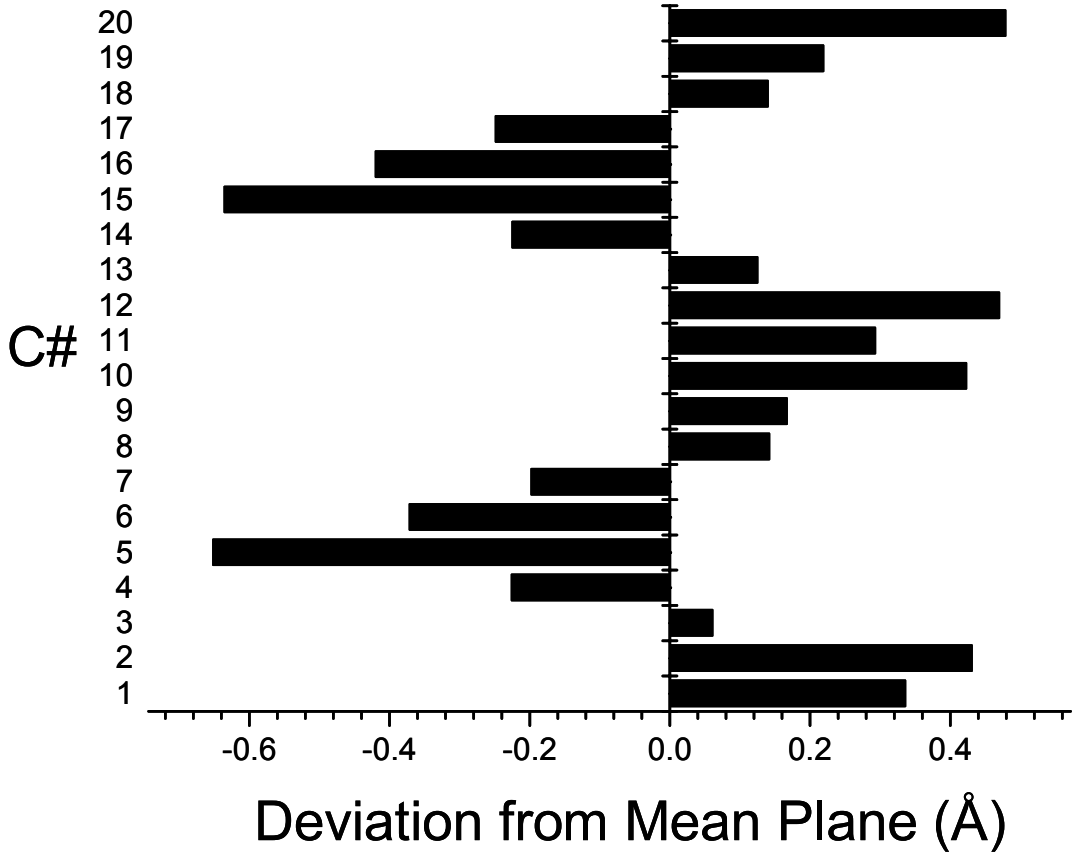

Figure 5-23. Histogram illustrating the displacement of the core carbon atoms from the N-normal plane of **5-10** illustrating the ruffled deformation of the macrocycle.

The mean deformation of **5-11** is not as pronounced as that found for **5-10**, resulting in an average deviation of 0.25 Å for the 20 core carbon atoms from the N-normal plane. The angle between the N-normal plane and the two average planes containing the naphthyl moieties are 37.9(2)^{o} and 38.5(2)^{o}, with C23 having the largest displacement [2.930(6) Å] from the mean plane defined by the coordinated palladium and all of the fused sp^2 atoms in the polycyclic ring system. The palladium is situated 0.457(5) Å below the plane defined by the 20 core carbon atoms.

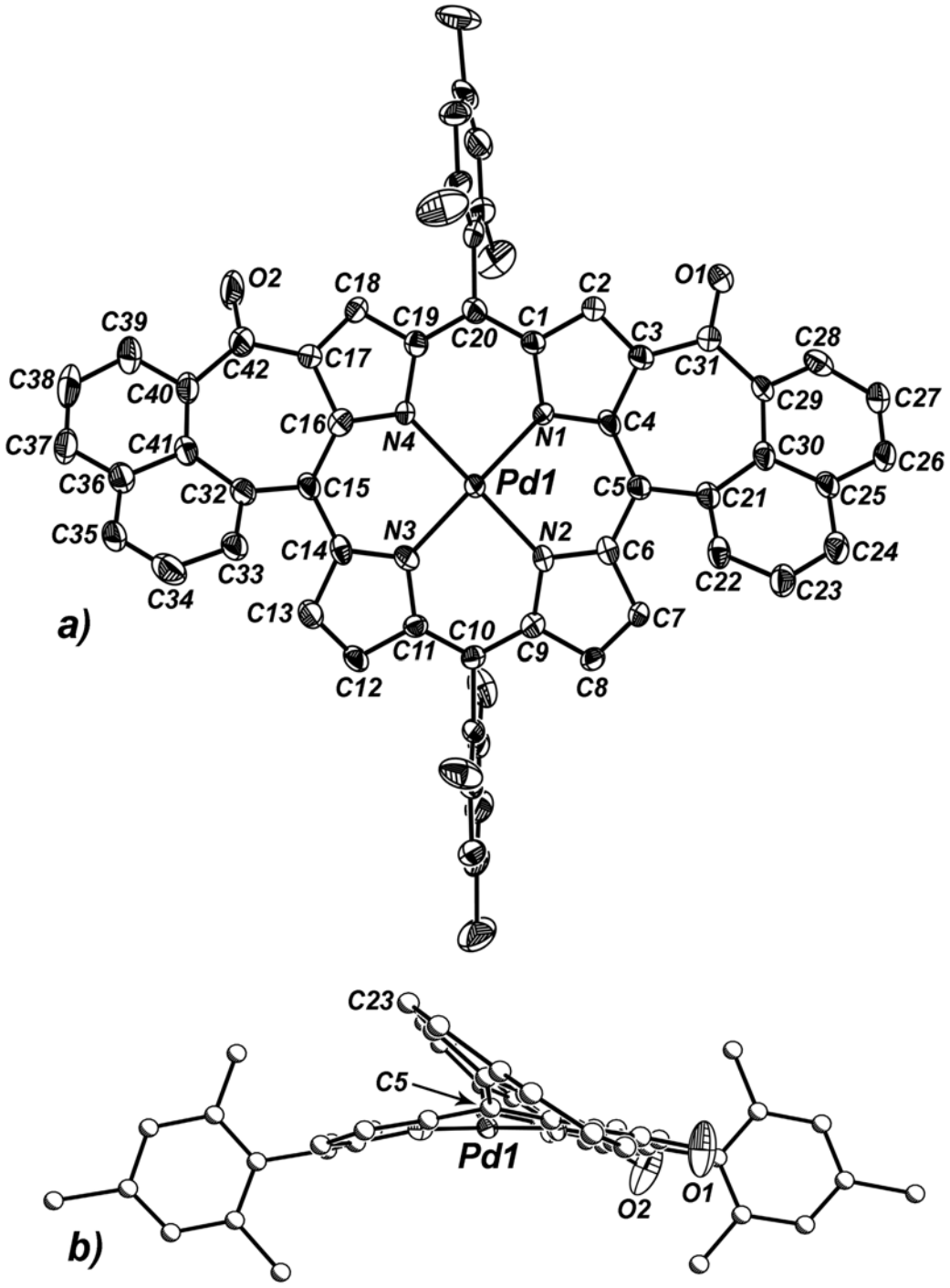

Figure 5-24. Diagram of the X-ray structure of **5-11**. a) Top view (ellipsoids at 30 % probability). b) Side view of **5-11** (arbitrary radii for carbon atoms). Hydrogen atoms omitted for clarity.

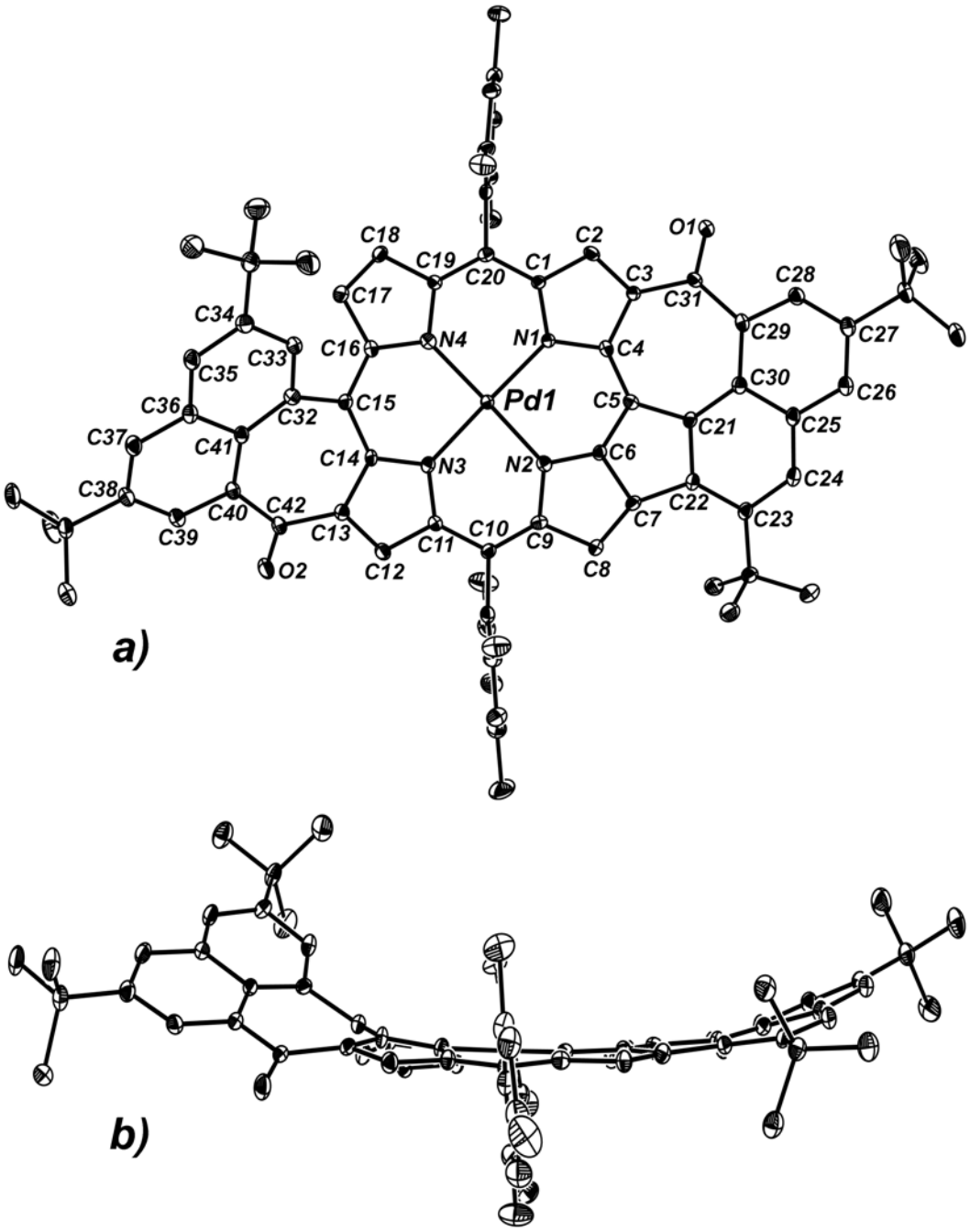

Figure 5-25. Diagram of the X-ray structure of **5-32** (30 % ellipsoids). a) Top view and b) side view. Hydrogen atoms have been omitted for clarity.

Compound **5-32** adopts an extremely non-planar structure in the solid-state (Figure 5-25). The C_i symmetry apparent in the X-ray structure is consistent with the four distinct *t*-butyl and six mesityl methyl signals observed in its ^{1}H NMR spectrum. Non-planar distortions and the delocalization of electron densities through the fused ring systems likely contribute to the bathochromic shifts observed in the electronic absorption spectra of the porphyrins bearing naphthocycloheptenone moieties. Complete oxidation to the bis-naphthoazulenone porphyrins relieves the distortion from planarity as, illustrated in Figure 5-26, but the degree of delocalization through the ring system is increased, producing greater bathochromic shifts, and smaller differences in primary redox potentials.

Single crystals suitable for X-ray diffraction were obtained by the slow diffusion of diethyl ether into a saturated CH_2Cl_2 solution of **5-25**, providing purple plates with a green metallic luster. X-ray diffraction structural analysis reveals a relatively planar porphyrin interior, with a mean deviation of only 0.08(6) Å for the 20 carbon atoms in the porphyrin core from the average plane defined by the four nitrogens (Figure 5-27). The naphthyl moieties on the periphery of the ring system deviate only slightly from this nitrogen plane with a mean deviation of 0.27(16) Å for the 22 carbon atoms in the two naphthyl groups (max deviation 0.532 Å for C26), and these minor deviations are likely induced by packing forces in the solid state. Interestingly, the largest displacement (0.78 Å) from the N4 plane in the macrocyclic core structure is found at one of the carbonyl oxygens, O2. Many unusual bond angles are found in this ring system, which, discounting *t*-butyl and mesityl aryl groups, contains 49 non-hydrogen nuclei arranged as eight 6-, six 5-, and two 7-membered rings, interlocked in a highly delocalized π-system,

with two carbonyls in the plane of hybridization. Among the 42-sp^2 carbons in the porphyrin plane, 17 have a bond angle of 110° or less, and 9 have a bond angle of 130° or more, with extremes represented at the C7 and C13 vertices [C8-C7-C6: 104.5°(2); C8-C7-C22: 149.8°(2)]. The distance from the two most separated sp^2 carbon atoms in the sheet-like macrocycle is 1.69 nm.

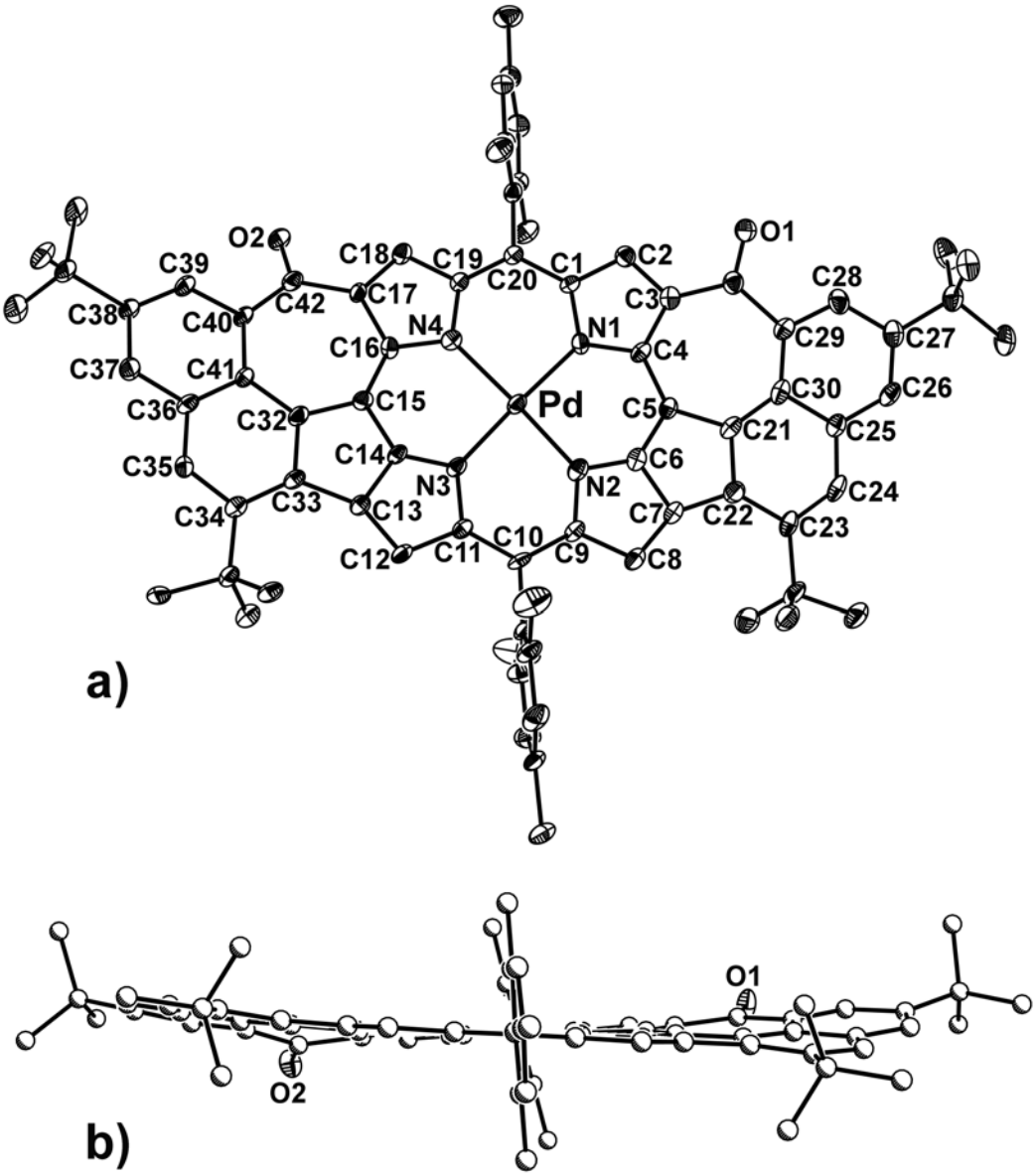

Figure 5-26. Diagram of the X-ray structure of **5-27** . a) Top view (ellipsoids at 30 % probability) and b) side view (arbitrary radii for carbon atoms). Hydrogen atoms omitted for clarity.

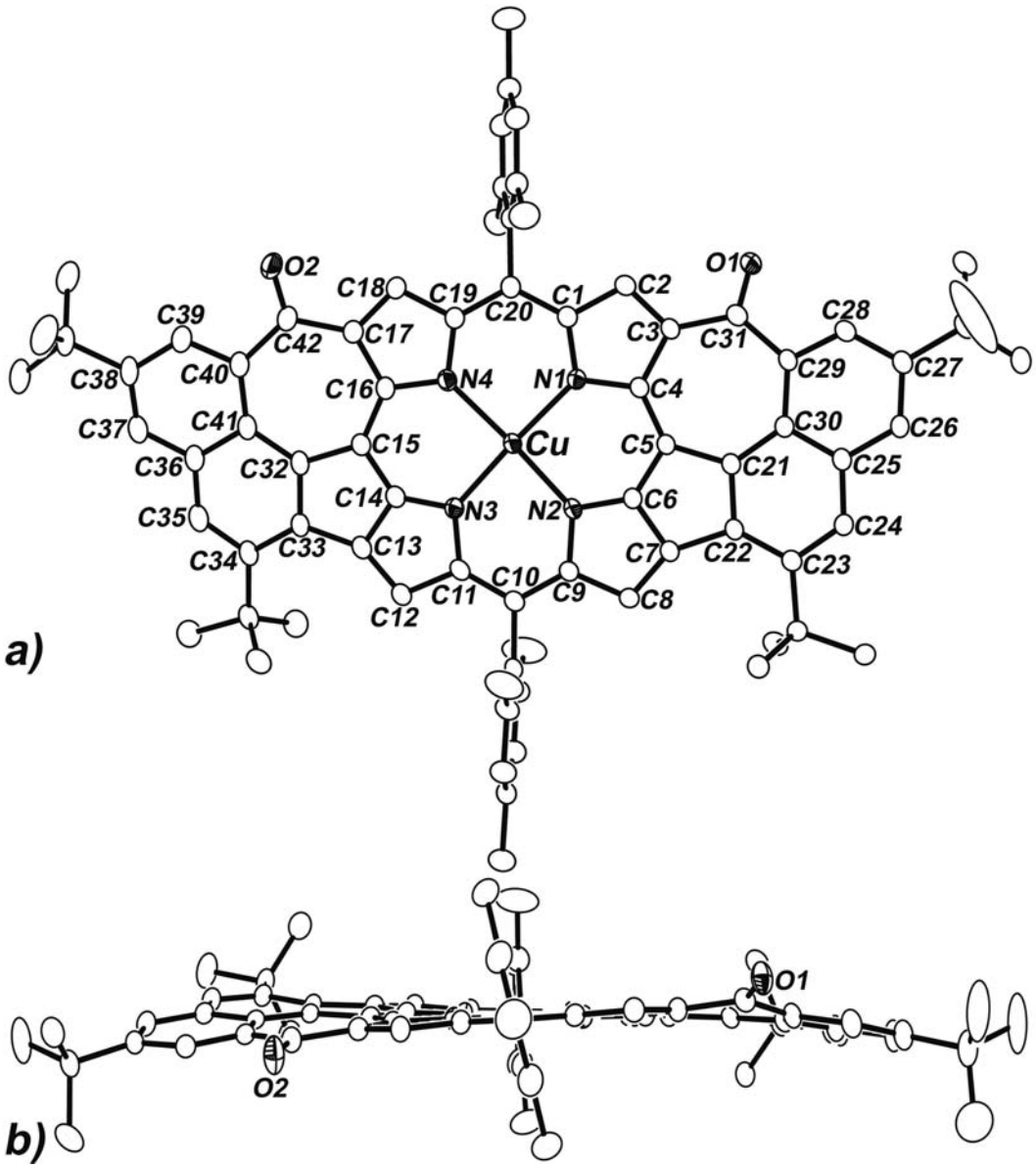

Figure 5-27. Diagram of the X-ray structure of **5-25** (30 % ellipsoids). a) Top view and b) side view . Hydrogen atoms have been omitted for clarity.

As illustrated in Figure 5-28, the metal-free porphyrin, **5-33**,retains the planar situation observed for **5-25** and **5-32**in the solid state. Among the sp^2 atoms in the fused ring system, none deviate from the plane defined by the three *meso*-carbon atoms and two nitrogen atoms in the asymmetric unit by more than 0.6 Å, with a mean displacement of less than 0.01 Å. This interesting ligand has a core size of 4.061(4) Å, as defined by the

distance between two opposing nitrogen atoms. Interestingly, the nitrogen atoms are quite asymmetrically distributed with respect to each other. The distance between N1 and N4, on the side of the carbonyl functionalities, is 2.887(4) Å, while the N2 – N3 distance is only 2.580(3) Å. A larger separation of 3.007(4) Å is found for N1 and N2 and their symmetrical equivalents N3 and N4.

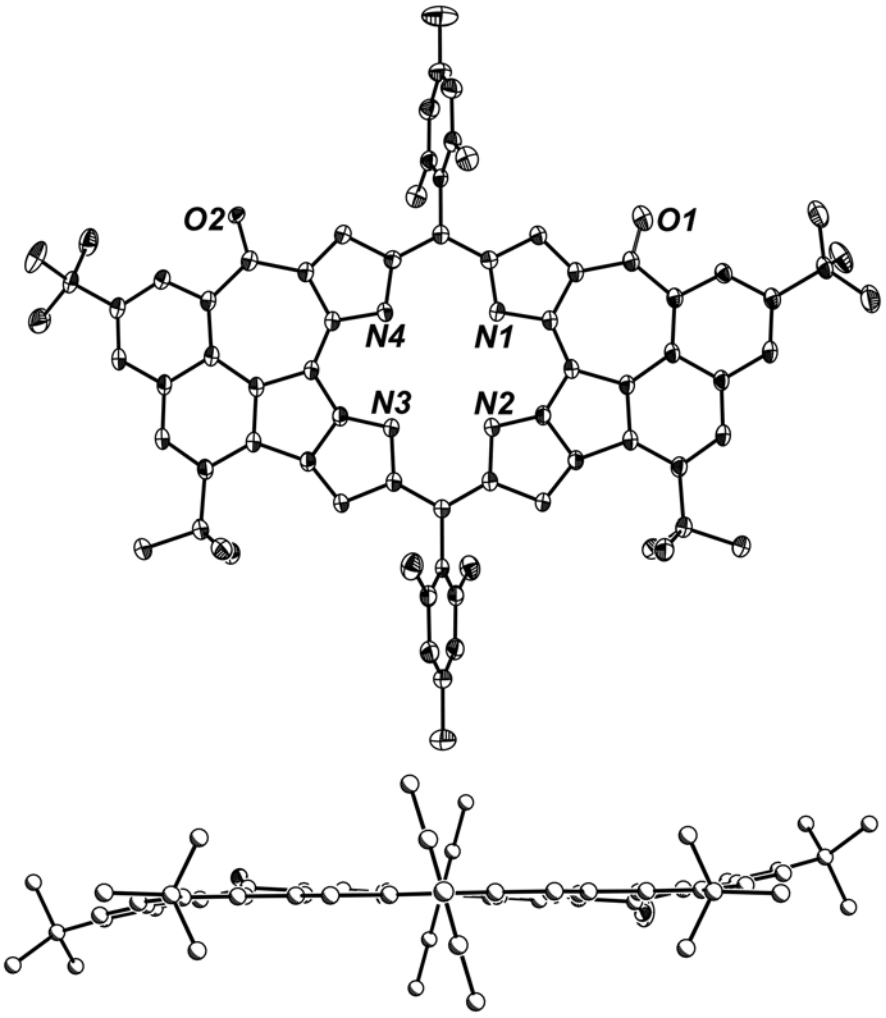

Figure 5-28. Diagram of the X-ray structure of **5-33**. a) Top view (30 % ellipsoids) and b) side view (arbitrary radii for carbon atoms). Hydrogen atoms have been omitted for clarity.

Table 5-4. Selected parameters from the solid-state structure of some porphyrins bearing fused exocyclic ring systems.

	5-10	**5-11**	**5-32**	**5-25**
M-N1	1.990(7)	2.000(5)	2.039(5)	2.002(2)
M-N2	1.986(6)	2.009(5)	1.968(5)	1.952(2)
M-N3	2.005(7)	2.002(5)	2.011(5)	1.949(2)
M-N4	2.002(6)	1.986(5)	1.971(5)	1.997(2)
N1-M-N2	88.4(2)	92.2(2)	90.7(1)	92.3(1)
N2-M-N3	91.8(2)	88.4(2)	87.9(2)	84.6(1)
N3-M-N4	88.5(2)	91.1(2)	90.8(2)	92.0(1)
N4-M-N1	91.2(2)	88.3(2)	90.6(2)	91.0(1)
O1-C31	1.218(10)	1.187(9)	1.244(7)	1.232(3)
O2-C42	1.239(9)	1.223(9)	-	1.223(3)

Electrochemical investigations

In light of the spectral features in the near-IR region indicating very small energy-gaps, cyclic voltammetric studies of several of these compounds were carried out, with special attention paid to the difference in first oxidation and first reduction potentials in comparison with each other and those of Cu(II)tetramesitylporphyrin [Cu(TMP)]. As expected based upon their spectrophotometry, the first oxidation potential was less positive and the first reduction potential less negative for **5-24** (ox1 = 0.73 V; red1 = -0.44 V) compared to **5-25** (ox1 = 0.87 V; red1 = -0.46 V). Relative to Cu(TMP) (ox1 = 1.18 V; red1 = -1.36 V), the differences in these potentials are quite small (Figure 5-28), and even the second reduction for both **5-24** (-0.85 V) and **5-25** (-0.89 V) occurs at a potential far less negative than the first reduction for Cu(TMP). Additional currents were observed in the CVs for these compounds, including two more quasi-reversible reductive waves for **5-25** at more negative potentials (-1.56 V and -1.89 V).

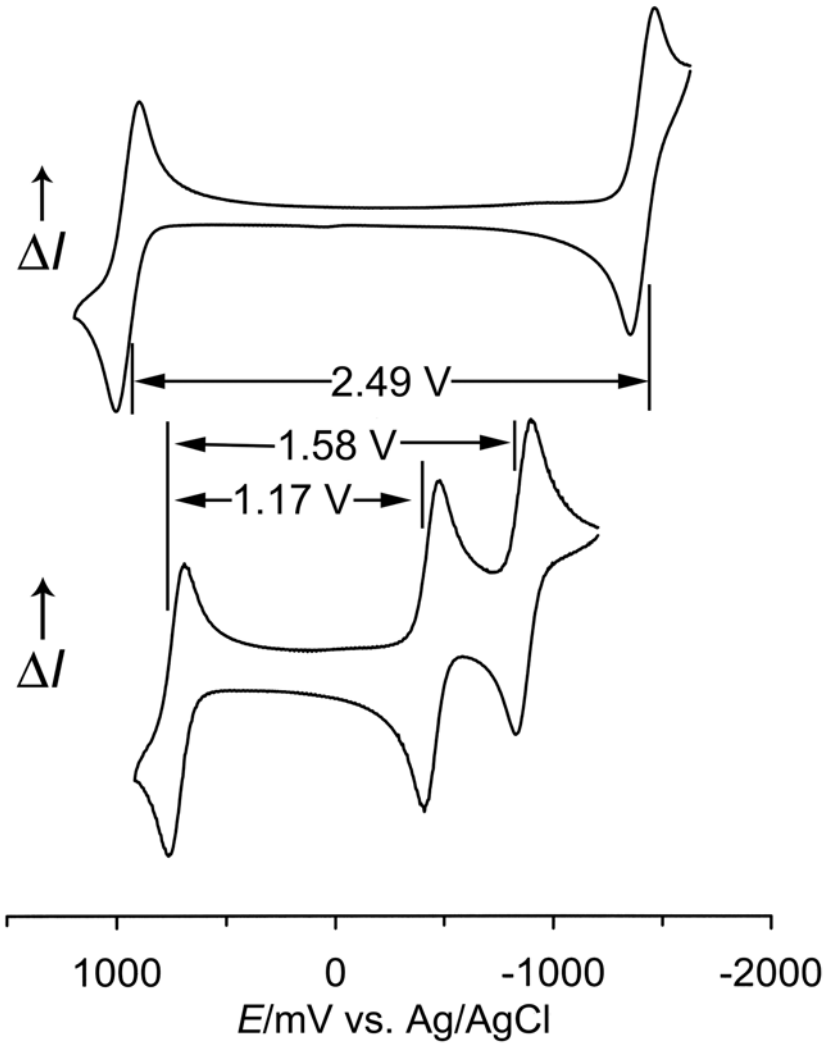

Figure 5-28. Cyclic voltammogram of **5-24** (bottom) compared to that of Cu(TMP) (top).

For the bis-naphthoazulenone porphyrins whose electrochemical potentials were measured, the differences in their primary redox potentials were found to be consistent with the lowest energy absorption in their UV-visible spectra. As depicted in Figure 5-29, a correlation plot comparing these two energies was generated and a good linear fit was made ($R^2 = 0.95$), with a slope of 1.35 and a y-intercept of –0.41. When the line of best-fit was constrained to the origin, the R^2 value decreased to 0.90, but the slope approached unity (1.03).

Table 5-5. Summary of the electrochemical data for selected metalloporphyrins bearing fused exocyclic ring systems. † => $E_{½}$ for reversible process.

Entry	M	isomer	Ox (2)	Ox (1)	Red (1)	Red (2)	Red (3)	Red (4)
5-8	Cu	*trans*	1.30	0.96†	-0.69†	-1.05†	-1.57†	
5-9	Cu	*cis*	1.36	0.97†	-0.83†	-1.24†	-1.56†	-1.89†
5-24	Cu	*trans*		0.73†	-0.44†	-0.85†	-1.74	
5-25	Cu	*cis*		0.87†	-0.46†	-0.89†	-1.57†	-1.96
5-27	Pd	*cis*		0.98†	-0.44†	-0.88†	-1.52†	
5-28	Zn	*trans*	0.83†	0.55†	-0.55†	-0.93†		
5-29	Zn	*cis*		0.60†	-0.64†	-1.04†		
5-31	Ni	*cis*		0.92†	-0.46†	-0.90†	-1.53†	
5-33	2H	*cis*		0.96†	-0.33†	-0.75†	-1.46†	

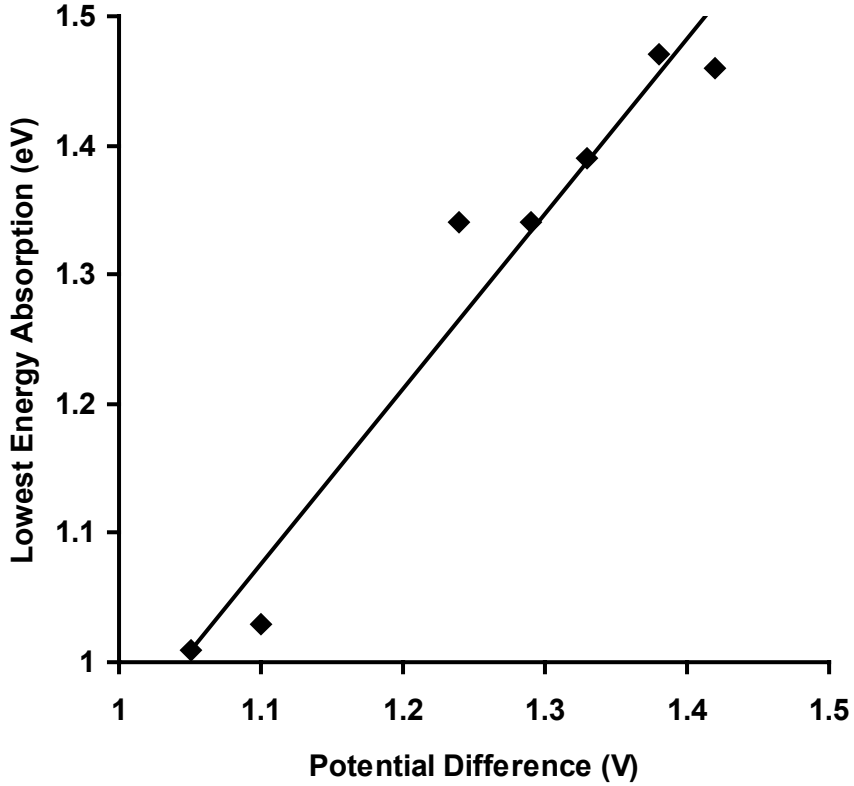

Figure 5-29. Illustration of the correlation between the difference in first oxidation and first reduction potentials of selected bis-naphthoazulenone porphyrins and the lowest energy transition in their electronic absorption spectra. R^2 value for the line depicted is 0.95.

Conclusions

With their tendency to form fully aromatic porphyrins, dispiro-porphodimethene macrocycles are excellent synthons for the preparation of distorted porphyrins bearing two naphthocycloheptenone moieties fused to the macrocycle core as well as 1.69 nm wide, planar porphyrins with two naphthoazulen-8-one ring-systems. These unusual, soluble macrocycles can be isolated in high yields in one or two pot procedures from metalloporphodimethenes, allowing for the preparation of large quantities of material. Detailed investigations into the reactivity and photochemistry of the macrocycles as well as the extension of the rearrangement and coupling procedures to other dispiro-porphodimethenes and biaryl systems, respectively, are underway.

Experimental

General Procedures

The University of Florida Mass Spectrometry Services measured all mass spectral data. Atlantic Microlabs, Norcross, GA or Complete Analysis Laboratories, Parsippany, NJ performed elemental analyses. ^{1}H NMR spectra were recorded on Varian Mercury or VXR spectrometers at 300 MHz in $CDCl_3$ at 25^{o} C (unless otherwise noted), and the chemical shifts were referenced to the solvent residual peak of chloroform at 7.26 MHz. Electronic absorption spectra were collected on either a Varian Cary 50 (UV/ Vis) or 500 (UV/ Vis/ near-IR) spectrophotometer. All reagents were used as received from Aldrich, and all solvents were used as received from Fisher, unless otherwise specified. Compounds **5-1**, **5-2**, and **5-4** were prepared following literature procedures. Refer to Chapter 2 for the preparation of metalloporphodimethenes **5-3**, **5-5**, and **5-12** - **5-15**. Metalloporphodimethenes have been found to undergo decomposition reactions in the presence of air and light; hence light exposure should be minimized when handling these

compounds in solution, and they should be stored as solids, protected from light, under an inert atmosphere.

Chromatography

Absorption column chromatography was preformed using chromatographic silica gel (Fisher, 200 – 425 mesh).

Synthesis of 5-7

Under standard Schlenk conditions, a toluene solution (250 mL, dry, degassed) containing 200 mg of **5-5** was treated with 10 mL of a solution containing 0.200 g $FeCl_3 \cdot 6H_2O$ in MeOH (dry, degassed) which had been stored over 3.5 Å molecular sieves to remove the water of hydration. The reaction mixture was heated to reflux for 30 min, whereupon an additional 10 mL of the $FeCl_3$ solution was added. This incremental addition was repeated 3 times until a total of 50 mL (1.00 g) had been added. Filtration over a small pad of alumina (elution with CH_2Cl_2) and column chromatography (silica, 3x15 cm, 1:1 CH_2Cl_2/ hexanes) provided **5-7** as the second colored fraction (green) following the starting material (red). Recrystallization from $CHCl_3$/ hexanes afforded **5-7** as a green microcrystalline solid.

Yield (**5-7**): 74% (154 mg). UV/ Vis [CH_2Cl_2, λ(log ε)]: 468 (5.4), 630 (4.5) , 678 (4.5) nm. ^{1}H NMR (300 MHz, $CDCl_3$): δ = 9.50 (s, 1H), 9.40 (dd, 1H, J_1 = 1.5, J_2 = 7.5 Hz), 8.70 (dd, 1H, J_1 = 1.2, J_2 = 3.0 Hz), 8.47 – 8.40 (m, 2H), 8.36 (d, 2H, J = 1.5 Hz), 8.26 (dd, 1H, J_1 = 1.2, J_2 = 7.2 Hz), 8.16 – 8.11 (m, 2H), 8.00 – 7.93 (m, 2H), 7.71 – 7.62 (m, 2H), 7.44 (dd, 1H, J_1 = J_2 = 8.1 Hz), 7.34 (s, 1H), 7.30 (s, 1H), 7.15 (dd, 1H, J_1 = 1.2, J_2 = 7.2 Hz), 7.06 (s, 1H), 6.98 (s, 1H), 6.67 (d, 1H, J_1 = 6.6 Hz), 2.60 (s, 3H), 2.56 (s,

3H), 2.34 (s, 3H), 1.37 (s, 3H), 1.18 (s, 3H), -0.90 (t, 3H, J = 7.2 Hz). HRMS (FAB) calculated for $[M+H]^+$ ($C_{62}H_{47}N_4O_3Ni$): 953.3002. Found: 953.2967.

Synthesis of 5-8 and 5-9

Under an inert atmosphere, 201 mg (0.220 mmol) of **5-1** and 60 mg (0.263 mmol) of DDQ were dissolved in 200 mL of dry, degassed CH_2Cl_2. The solution was stirred and irradiated from a distance of 10 cm with a 20 W halogen light source fitted with a UV filter. The reaction mixture darkened immediately, and after 1 min, the title compounds were detected by TLC (silica, 2:1 CH_2Cl_2/ hexanes) as the major green band with the highest R_f value (*trans*) and the red-green band slightly below (*cis*). After 10 min, a supplementary portion of 60 mg (0.263 mmol) of DDQ was added, and the reaction was allowed to proceed for an additional 15 min. The reaction mixture was then diluted, washed with water (600 mL, 3x), dried over Na_2SO_4, and the solvent was removed. Column chromatography (silica, 5x25 cm, 3:1:1 dichloromethane/ hexanes/ toluene) afforded the *trans*-isomer as the first major green band to elute. The *cis*-isomer appears brown on the column, but it elutes as a dark green solution following the *trans*-isomer. The solvents were removed from these two fractions, and the *trans*-isomer was crystallized from CH_2Cl_2/ hexanes to produce a green microcrystalline solid. Diffusion of pentanes into a concentrated toluene solution of the *cis*-isomer provided clusters of green, needle-like crystals.

Yield (**5-8**): 36% (72 mg). UV/ Vis [CH_2Cl_2, λ(log ε)]: 470(5.2), 700(4.5) nm. Analysis Calculated for $C_{60}H_{40}N_4O_2Cu \cdot 2CH_2Cl_2$: C, 68.80; H, 4.10; N, 5.18. Found: C, 69.29; H, 3.89; N, 5.18. HRMS (ESI-FTICR) calculated for $[M+Na]^+$ ($C_{60}H_{40}N_4O_2CuNa$): 934.2339. Found: 934.2379.

Yield (**5-9**): 59% (123 mg). UV/ Vis [CH_2Cl_2, λ(log ε)]: 488(5.2), 678(4.5) nm. Analysis calculated for $C_{60}H_{40}N_4O_2Cu$: C, 78.97; H, 4.42; N, 6.14. Found: C, 78.74; H, 4.65; N, 6.27. HRMS (ESI-FTICR) calculated for $[M+H]^+$ ($C_{60}H_{41}N_4O_2Cu$): 912.2520. Found: 912.2544.

Synthesis of 5-10 and 5-11

As described for **5-8** and **5-9**, 150 mg (0.157 mmol) of **5-3** dissolved in 200 mL of CH_2Cl_2 was treated with two portions of 43 mg (0.189 mmol) of DDQ under an inert atmosphere with light irradiation for a total of 1.5 h. Column chromatography (silica, 5x25 cm, 3:1:1 CH_2Cl_2/ hexanes/ toluene) yielded the *trans*-isomer as the first major green band to elute. The *cis*-isomer elutes as the second green fraction. The solvents were removed, and each isomer was crystallized from $CHCl_3$/ hexanes to produce green, microcrystalline solids. Single crystals suitable for X-ray diffraction were afforded by the slow diffusion of pentanes into either a saturated $CHCl_3$ solution for **5-10** or a saturated THF solution for **5-11**.

Yield (**5-10**): 37% (56 mg). UV/ Vis [CH_2Cl_2, λ(log ε)]: 466(5.3), 674(4.6) nm. ^{1}H NMR (300 MHz, $CDCl_3$): δ = 9.59 (s, 2H), 9.37 (dd, 2H, J_1 = 7.5, J_2 = 1.6 Hz), 8.51 (dd, 2H, J_1 = 8.0, J_2 = 1.7 Hz), 8.49 (d, 2H, J = 5.0 Hz), 8.37 (d, 2H, J = 5.2), 8.20 (dd, 2H, J_1 = 8.2, J_2 = 1.3 Hz), 8.00 (dd, 2H, J_1 = J_2 = 7.7 Hz), 7.72 (dd, 2H, J_1 = J_2 = 7.6 Hz), 7.37 (s, 2H), 7.10 (s, 2H), 6.85 (dd, 2H, J_1 = 7.4, J_2 = 1.2 Hz), 2.59 (s, 6H), 2.45 (s, 6H), 1.29 (s, 6H). Analysis calculated for $C_{60}H_{40}N_4O_2Pd$·0.5 $CHCl_3$: C, 71.58; H, 4.02; N, 5.52. Found: C, 71.67; H, 4.00; N, 5.62. HRMS (FAB) calculated for M^+ ($C_{60}H_{40}N_4O_2Pd$): 954.2204. Found: 954.2266.

Yield (**5-11**): 59% (88 mg). UV/ Vis [CH_2Cl_2, λ(log ε)]: 483(5.4), 652(4.6) nm. ^{1}H NMR (300 MHz, $CDCl_3$): δ = 9.66 (s, 2H), 9.35 (dd, 2H, J_1 = 7.5, J_2 = 1.7 Hz), 8.49 (dd, 2H, J_1 = 8.3, J_2 = 1.4 Hz), 8.41 (d, 2H, J = 5.0 Hz), 8.30 (dd, 2H, J_1 = 5.0, J_2 = 0.5 Hz), 8.20 (dd, 2H, J_1 = 8.2, J_2 = 1.1 Hz), 8.00 (dd, 2H, J_1 = J_2 = 7.6 Hz), 7.75 (dd, 2H, J_1 = J_2 = 7.6 Hz), 7.41 (s, 1H), 7.35 (s, 1H), 7.18 (s, 1H), 7.02 (s, 1H), 6.86 (dd, 2H, J_1 = 7.4, J_2 = 1.2 Hz), 2.67 (s, 3H), 2.63 (s, 3H), 2.56 (s, 3H), 2.29 (s, 3H), 1.45 (s, 3H), 1.13 (s, 3H). Analysis calculated for $C_{60}H_{40}N_4O_2Pd$: C, 75.43; H, 4.22; N, 5.86. Found: C, 75.12; H, 4.27; N, 5.58. HRMS (FAB) calculated for M^+ ($C_{60}H_{40}N_4O_2Pd$): 954.2204. Found: 954.2191.

Synthesis of 5-16 and 5-17

As described for **5-8** and **5-9**, a solution containing 202 mg (0.177 mmol) of **5-12** in 200 mL of CH_2Cl_2 was treated with two portions of 48 mg (0.212 mmol) of DDQ under an inert atmosphere with light irradiation for a total of 40 min. Column chromatography (silica, 5x25 cm, 2:1:1 CH_2Cl_2/ hexanes/ toluene) yielded the *trans*-isomer as the first major green band to elute. The *cis*-isomer appears brown on the column, but it elutes as the second green fraction. The solvents were removed from these two fractions, and the *trans*-isomer was crystallized from $CHCl_3$/ hexanes to produce a green microcrystalline solid. The *cis*-isomer was crystallized from pentanes to produce thin needles of **5-17**.

Yield (**5-16**): 32% (62 mg). UV/ Vis [CH_2Cl_2, λ(log ε)]: 473(5.3), 705(4.6) nm. Analysis calculated for $C_{76}H_{72}N_4O_2Cu$: C, 80.29; H, 6.38; N, 4.93. Found: C, 80.09; H, 6.38; N, 5.27. HRMS (ESI-FTICR) calculated for $[M+Na]^+$ ($C_{76}H_{72}N_4O_2CuNa$): 1158.4843. Found: 1158.4837.

Yield (**5-17**): 57% (114 mg). UV/ Vis [CH_2Cl_2, λ(log ε)]: 490(5.3), 681(4.6) nm. Analysis calculated for $C_{76}H_{72}N_4O_2Cu$: C, 80.29; H, 6.38; N, 4.93. Found: C, 79.91; H, 6.31; N, 4.65. HRMS (ESI-FTICR) calculated for $[M+H]^+$ ($C_{76}H_{73}N_4O_2Cu$): 1136.5023. Found: 1136.5015.

Synthesis of 5-18 and 5-19

As described for **5-8** and **5-9**, a solution containing 160 mg (0.136 mmol) of **5-13** in 200 mL of CH_2Cl_2 was treated with two portions of 37 mg (0.162 mmol) of DDQ under an inert atmosphere with light irradiation for total of 2h. Column chromatography (silica, 5x25 cm, 3:1:1 CH_2Cl_2/ hexanes/ toluene) yielded the *trans*-isomer as the first major green band to elute. The *cis*-isomer elutes as the second green fraction. The *trans*-isomer was crystallized from $CHCl_3$/ hexanes to produce a green, microcrystalline solid. The *cis*-isomer was crystallized from pentanes to produce thin needles that were dried under vacuum.

Yield (**5-18**): 32% (52 mg). UV/ Vis [CH_2Cl_2, λ(log ε)]: 470(5.4), 678(4.7) nm. ^{1}H NMR (300 MHz, $CDCl_3$): δ = 9.57 (s, 2H), 9.46 (d, 2H, *J* = 2.0 Hz), 8.52 (d, 2H, *J* = 4.8 Hz), 8.43 (d, 2H, *J* = 2.0 Hz), 8.40 (d, 2H, *J* = 5.0 Hz), 8.07 (d, 2H, *J* = 1.4 Hz), 7.37 (s, 2H), 7.12 (s, 2H), 6.74 (d, 2H, *J* = 1.6 Hz), 2.59 (s, 6H), 2.42 (s, 6H), 1.66 (s, 18H), 1.35 (s, 6H), 1.31 (s, 18H). HRMS (FAB) calculated for M^+ ($C_{76}H_{72}N_4O_2Pd$): 1178.4689. Found: 1178.4685.

Yield (**5-19**): 62% (99 mg). UV/ Vis [CH_2Cl_2, λ(log ε)]: 486(5.4), 656(4.6) nm. ^{1}H NMR (300 MHz, $CDCl_3$): δ = 9.66 (s, 2H), 9.44 (d, 2H, *J* = 2.0 Hz), 8.45 (d, 2H, *J* = 5.0 Hz), 8.43 (d, 2H, *J* = 2.0 Hz), 8.32 (d, 2H, *J* = 5.0 Hz), 8.09 (d, 2H, *J* = 1.6 Hz), 7.44 (s, 1H), 7.34 (s, 1H), 7.19 (s, 1H), 7.04 (s, 1H), 8.65 (d, 2H, *J* = 1.6 Hz), 2.71 (s, 3H),

2.63 (s, 3H), 2.57 (s, 3H), 2.28 (s, 3H), 1.65 (s, 18H), 1.48 (s, 3H), 1.36 (s, 18H), 1.16 (s, 3H). HRMS (FAB) calculated for M^+ ($C_{76}H_{72}N_4O_2Pd$): 1178.4689. Found: 1178.4664.

Synthesis of 5-20 and 5-21

A solution containing 614 mg (0.54 mmol) of **5-14** in 600 mL of CH_2Cl_2 was treated with 120 mg (0.53 mmol) of DDQ under an inert atmosphere with light irradiation for a total of 2h. Column chromatography (silica, 5x35 cm, 4:1 CH_2Cl_2/ hexanes) yielded the *trans*-isomer as the first major green band to elute. The *cis*-isomer appears red-brown on the column but elutes as the second green fraction. The solvents were removed, and the *trans*-isomer was crystallized from $CHCl_3$/ hexanes to produce a green, microcrystalline solid. The *cis*-isomer was crystallized from pentanes to produce thin needles.

Yield (**5-20**): 35% (213 mg). UV/ Vis [CH_2Cl_2, λ(log ε)]: 715 (4.7), 680 (s), 473 (5.4), 395 (4.4), 303 (4.6) nm. ^{1}H NMR (300 MHz, $CDCl_3$): δ = 9.58 (s, 2H), 9.44 (d, 2H, *J* = 2.1 Hz), 8.62 (d, 2H, *J* = 4.8 Hz), 8.47 (d, 2H, *J* = 4.8 Hz), 8.45 (d, 2H, *J* = 2.4 Hz), 8.09 (d, 2H, *J* = 2.1 Hz), 7.38 (s, 2H), 7.15 (s, 2H), 6.81 (d, 2H, *J* = 2.1 Hz), 2.61 (s, 6H), 2.41 (s, 6H), 1.65 (s, 18H), 1.36 (s, 6H), 1.35 (s, 18H). Analysis calculated for $C_{76}H_{80}N_4O_4Zn$ (**5-20**·$2H_2O$): C, 77.70; H, 6.52; N, 4.77. Found: C, 77.22; H, 6.55; N, 4.40. HRMS (FAB) calculated for M^+ ($C_{76}H_{72}N_4O_2Zn$): 1136.4947. Found: 1136.5014. Calculated for $[M+H]^+$ ($C_{76}H_{73}N_4O_2Zn$): 1137.503. Found: 1136.506.

Yield (**5-21**): 59% (356 mg). UV/ Vis [CH_2Cl_2, λ(log ε)]: 688 (4.6), 624 (4.1), 489 (5.4), 313 (4.5) nm. ^{1}H NMR (300 MHz, $CDCl_3$): δ = 9.73 (s, 2H), 9.47 (d, 2H, *J* = 2.1 Hz), 8.55 (d, 2H, *J* = 4.5 Hz), 8.47 (d, 2H, *J* = 2.1 Hz), 8.45 (d, 2H, *J* = 4.8 Hz), 8.14 (d, 2H, *J* = 1.9 Hz), 7.49 (s, 1H), 7.37 (s, 1H), 7.25 (s, 1H), 7.10 (s, 1H), 6.89 (d, 2H, *J* = 1.9

Hz), 2.74 (s, 3H), 2.67 (s, 3H), 2.61 (s, 3H), 2.30 (s, 3H), 1.68 (s, 18H), 1.53 (s, 3H), 1.41 (s, 18H), 1.23 (s, 3H). Analysis calculated for $C_{153}H_{145}N_8O_8Cl_3Zn_2$ [2(**5-21**)·$CHCl_3$)]: C, 76.92; H, 5.78; N, 4.69. Found: C, 76.63; H, 6.20; N, 4.30. HRMS (FAB) calculated for $[M+H]^+$ ($C_{76}H_{73}N_4O_2Zn$): 1137.5025. Found: 1137.5043.

Synthesis of 5-22 and 5-23

A solution containing 190 mg (0.177 mmol) of **5-15** in 250 mL of CH_2Cl_2 was treated with 80 mg (0.354 mmol) of DDQ under an inert atmosphere with light irradiation for 1 h. Column chromatography (silica, 3x20 cm; toluene/ hexanes/ $CHCl_3$, 1:1:1) provided the *trans*-isomer as the first major green band to elute. The *cis*-isomer elutes as the second green fraction. The solvents were removed, and the *trans*-isomer was crystallized from CH_2Cl_2/ hexanes to produce a green, microcrystalline solid. The *cis*-isomer was crystallized from pentanes to produce thin needles that were dried under vacuum.

Yield (**5-22**): 32% (64 mg). UV/ Vis [CH_2Cl_2, λ(log ε)]: 692 (4.7), 476 (5.2). ^{1}H NMR (300 MHz, $CDCl_3$): δ = 9.46 (d, 2H, *J* = 2.4 Hz), 9.41 (s, 2H), 8.38 (m, 6H), 7.97 (d, 2H, *J* = 1.9 Hz), 7.33 (s, 2H), 7.03 (s, 2H), 6.62 (d, 2H, *J* = 2.1 Hz), 2.54 (s, 6H), 2.52 (s, 6H), 1.64 (s, 18H), 1.30 (s, 6H), 1.26 (s, 18H). HRMS (FAB) calculated for $[M+H]^+$ ($C_{76}H_{73}N_4O_2Ni$): 1131.5087. Found: 1131.5090.

Yield **5-23**: 65% (110 mg). UV/ Vis [CH_2Cl_2, λ(log ε)]: 672 (4.4), 494 (5.1). ^{1}H NMR (300 MHz, $CDCl_3$): δ = 9.45 (s, 2H), 9.41 (s, 2H), 8.36 (s, 2H), 8.33 (s, 4H), 8.00 (s, 2H), 7.38 (s, 1H), 7.29 (s, 1H), 7.09 (s, 1H), 6.97 (s, 1H), 6.77 (s, 2H), 2.71 (s, 3H), 2.58 (s, 3H), 2.51 (s, 3H), 2.32 (s, 3H), 1.62 (s, 18H), 1.41 (s, 3H), 1.33 (s, 18H), 1.19 (s,

3H). HRMS (FAB) calculated for $[M+H]^+$ ($C_{76}H_{72}N_4O_2Ni$): 1131.5087. Found: 1131.5028.

Synthesis of 5-24

A portion of 60 mg (0.053 mmol) of **5-16** was added to 100 mL of CH_2Cl_2 containing 58 mg (0.254 mmol) of DDQ and 142 mg (0.528 mmol) of $FeCl_3 \cdot 6H_2O$. The reaction mixture was heated to reflux with stirring. After 4 h, an additional 29 mg (0.127 mmol) of DDQ and 142 mg (0.528 mmol) of $FeCl_3 \cdot 6H_2O$ were added. Reflux was continued for another 2 h. The reaction mixture was allowed to cool to room temperature and decanted, leaving behind most of the iron salts as a residue. The solution was treated with 100 mL of a freshly prepared aqueous solution containing 200 mg of $NaBH_4$. The resulting biphasic mixture was stirred for 5 min, and diluted with 200 mL of CH_2Cl_2. The organic phase was then washed with water (600 mL, 3x), dried over Na_2SO_4, and filtered over silica (4x4 cm, *o*-$C_6H_4Cl_2$). The addition of hexanes to the filtrate caused precipitation of the title compound, which was dried under vacuum to produce a metallic, red-gray powder.

Yield (**5-24**): 90% (54 mg). UV/ Vis [$CHCl_3$, λ(log ε)]: 314(4.8), 449(4.8), 519(4.7), 579(4.9), 706(3.8), 1038(3.9), 1204(3.9) nm. Analysis calculated for $C_{76}H_{68}N_4O_2Cu \cdot C_6H_4Cl_2$: C, 76.95; H, 5.67; N, 4.38. Found: C, 76.68; H, 5.96; N, 4.85. HRMS (FAB) calculated for M^+ ($C_{76}H_{68}N_4O_2Cu$): 1131.4632. Found: 1131.4611.

Synthesis of 5-25

A portion of 50 mg (0.044 mmol) **5-17** was added to 100 mL of CH_2Cl_2 containing 24 mg (0.106 mmol) of DDQ and 118 mg (0.440 mmol) of $FeCl_3 \cdot 6H_2O$. The reaction mixture was heated to reflux with stirring. An additional portion of 24 mg (0.106 mmol) of DDQ was added to the flask. After 15 min, TLC indicated the complete consumption

of the starting material. The reaction mixture was washed with water (600 mL, 3x), dried over Na_2SO_4, and concentrated to 20 mL. Filtration over silica (6x4 cm, elution with CH_2Cl_2/ hexanes 1:1) and slow removal of the solvents produced **5-25** as a purple-green microcrystalline solid. Single crystals suitable for X-ray diffraction were grown by diffusion of pentanes into a saturated CH_2Cl_2 solution of **5-25**.

Yield (**5-25**): 98% (49 mg). UV/ Vis [$CHCl_3$, λ(log ε)]: 308(4.6), 441(4.6), 540(4.9), 894(4.2) nm. Analysis calculated for $C_{76}H_{68}N_4O_2Cu$: C, 80.57; H, 6.05; N, 4.95. Found: C, 80.60; H, 5.98; N, 4.86. HRMS (FAB) calculated for M^+ ($C_{76}H_{68}N_4O_2Cu$): 1132.4670. Found: 1132.4682.

Synthesis of 5-26

As described for **5-24**, 48 mg (0.041 mmol) **5-18** was added to 100 mL of CH_2Cl_2 containing 44 mg (0.196 mmol) of DDQ, and 109 mg (0.407 mmol) of $FeCl_3 \cdot 6H_2O$. The reaction mixture was heated to reflux with stirring. After 4 h, an additional portion of 22 mg (0.098 mmol) of DDQ and 109 mg (0.407 mmol) of $FeCl_3 \cdot 6H_2O$ was added. Reflux was continued for another 1 h. The reaction mixture was allowed to cool to room temperature and decanted, leaving behind most of the iron salts as a residue, and it was then treated with 100 mL of a freshly prepared aqueous solution containing 200 mg of $NaBH_4$. The resulting biphasic mixture was stirred for 5 min and diluted with 200 mL of CH_2Cl_2. The organic phase was then washed with water (600 mL, 3x), dried over Na_2SO_4, and filtered over silica (4x4 cm, *o*-$C_6H_4Cl_2$). The addition of hexanes to the filtrate caused precipitation of the title compound, which was collected on a fine-fritted funnel, washed with pentanes, and dried under vacuum to produce a metallic, red-gray powder.

Yield (**5-26**): 92% (44 mg). UV/ Vis [$CHCl_3$, λ(log ε)]: 307(4.6), 445(4.7), 502(4.5), 522(4.5), 567(4.9), 682(3.8), 994(3.8), 1145(3.8) nm. ^{1}H NMR (300 MHz, $CDCl_3$): δ = 8.70 (d, 2H, *J* = 2.1 Hz), 8.29 (s, 2H), 7.52 (d, 2H, *J* = 2.4 Hz), 7.21 (s, 2H), 7.09 (s, 4H), 6.69 (s, 2H), 2.50 (s, 6H), 2.01 (s, 12H), 1.45 (s, 18H), 1.40 (s, 18H). Analysis calculated for $C_{76}H_{68}N_4O_2Pd \cdot C_6H_4Cl_2$: C, 74.45; H, 5.49; N, 4.24. Found: C, 74.59; H, 5.90; N, 4.37. HRMS (ESI-FTICR) calculated for M^+ ($C_{76}H_{68}N_4O_2Pd$): 1174.4376. Found: 1174.4334.

Synthesis of 5-27

As described for **5-25**, 55 mg (0.047 mmol) **5-19** was added to 100 mL of CH_2Cl_2 containing 25 mg (0.112 mmol) of DDQ and 126 mg (0.470 mmol) of $FeCl_3 \cdot 6H_2O$. The reaction mixture was heated to reflux with stirring. Once reflux was reached, an additional portion of 25 mg (0.112 mmol) of DDQ was added to the flask. After 15 min, TLC indicated the complete consumption of the starting material. The reaction mixture was washed with water (600 mL, 3x), dried over Na_2SO_4, and concentrated to 20 mL. Filtration over silica (6x4 cm, elution with CH_2Cl_2/ hexanes 1:1) and slow removal of the solvents produced the title compound as a purple-green microcrystalline solid. Single crystals suitable for X-ray diffraction were grown by diffusion of pentanes into a saturated CH_2Cl_2 solution.

Yield (**5-27**): 96% (53 mg). UV/ Vis [$CHCl_3$, λ(log ε)]: 285(4.6), 445(4.8), 553(4.9), 850(4.2) nm. ^{1}H NMR (300 MHz, $CDCl_3$): δ = 8.78 (d, 2H, *J* = 2.1 Hz), 8.51 (s, 2H), 7.63 (d, 2H, *J* = 2.4 Hz), 7.34 (s, 2H), 7.11 (s, 4H), 6.72 (s, 2H), 2.52 (s, 3H), 2.51 (s, 3H), 2.19 (s, 6H), 1.87 (s, 6H), 1.49 (s, 18H), 1.42 (s, 18H). Analysis calculated

for $C_{76}H_{68}N_4O_2Pd$: C, 77.63; H, 5.83; N, 4.77. Found: C, 77.44; H, 5.93; N, 4.85. HRMS (FAB) calculated for M^+ ($C_{76}H_{68}N_4O_2Pd$): 1174.4376. Found: 1174.4359.

Synthesis of 5-28

A portion of 102 mg (0.090 mmol) **5-20** was added to 120 mL of CH_2Cl_2. This solution was treated with 50.0 mg (0.220 mmol) of DDQ, and 109 mg (0.187 mmol) of $FeCl_3 \cdot 6H_2O$. The reaction mixture was heated to reflux with stirring. After 2 h, an additional portion of 100 mg (0.440 mmol) of DDQ and 100 mg (0.373 mmol) of $FeCl_3 \cdot 6H_2O$ was added. Reflux was continued for another 6 h. The reaction mixture was allowed to cool to room temperature and decanted, leaving behind most of the iron salts as a residue, and it was then treated with 150 mL of a freshly prepared aqueous solution containing 500 mg of $NaBH_4$. The resulting biphasic mixture was stirred for 5 min and diluted with 200 mL of CH_2Cl_2. The organic phase was then washed with water (800 mL, 3x), dried over Na_2SO_4, and filtered over silica (4x4 cm, $CHCl_3$/ THF 9:1). The addition of hexanes to the filtrate caused precipitation of the title compound, which was washed with pentanes to produce a metallic, red-brown powder.

Yield (**5-28**): 74% (76 mg). UV/ Vis [$CHCl_3$, λ(log ε)]: 1228 (4.0), 1060 (4.0), 720 (4.0), 593 (4.9), 524 (4.9), 456 (4.9), 313 (4.9) nm. ^{1}H NMR (300 MHz, $CDCl_3$): δ = 8.66 (s, 2H), 8.22 (s, 2H), 7.45 (s, 2H), 7.13 (s, 2H), 7.07 (s, 4H), 6.70 (s, 2H), 2.49 (s, 6H), 2.01 (s, 12H), 1.43 (s, 18H), 1.38 (s, 18H). HRMS (EI) calculated for M^+ ($C_{76}H_{68}N_4O_2Zn$): 1132.4634. Found: 1132.4655.

Synthesis of 5-29

A solution containing 100 mg (0.088 mmol) **5-21** in 100 mL of CH_2Cl_2 was treated with 50 mg (0.220 mmol) of DDQ and 240 mg (0.889 mmol) of $FeCl_3 \cdot 6H_2O$. The

reaction mixture was heated to reflux with stirring for 20 min. The reaction mixture was filtered over silica (4x4 cm, elution with CH_2Cl_2). The solvent was reduced to 10 mL, and the product was precipitated with hexanes to produce the title compound as a purple microcrystalline solid. Single crystals suitable for X-ray diffraction were grown by slow diffusion of pentane into a saturated solution of **5-29** in THF/ $CHCl_3$ (1:5). Yield **5-29**: 89% (89 mg). UV/ Vis [$CHCl_3$, $\lambda(\log \varepsilon)$]: 923 (4.3), 546 (5.1), 445 (4.7), 302 (4.8) nm. ^{1}H NMR (300 MHz, $CDCl_3$): δ = 8.68 (d, 2H, J = 2.4 Hz), 8.38 (s, 2H), 7.51 (d, 2H, J = 2.1 Hz), 7.20 (s, 2H), 7.08 (s, 2H), 7.07 (s, 2H), 6.51 (s, 2H), 2.50 (s, 3H), 2.49 (s, 3H), 2.18 (s, 6H), 1.89 (s, 6H), 1.44 (s, 18H), 1.39 (s, 18H). Analysis calculated for $C_{84.5}H_{76.5}N_4O_4Cl_{1.5}Zn$ [**5-28**·2THF·0.5$CHCl_3$(as found in the solid-state): C, 76.46; H, 6.10; N, 4.43. Found C, 76.63; H, 6.20; N, 4.30. HRMS (EI) calculated for M^+ ($C_{76}H_{68}N_4O_2Zn$): 1132.4634. Found 1132.4638.

Synthesis of 5-30

A portion of 60 mg (0.053 mmol) **5-22** was added to 120 mL of CH_2Cl_2. This solution was treated with 40.0 mg (0.055 mmol) of DDQ, and 85 mg (0.146 mmol) of $FeCl_3{\cdot}6H_2O$. The reaction mixture was heated to reflux with stirring. After 2 h, an additional portion of 90 mg (0.396 mmol) of DDQ and 100 mg (0.373 mmol) of $FeCl_3{\cdot}6H_2O$ was added. Reflux was continued for another 8 h. The reaction mixture was allowed to cool to room temperature and decanted, leaving behind most of the iron salts as a residue, and the solution was treated with 150 mL of a freshly prepared aqueous solution containing 500 mg of $NaBH_4$. The resulting biphasic mixture was stirred for 5 min and diluted with 300 mL of CH_2Cl_2. The organic phase was then washed with water (800 mL, 3x), dried over Na_2SO_4, and filtered over silica (4x4 cm, $CHCl_3$/ THF 9:1).

The addition of hexanes to the filtrate caused precipitation of the title compound, which was washed with pentanes and dried under vacuum to produce a metallic, red-gray powder. Yield: **5-30**: 74% (76 mg). UV/ Vis [$CHCl_3$, λ(log ε)]: 1147 (3.9), 1038 (4.2), 894 (3.7), 751 (3.5), 564 (4.9), 507 (4.7), 447 (4.8), 307 (4.8) nm. ^{1}H NMR (300 MHz, d_8-toluene, 105^o C): δ = 8.91 (d, 2H, *J* = 2.1 Hz), 8.55 (s, 2H), 8.34 (s, 2H), 8.00 (d, 2H, *J* = 8.5 Hz), 7.49 (d, 2H, *J* = 7.9 Hz), 7.41 (s, 2H), 7.32 (s, 2H), 2.28 (s, 6H), 1.95 (s, 12H), 1.39 (s, 18H), 1.22 (s, 18H). HRMS (EI) calculated for M^+ ($C_{76}H_{68}N_4O_2Ni$): 1126.4696. Found: 1126.4758.

Synthesis of 5-31

A solution containing 102 mg (0.088 mmol) **5-23** in 100 mL of CH_2Cl_2 was treated with 50 mg (0.220 mmol) of DDQ and 240 mg (0.889 mmol) of $FeCl_3{\cdot}6H_2O$. The reaction mixture was heated to reflux with stirring for 20 min. The reaction mixture was filtered over silica (4x4 cm, elution with CH_2Cl_2). The solvent was reduced to 10 mL, and the product was precipitated with hexanes to produce the title compound as a purple microcrystalline solid. Single crystals suitable for X-ray diffraction were grown by diffusion of Et_2O into a saturated CH_2Cl_2 solution. Yield: **5-31**: 89% (89 mg). UV/ Vis [$CHCl_3$, λ(log ε)]: 846 (4.2), 558 (4.8), 513 (4.8), 454 (4.8) nm. ^{1}H NMR (300 MHz, $CDCl_3$): δ = 8.71 (d, 2H, *J* = 2.1 Hz), 8.46 (s, 2H), 7.60 (d, 2H, *J* = 2.1 Hz), 7.30 (s, 2H), 7.09 (s, 4H), 6.74 (s, 2H), 2.50 (s, 3H), 2.49 (s, 3H), 2.16 (s, 6H), 1.85 (s, 6H), 1.45 (s, 18H), 1.41 (s, 18H). HRMS (FAB) calculated for $[M+H]^+$ ($C_{76}H_{69}N_4O_2Ni$): 1127.4774. Found 1127.4786.

Synthesis of 5-32

A solution containing 235 mg (0.200 mmol) **5-18** in 200 mL of CH_2Cl_2 was treated with 50 mg (0.220 mmol) of DDQ and 240 mg (0.889 mmol) of $FeCl_3 \cdot 6H_2O$. The reaction mixture was heated to reflux with stirring for 3 h, and was then filtered over silica (4x4 cm, elution with CH_2Cl_2). The solvent was reduced to 10 mL, and the product was precipitated with hexanes to produce the title compound as a red-brown microcrystalline solid. Single crystals suitable for X-ray diffraction were grown by diffusion of pentanes into a saturated $CHCl_3$/ THF solution (1:1).

Yield: **5-32**: 82% (193 mg). UV/ Vis [$CHCl_3$, λ(log ε)]: 825 (4.0), 646 (4.0), 577 (4.7), 515 (4.8), 464 (5.0)nm. ^{1}H NMR (300 MHz, $CDCl_3$): δ = 9.21 (d, 1H, *J* = 2.4 Hz), 8.86 (d, 2H, *J* = 6.4 Hz), 8.82 (d, 1H, *J* = 2.1 Hz), 8.31 (d, 1H, *J* = 2.4 Hz), 8.06 (d, 1H, *J* = 1.9 Hz), 7.85 (d, 1H, *J* = 5.0 Hz), 7.58 – 7.62 (m, 3H), 7.29 (s, 1H), 7.25 (s, 1H), 7.17 (s, 1H), 7.15 (s, 1H), 7.12 (s, 1H), 7.05 – 7.09 (m, 2H), 2.55 (s, 3H), 2.53 (s, 3H), 2.21 (s, 3H), 2.11 (s, 3H), 1.97 (s, 3H), 1.58 (s, 9H), 1.55 (s, 9H) 1.45 (s, 9H), 1.38 (s, 9H), 1.26 (s, 3H). HRMS (FAB) calculated for $[M+H]^+$ ($C_{76}H_{71}N_4O_2Pd$): 1176.4556. Found 1176.4531.

Synthesis of 5-33

A $CHCl_3$ solution (25 mL) containing 90 mg (0.088 mmol) **5-29** was treated with 3 mL of 12 M HCl at room temperature for 10 h. This solution was diluted with 50 mL of $CHCl_3$, washed with water (400 mL, 3x), and dried over Na_2SO_4. Column chromatography (silica, 2x10 cm, $CHCl_3$/ hexanes 3:2) provided **5-33** as the second, purple fraction, following a minor first fraction of similar color. Recrystallization from CH_2Cl_2/ hexanes afforded a purple, microcrystalline solid. Single crystals suitable for X-

ray diffraction were grown by slow diffusion of pentane into a saturated solution of **5-33** in $CHCl_3$.

Yield (**5-33**): 85% (80 mg). UV/ Vis [$CHCl_3$, λ(log ε)]: 923 (4.2), 879 (sh), 541 (5.0), 437 (4.7), 316 (4.9) nm. ^{1}H NMR (300 MHz, $CDCl_3$): δ = 8.67 (d, 2H, *J* = 2.4 Hz), 8.29 (s, 2H), 7.64 (bs, 2H), 7.55 (d, 2H, *J* = 2.1 Hz), 7.09 (s, 2H), 7.08 (s, 2H), 6.49 (bs, 2H), 2.49 (s, 3H), 2.48 (s, 3H), 2.18 (s, 6H), 1.94 (s, 6H), 1.44 (s, 18H), 1.40 (s, 18H). HRMS (ESI-FTICR) calculated for $[M+H]^+$ ($C_{76}H_{71}N_4O_2$): 1071.5577. Found: 1071.5570.

Synthesis of 5-34

A $CHCl_3$ solution (25 mL) containing 50 mg (0.088 mmol) **5-28** was treated with 3 mL of TFA at room temperature for 4 h. This solution was diluted with 100 mL of $CHCl_3$, washed with aqueous K_2CO_3 (400 mL) and water (400 mL, 3x), and dried over Na_2SO_4. Filtration through a small pad of silica (3x5 cm, $CHCl_3$/ hexanes 1:1) provided **5-34** as the only colored filtrite.

Yield (**5-34**): 87% (44 mg). UV/ Vis [$CHCl_3$, λ(log ε)]: 1101 (3.9), 856 (3.8), 582 (4.5), 430 (4.8) nm. ^{1}H NMR (300 MHz, d_8-toluene, 105^o C): δ = 8.81 (s, 2H), 8.09 (d, 2H, *J* = 2.4 Hz), 7.31 (s, 2H), 6.69 (s, 2H), 6.41 (s, 2H), 6.33 (s, 4H), 2.24 (s, 6H), 2.15 (s, 12H), 1.24 (s, 18H), 1.23 (s, 18H). HRMS (FAB) calculated for $[M+H]^+$ ($C_{76}H_{71}N_4O_2$): 1071.5577. Found: 1071.5524.

Electrochemistry

Electrochemical measurements were made using an EG&G PAR Versa Stat II potentiostat with a Pt disc working electrode, a Pt wire counter electrode, and an aqueous Ag/ AgCl reference electrode (NaCl, 3M) fitted with a Vicor frit as a salt bridge. In all

cases, dry, degassed benzonitrile was the solvent, and tetra-n-butylammoniumhexafluorophosphate, at a concentration of 0.10 M, was used for the supporting electrolyte. Ferrocene was added to the cell after each series of measurements to confirm the potential of the reference electrode (the $E_{1/2}$ for the Fc/Fc^{+} couple remained constant at 0.46(1) V vs. the Ag/ AgCl reference electrode). The analyte concentration was 2.5(2) mM. All measurements were made at room temperature, with the exception of **5-22**, which for solubility reasons was measured at 65°C.

X-ray Crystallography

Unit cell dimensions were obtained (Tables 5-4 and 5-5) and intensity data collected by Prof. Michael Scott on a Siemens CCD SMART diffractometer at low temperature, with monochromatic Mo-Kα X-rays (λ = 0.71073 Å). The data collections nominally covered over a hemisphere of reciprocal space, by a combination of three sets of exposures; each set had a different ϕ angle for the crystal and each exposure covered 0.3° in ω. The crystal to detector distance was 5.0 cm. The data sets were corrected empirically for absorption using SADABS.[66] The structure was solved using the Bruker SHELXTL software package for the PC, by direct method option of SHELXS. The space group was determined from an examination of the systematic absences in the data, and the successful solution and refinement of the structure confirmed these assignments. All hydrogen atoms were assigned idealized locations and were given a thermal parameter equivalent to 1.2 or 1.5 times the thermal parameter of the carbon atom to which it were attached. For the methyl groups, where the location of the hydrogen atoms was uncertain, the AFIX 137 card was used to allow the hydrogen atoms to rotate to the maximum area of residual density, while fixing their geometry.

Table 5-7. Crystallographic data for compounds **5-10**, **5-11**, and **5-32**.

	5-10·4$CHCl_3$·0.5C_5H_{12}	**5-11**·C_4H_8O	**5-32**·$CHCl_3$
Formula	$C_{66.5}H_{50}Cl_{12}N_4O_2Pd$	$C_{64}H_{48}N_4O_3Pd$	$C_{77}H_{71}Cl_3N_4O_2Pd$
Formula weight	1469.01	1027.53	1297.22
Crystal system	Monoclinic	Orthorhombic	Monoclinic
Space group	$P2_1/c$	$Pna2_1$	$I2/a$
Z	8	8	8
Temp, K	193(2)	193(2)	193(2)
D_{calc} gcm^{-3}	1.515	1.354	1.395
a Å	12.085(3)	27.078(3)	29.576(1)
b Å	31.100(8)	13.077(1)	16.355(4)
c Å	28.596(7)	29.018(3)	30.068(9)
β, deg	98.472(4)		105.489(9)
V $Å^3$	10630(4)	10275(2)	14016(7)
μ, mm^{-1}	0.702	0.414	0.387
Uniq. data coll./obs.	8505/16688	20174/ 12188	16231/ 11610
$R_1[I \geq 2\sigma(I)data]$[a]	0.0700	0.0543	0.1040
$wR_2[I \geq 2\sigma(I)data]$[b]	0.1543	0.1355	0.3162

[a] $R_1 = \Sigma||F_o| - |F_c||/ \Sigma| F_o|$

[b] $wR_2 = \{ \Sigma[w (F_o^2 - F_c^2)^2 / \Sigma[w (F_o^2)^2$

Table 5-8. Crystallographic data for **5-25** and **5-34**.

	5-25·CH_2Cl_2	**5-34**·$2CHCl_3$
Formula	$C_{77}H_{70}Cl_2CuN_4O_2$	$C_{78}H_{72}Cl_6N_4O_2$
Formula weight	1339.80	1310.17
Crystal system	Monoclinic	Monoclinic
Space group	*C*2/c	*C*2/c
Z	8	4
Temp, K	193(2)	193(2)
D_{calc} gcm^{-3}	1.193	1.236
a Å	29.574(1)	22.561(2)
b Å	12.4738(6)	31.346(3)
c Å	41.109(2)	10.0498(9)
β, deg	100.309(1)	107.369(2)
V $Å^3$	14920(1)	6783(1)
μ, mm^{-1}	0.484	0.301
Uniq. data coll./obs.	14679/10048	8000/4318
$R_1[I \geq 2\sigma(I)data]$[a]	0.0558	0.0500
$wR_2[I \geq 2\sigma(I)data]$[b]	0.1398	0.1258

[a] $R_1 = \Sigma||F_o| - |F_c||/ \Sigma| F_o|$

[b] $wR_2 = \{ \Sigma[w (F_o^2 - F_c^2)^2 / \Sigma[w (F_o^2)^2$

Table 5-9. Crystallographic data for **5-27** and **5-27a**.

	5-27·0.5CH_2Cl_2·0.5C_5H_{12}	**5-27a**·2CH_2Cl_2
Formula	$C_{79}H_{75}ClPdN_4O_2$	$C_{78}H_{71}Cl_5PdN_4O_2$
Formula weight	1254.36	1380.13
Crystal system	Monoclinic	Triclinic
Space group	*C*2/c	*P*-1
Z	8	2
Temp, K	193(2)	193(2)
D_{calc} gcm^{-3}	1.428	1.193
a Å	29.727(5)	13.9683(7)
b Å	12.710(2)	14.6890(7)
c Å	39.668(7)	17.1512(8)
α, deg		84.604(1)
β, deg	98.815(3)	72.978(1)
γ, deg		72.450(1)
V $Å^3$	14811(5)	3208.2(3)
μ, mm^{-1}	0.534	0.423
Uniq. data coll./obs.	10825/8447	14424/8668
$R_1[I \geq 2\sigma(I)data]$[a]	0.0935	0.0614
$wR_2[I \geq 2\sigma(I)data]$[b]	0.2295	0.1548

[a] $R_1 = \Sigma||F_o| - |F_c||/ \Sigma| F_o|$

[b] $wR_2 = \{ \Sigma[w (F_o^2 - F_c^2)^2 / \Sigma[w (F_o^2)^2$

LIST OF REFERENCES

(1) Gouterman, M. *Porphyrins*; Ameican Chemical Society: Washington DC, 1986.

(2) Dennstedt, M.; Zimmermann, J. *Chem. Berichte* **1887**, *20*, 2449.

(3) Kadish, K. M.; Smith, K. M.; Guilard, R., Eds. *The Porphyrin Handbook*; Academic Press: Burlington MA, 1999; Vol. 6.

(4) Moss, G. P. *Pure Appl. Chem.* **1987**, *59*, 779.

(5) Mauzerall, D. *J. Am. Chem. Soc.* **1960**, *82*, 2605.

(6) Dolphin, D. *J. Heterocycl. Chem.* **1970**, *7*, 275.

(7) Evans, B.; Smith, K. M.; Fuhrhop, J. H. *Tetrahedron Lett.* **1977**, 443.

(8) Buchler, J. W.; Puppe, L. *Annalen Der Chemie-Justus Liebig* **1974**, 1046.

(9) Buchler, J. W.; Lay, K. L.; Smith, P. D.; Scheidt, W. R.; Rupprecht, G. A.; Kenny, J. E. *J. Organometal. Chem.* **1976**, *110*, 109.

(10) Buchler, J. W.; Dreher, C.; Lay, K. L.; Lee, Y. J.; Scheidt, W. R. *Inorg. Chem.* **1983**, *22*, 888.

(11) Botulinski, A.; Buchler, J. W.; Tonn, B.; Wicholas, M. *Inorg. Chem.* **1985**, *24*, 3239.

(12) Botulinski, A.; Buchler, J. W.; Wicholas, M. *Inorg. Chem.* **1987**, *26*, 1540.

(13) Botulinski, A.; Buchler, J. W.; Lee, Y. J.; Scheidt, W. R.; Wicholas, M. *Inorg. Chem.* **1988**, *27*, 927.

(14) Renner, M. W.; Buchler, J. W. *J. Phys. Chem.* **1995**, *99*, 8045.

(15) Dwyer, P. N.; Buchler, J. W.; Scheidt, W. R. *J. Chem. Soc.* **1974**, *96*, 2789.

(16) Dwyer, P. N.; Puppe, L.; Buchler, J. W.; Scheidt, W. R. *Inorg. Chem.* **1975**, *14*, 1782.

(17) Buchler, J. W.; Lay, K. L.; Lee, Y. J.; Scheidt, W. R. *Angew. Chem.-Int. Edit.* **1982**, *21*, 432.

(18) Botulinski, A.; Buchler, J. W.; Lay, K. L.; Ensling, J.; Twilfer, H.; Billecke, J.; Leuken, H.; Tonn, B. *Advances in Chemistry Series* **1982**, 253.

(19) Lindsey, J. S. In *The Porphyrin Handbook*; Kadish, K. M., Smith, K. M., Guilard, R., Eds.; Academic Press: Burlington MA, 1999; Vol. 1.

(20) Lindsey, J. S. In *Metalloporphyrin-Catalyzed Oxidations*; Montanari, F., Casella, L., Eds.; Kluwer Academic Publishers: Dordrecht, 1994; Vol. 17.

(21) Rothemund, P. *J. Am. Chem. Soc.* **1935**, *57*, 2010.

(22) Rothemund, P.; Menotti, A. R. *J. Am. Chem. Soc.* **1941**, *63*, 267.

(23) Adler, A. D.; Shergali.W; Longo, F. R. *J. Am. Chem. Soc.* **1964**, *86*, 3145.

(24) Lindsey, J. S.; Hsu, H. C.; Schreiman, I. C. *Tetrahedron Lett.* **1986**, *27*, 4969.

(25) Lindsey, J. S.; Schreiman, I. C.; Hsu, H. C.; Kearney, P. C.; Marguerettaz, A. M. *J. Org. Chem.* **1987**, *52*, 827.

(26) Banfi, S.; Manfredi, A.; Montanari, F.; Pozzi, G.; Quici, S. *J. Mol. Catal. A-Chem.* **1996**, *113*, 77.

(27) Staley, S. W.; Eliasson, B.; Kearney, P. C.; Schreiman, I. C.; Lindsey, J. S. In *Molecular Electronic Devices*; 3rd ed.; Carter, F. L., Siatkowski, R. E., Wohltjen, H., Eds.; Elsevier: North Holland, 1988.

(28) Lee, C. H.; Lindsey, J. S. *Tetrahedron* **1994**, *50*, 11427.

(29) French, R. R.; Wirz, J.; Woggon, W. D. *Helv. Chim. Acta* **1998**, *81*, 1521.

(30) Geier, G. R.; Littler, B. J.; Lindsey, J. S. *J. Chem. Soc.-Perkin Trans. 2* **2001**, 701.

(31) Littler, B. J.; Ciringh, Y.; Lindsey, J. S. *J. Org. Chem.* **1999**, *64*, 2864.

(32) Balakumar, A.; Lysenko, A. B.; Carcel, C.; Malinovskii, V. L.; Gryko, D. T.; Schweikart, K. H.; Loewe, R. S.; Yasseri, A. A.; Liu, Z. M.; Bocian, D. F.; Lindsey, J. S. *J. Org. Chem.* **2004**, *69*, 1435.

(33) Schweikart, K. H.; Malinovskii, V. L.; Yasseri, A. A.; Li, J. Z.; Lysenko, A. B.; Bocian, D. F.; Lindsey, J. S. *Inorg. Chem.* **2003**, *42*, 7431.

(34) Tornizaki, K. Y.; Thamyongkit, P.; Loewe, R. S.; Lindsey, J. S. *Tetrahedron* **2003**, *59*, 1191.

(35) Tour, J. M.; Rawlett, A. M.; Kozaki, M.; Yao, Y. X.; Jagessar, R. C.; Dirk, S. M.; Price, D. W.; Reed, M. A.; Zhou, C. W.; Chen, J.; Wang, W. Y.; Campbell, I. *Chem.-Eur. J.* **2001**, *7*, 5118.

(36) Yu, L. H.; Lindsey, J. S. *J. Org. Chem.* **2001**, *66*, 7402.

(37) Rao, P. D.; Dhanalekshmi, S.; Littler, B. J.; Lindsey, J. S. *J. Org. Chem.* **2000**, *65*, 7323.

(38) Gouterman, M. In *The porphyrins*; Dolphin, D., Ed.; Academic Press: New York, 1978; Vol. III.

(39) Anderson, H. L. *Chem. Commun* **1999**, 2323-2330.

(40) Mamardashvili, N. Z.; Golubchikov, O. A. *Uspekhi Khimii* **2001**, *70*, 656.

(41) Sanders, J. K. M. In *The Porphyrin Handbook*; 1 ed.; K. M. Kadish, K. M. S., and R. Guilard, Ed.; Academic press: San Diego, CA, 2000; Vol. 3, pp 1-40.

(42) Kaim, W.; Schwederski, B. *Bioinorganic Chemistry: Inorganic Elements in the Chemistry of Life*; 3rd ed.; Wiley: Chichester, 1994.

(43) Botulinski, A.; Buchler, J. W.; Abbes, N. E.; Scheidt, W. R. *Liebigs Ann.* **1987**, 305.

(44) Chang, C. K.; Kondylis, M. P. *Chem. Commun.* **1986**, 316.

(45) Harmjanz, M.; Scott, M. J. *Chem. Commun.* **2000**, 397.

(46) Bonomo, L.; Solari, E.; Scopelliti, R.; Latronico, M.; Floriani, C. *Chem. Commun.* **1999**, 2227.

(47) Bucher, C.; Seidel, D.; Lynch, V.; Kral, V.; Sessler, J. L. *Org. Lett.* **2000**, *2*, 3103.

(48) Fontecave, M.; Battioni, J. P.; Mansuy, D. *J. Am. Chem. Soc.* **1984**, *106*, 5217.

(49) Rhee, S. W.; Na, Y. H.; Do, Y.; Kim, J. *Inorg. Chim. Acta* **2000**, *309*, 49.

(50) Senge, M. O.; Runge, S.; Speck, M.; Ruhlandt-Senge, K. *Tetrahedron* **2000**, *56*, 8927.

(51) Senge, M. O.; Kalisch, W. W.; Bischoff, I. *Chem.-Eur. J.* **2000**, *6*, 2721.

(52) Gill, H. S.; Harmjanz, M.; Santamaria, J.; Finger, I.; Scott, M. J. *Angew. Chem.-Int. Edit.* **2003**.

(53) Harmjanz, M.; Scott, M. J. *Inorg. Chem.* **2000**, *39*, 5428.

(54) Harmjanz, M.; Gill, H. S.; Scott, M. J. *J. Am. Chem. Soc.* **2000**, *122*, 10476.

(55) Harmjanz, V.; Bozidarevic, I.; Scott, M. J. *Org. Lett.* **2001**, *3*, 2281.

(56) Harmjanz, M.; Gill, H. S.; Scott, M. J. *J. Org. Chem.* **2001**, *66*, 5374.

(57) Gill, H. S.; Scott, M. J., Unpublished results.

(58) Bozidarevic, I.; Haskins-Glusac, K.; Gill, H. S.; Shanze, K. S.; Scott, M. J. *Inorg. Chem.* **In preparation**.

(59) Re, N.; Bonomo, L.; Da Silva, C.; Solari, E.; Scopelliti, R.; Floriani, C. *Chem.-Eur. J.* **2001**, *7*, 2536.

(60) Billecke, J.; Botulinski, A.; Buchler, J. W.; Kokisch, W.; Lay, K. L.; Oesten, K.; Smith, P. D. *Abstr. Pap. Am. Chem. Soc.* **1981**, *181*, 107.

(61) Kral, V.; Sessler, J. L.; Zimmerman, R. S.; Seidel, D.; Lynch, V.; Andrioletti, B. *Angew. Chem.-Int. Edit.* **2000**, *39*, 1055.

(62) Bonomo, L.; Solari, E.; Scopelliti, R.; Floriani, C.; Re, N. *J. Am. Chem. Soc.* **2000**, *122*, 5312.

(63) Da Silva, C.; Bonomo, L.; Solari, E.; Scopelliti, R.; Floriani, C.; Re, N. *Chem.-Eur. J.* **2000**, *6*, 4518.

(64) Illingworth, E.; Peters, A. T. *J. Chem. Soc.* **1952**, 1602.

(65) Fieser, L. F.; Cason, J. *J. Am. Chem. Soc.* **1940**, *62*, 432.

(66) Blessing, R. H. *Acta Crystallogr. Sect. A* **1995**, *51*, 33.

(67) Ortiz de Montellano, P. R., Ed. *Cytochrome P450, Structure, Mechanism and Biochemistry*; 2nd ed.; Plenum: New York, 1995.

(68) James, M. O.; Boyle, S. M. *Comparative Biochemistry and Physiology C-Toxicology & Pharmacology* **1998**, *121*, 157.

(69) Kagawa, N.; Waterman, M. R. In *Cytochrome P450, Structure, Mechanism and Biochemistry*; 2nd ed.; Ortiz de Montellano, P. R., Ed.; Plenum: New York, 1995, pp 419-442.

(70) Lathe, R. *Steroids* **2002**, *67*, 967.

(71) Stoffel-Wagner, B. *European Journal of Endocrinology* **2001**, *145*, 669.

(72) Lewis, D. F. V. *Pharmacogenomics* **2004**, *5*, 305.

(73) Danielson, P. B. *Current Drug Metabolism* **2002**, *3*, 561.

(74) Staab, H. A.; Feurer, A.; Hauck, R. *Angew. Chem.-Int. Edit.* **1995**, *33*, 2428.

(75) Staab, H. A.; Feurer, A.; Krieger, C.; Kumar, A. S. *Liebigs Ann.-Recl.* **1997**, 2321.

(76) Ward, B.; Wang, C. B.; Chang, C. K. *J. Am. Chem. Soc.* **1981**, *103*, 5236.

(77) Chang, C. K.; Abdalmuhdi, I. *J. Org. Chem.* **1983**, *48*, 5388-5390.

(78) Barley, M. H.; Dolphin, D.; James, B. R. *J. Chem. Soc.-Chem. Commun.* **1984**, 1499.

(79) Chang, C. K.; Liu, H. Y.; Abdalmuhdi, I. *J. Am. Chem. Soc.* **1984**, *106*, 2725.

(80) Chang, C. K.; Abdalmuhdi, I. *Angew. Chem.-Int. Edit. Engl.* **1984**, *23*, 164.

(81) Eaton, S. S.; Eaton, G. R.; Chang, C. K. *J. Am. Chem. Soc.* **1985**, *107*, 3177.

(82) Liu, H. Y.; Abdalmuhdi, I.; Chang, C. K.; Anson, F. C. *J. Phys. Chem.* **1985**, *89*, 665.

(83) Ni, C. L.; Abdalmuhdi, I.; Chang, C. K.; Anson, F. C. *J. Phys. Chem.* **1987**, *91*, 1158.

(84) Osuka, A.; Maruyama, K. *J. Am. Chem. Soc.* **1988**, *110*, 4454-.

(85) Naruta, Y.; Maruyama, K. *J. Am. Chem. Soc.* **1991**, *113*, 3595.

(86) Cammidge, A. N.; Ozturk, O. *Tetrahedron Lett.* **2001**, *42*, 355.

(87) Liang, Y.; Chang, C. K. *Tetrahedron Lett.* **1995**, *36*, 3817.

(88) Bag, N.; Chern, S. S.; Peng, S. M.; Chang, C. K. *Inorg. Chem.* **1995**, *34*, 753.

(89) Ogoshi, H.; Mizutani, T.; Hayashi, T.; Kuroda, Y. In *The Porphyrin Handbook*; Kadish, K. M., Smith, K. M., Guilard, R., Eds.; Academic Press: Burlington MA, 2000; Vol. 6.

(90) Iovine, P. M.; Kellett, M. A.; Redmore, N. P.; Therien, M. J. *J. Am. Chem. Soc.* **2000**, *122*, 8717.

(91) Vangberg, T.; Ghosh, A. *J. Am. Chem. Soc.* **1998**, *120*, 6227.

(92) Kalsbeck, W. A.; Seth, J.; Bocian, D. F. *Inorg. Chem.* **1996**, *35*, 7935.

(93) Elkasmi, A.; Lexa, D.; Maillard, P.; Momenteau, M.; Saveant, J. M. *J. Am. Chem. Soc.* **1991**, *113*, 1586.

(94) Balch, A. L.; Koerner, R.; LatosGrazynski, L.; Noll, B. C. *J. Am. Chem. Soc.* **1996**, *118*, 2760.

(95) Chang, C. K.; Aviles, G.; Bag, N. Z. *J. Am. Chem. Soc.* **1994**, *116*, 12127.

(96) Smith, P. D.; James, B. R.; Dolphin, D. H. *Coord. Chem. Rev.* **1981**, *39*, 31.

(97) Renner, M. W.; Cheng, R. J.; Chang, C. K.; Fajer, J. *J. Phys. Chem.* **1990**, *94*, 8508.

(98) Medforth, C. J.; Senge, M. O.; Smith, K. M.; Sparks, L. D.; Shelnutt, J. A. *J. Am. Chem. Soc.* **1992**, *114*, 9859.

(99) Jentzen, W.; Unger, E.; Song, X. Z.; Jia, S. L.; TurowskaTyrk, I.; SchweitzerStenner, R.; Dreybrodt, W.; Scheidt, W. R.; Shelnutt, J. A. *J. Phys. Chem. A* **1997**, *101*, 5789.

(100) Shelnutt, J. A.; Song, X. Z.; Ma, J. G.; Jia, S. L.; Jentzen, W.; Medforth, C. J. *Chem. Soc. Rev.* **1998**, *27*, 31.

(101) Senge, M. O. *J. Porphyr. Phthalocyanines* **1998**, *2*, 107.

(102) Jia, S. L.; Jentzen, W.; Shang, M.; Song, X. Z.; Ma, J. G.; Scheidt, W. R.; Shelnutt, J. A. *Inorg. Chem.* **1998**, *37*, 4402.

(103) Neal, T. J.; Cheng, B. S.; Ma, J. G.; Shelnutt, J. A.; Schulz, C. E.; Scheidt, W. R. *Inorg. Chim. Acta* **1999**, *291*, 49.

(104) Senge, M. O. In *The Porphyrin Handbook*; 1 ed.; Kadish, K. M., Smith, K. M., Guilard, R., Eds.; Academic Press: San Diego, 2000; Vol. 1, pp 239-335.

(105) Barkigia, K. M.; Renner, M. W.; Fajer, J. *J. Porphyr. Phthalocyanines* **2001**, *5*, 415.

(106) Renner, M. W.; Barkigia, K. M.; Melamed, D.; Gisselbrecht, J. P.; Nelson, N. Y.; Smith, K. M.; Fajer, J. *Res. Chem. Intermed.* **2002**, *28*, 741.

(107) Nurco, D. J.; Smith, K. M.; Fajer, J. *Chem. Commun.* **2002**, 2982.

(108) Sigfridsson, E.; Ryde, U. *J. Biol. Inorg. Chem.* **2003**, *8*, 273.

(109) Callot, H. J.; Ocampo, R. In *The Porphyrin Handbook*; Kadish, K. M., Smith, K. M., Guilard, R., Eds.; Academic Press: San Diego, 2000; Vol. 1, pp 349-398.

(110) Lash, T. D. In *The Porphyrin Handbook*; Kadish, K. M., Smith, K. M., Guilard, R., Eds.; Academic Press: San Diego, 2000; Vol. 2.

(111) Richeter, S.; Jeandon, C.; Ruppert, R.; Callot, H. J. *Chem. Commun.* **2001**, 91.

(112) Aihara, H.; Jaquinod, L.; Nurco, D. J.; Smith, K. M. *Angew. Chem.-Int. Edit.* **2001**, *40*, 3439.

(113) Richeter, S.; Jeandon, C.; Gisselbrecht, J. P.; Ruppert, R.; Callot, H. J. *J. Am. Chem. Soc.* **2002**, *124*, 6168.

(114) Forman, A.; Renner, M. W.; Fujita, E.; Barkigia, K. M.; Evans, M. C. W.; Smith, K. M.; Fajer, J. *Isr. J. Chem.* **1989**, *29*, 57.

(115) Lash, T. D. *J. Porphyr. Phthalocyanines* **2001**, *5*, 267.

(116) Haddad, R. E.; Gazeau, S.; Pecaut, J.; Marchon, J. C.; Medforth, C. J.; Shelnutt, J. A. *J. Am. Chem. Soc.* **2003**, *125*, 1253.

(117) Chou, J. H.; Nalwa, H. S.; Kosal, M. E.; Rakow, N. A.; Suslick, S. S. In *The Porphyrin Handbook*; Kadish, K. M., Smith, K. M., Guilard, R., Eds.; Academic Press: San Diego, 2000; Vol. 6, pp 43-132.

(118) Pandey, R. K.; Zheng, G. In *The Porphyrin Handbook*; Kadish, K. M., Smith, K. M., Guilard, R., Eds.; Academic Press: San Diego, 2000; Vol. 6, pp 157-230.

(119) Wiehe, A.; Stollberg, H.; Runge, S.; Paul, A.; Senge, M. O.; Roder, B. *J. Porphyr. Phthalocyanines* **2001**, *5*, 853.

(120) Gazeau, S.; Pecaut, J.; Haddad, R.; Shelnutt, J. A.; Marchon, J. C. *Eur. J. Inorg. Chem.* **2002**, 2956.

(121) Mazzanti, M.; Marchon, J. C.; Shang, M. Y.; Scheidt, W. R.; Jia, S. L.; Shelnutt, J. A. *J. Am. Chem. Soc.* **1997**, *119*, 12400.

(122) Chapman, O. L.; Weiss, D. S. In *Organic Photochemistry*; 1 ed.; Chapman, O. L., Ed.; Dekker: New York, 1973; Vol. 3, pp 197-288.

(123) Bard, A. J.; Faulkner, L. R. *Electrochemical Methods*; Wiley: New York, 1980.

(124) Watson, M. D.; Fechtenkotter, A.; Mullen, K. *Chem. Rev.* **2001**, *101*, 1267.

(125) Chandrasekhar, S.; Sumithra, G.; Yadav, J. S. *Tetrahedron Lett.* **1996**, *37*, 1645.

(126) Kamo, M.; Tsuda, A.; Nakamura, Y.; Aratani, N.; Furukawa, K.; Kato, T.; Osuka, A. *Org. Lett.* **2003**, *5*, 2079.

(127) Tsuda, A.; Osuka, A. *Science* **2001**, *293*, 79.

(128) Yoon, D. H.; Lee, S. B.; Yoo, K. H.; Kim, J.; Lim, J. K.; Aratani, N.; Tsuda, A.; Osuka, A.; Kim, D. *J. Am. Chem. Soc.* **2003**, *125*, 11062.

BIOGRAPHICAL SKETCH

Hubert S. Gill, IV was born in Raleigh, N.C., on September 21, 1976, to Sue and Hubert Gill. He grew up in nearby Garner, N.C., where he played for 18 years, especially at the Boondocks, his grandparents' farm where his mother dropped him off to run amok. In high school Hubert played center on the varsity football team, was a set designer and stage manager for numerous musical theater productions, and participated in various mathematics and science competitions. He received two invitations to The National Science Olympiad and was awarded two "American Ingenuity Awards" from The Edison Society. In 1994 Hubert joined the Garner Fire Department, finally putting to good use his predilection towards playing with fire and dangerous chemicals. Throughout high school, he generally tried to pass himself off as a good student, and somehow this worked. In the spring of 1995, Hubert graduated from Garner Senior High School with high honors, and was awarded a National Merit Scholarship. That fall he departed the Old North State to attend Florida State University, where he majored in biochemistry and in chemistry, but spent more time sailing and gardening than he did in class. Despite of all of the leisure time that Hubert spent with his friends in Tallahassee, he remained active in the university, serving as a resident assistant for two years, a research technician for one year, a research assistant in both a molecular biophysics lab and an inorganic chemistry lab, and a full-time laboratory teaching assistant for two semesters. Hubert was also an active member of ΑΧΣ, the professional chemistry fraternity, and the historian and fleet captain for the FSU Sailing Association. In the spring of 1999 Hubert

was awarded the Undergraduate Research Award by the FSU Department of Chemistry, and he graduated with honors attaining degrees in both biochemistry and chemistry. That fall Hubert did what most good Seminoles consider the ultimate sacrilege by enrolling in the University of Florida for graduate school, where he has been working on this dissertation as an Alumni Fellow for the past five years.